Aalborg Universitet

AALBORG UNIVERSITY

DENMARK

Wave Overtopping of Marine Structures

Kofoed, Jens Peter

Jens Peter Kofoed

Wave Overtopping of Marine Structures — Utilization of Wave Energy

Wave Overtopping of Marine Structures — Utilization of Wave Energy

by

Jens Peter Kofoed

December 2002

Preface

The present thesis *Wave Overtopping of Marine Structures — Utilization of Wave Energy* is being submitted as one of the requirements set out in the Ministerial Order No. 114 of March 8, 2002 regarding Ph.D. studies. The thesis is being defended publicly on January 17, 2003 at Aalborg University.

The Ph.D. study *Overtopping of Marine Structures* has been supported by the Danish Wave Energy Programme under the Danish Energy Agency through the project *Optimization of Overtopping Ramps for Utilization of Wave Energy for Power Production* (J. no. 51191/98-0017) and *Power Pyramid — fase 2* (J. no. 51191/00-0050), and been co-financed by the Department of Civil Engineering, Aalborg University. The study has been conducted during the period from October 1998 to December 2002 at Hydraulics & Coastal Engineering Laboratory, Aalborg University, under the supervision of Associate Professor Peter B. Frigaard.

As a part of the Ph.D. study the author have benefitted from a five-month stay from March to July 1999 at Flanders Community, Flanders Hydraulics in Antwerp. Throughout the stay experimental work was carried out as part of EC MAST 3 project *OPTICREST — The optimization of crest level design of sloping coastal structures through prototype monitoring and modeling*. As part of this project the author also had the opportunity to work with the project organizers at Ghent University, Department of Civil Engineering. Special thanks to Marc Willems at FCFH for making this stay possible and a pleasant one.

In addition to the present thesis the research conducted has resulted in a number of other publications. Among these are:

- Kofoed J. P.: *Model study of overtopping of marine structures for a wide range of geometric parameters.* Poster presented at 27th Int. Conf. on Coastal Eng. (ICCE-2000), Sidney, Australia, July 2000.

Table of Contents

Appendices

List of Symbols

a	:	Amplitude of regular wave [m]
A_c	:	Armor crest freeboard defined as vertical distance from SWL to armor crest
c	:	Wave velocity defined as $c = \frac{L}{T}$ [m/s]
c_{rc}	:	Sector of the curved part of slope, circular curved slope [°]
d	:	Water depth [m]
d_r	:	Draft [m]
E_{f,d_r}	:	Energy flux integrated from the draft up to the surface [W/m]
$E_{f,d}$	:	Energy flux integrated from the sea bottom up to the surface [W/m]
f	:	Frequency [Hz]
f_p	:	Peak frequency [Hz]
g	:	Acceleration of gravity, where set to 9.82 m/s^2
H	:	Wave height [m]
$h_{c\ m,n}$	:	Horizontal distance between crest of reservoir m and n [m]
h_{hp}	:	Extension of horizontal plate at the draft of the slope [m]
$h_{l\ m,n}$	:	Horizontal opening between reservoir m and n [m]
H_{m0}	:	Significant wave height based on spectral estimate [m]
H_s	:	Significant wave height [m]
$h_{w,n}$	:	Horizontal distance from the line defined by the slope and crest of the reservoirs n [m]
k	:	Wave number defined as $\frac{2\pi}{L}$ [m^{-1}]
k_p	:	Wave number based on L_p defined as $\frac{2\pi}{L_p}$ [m^{-1}]
L	:	Wave length [m]
L_0	:	Deep water wave length [m]
L_m	:	Wave length based on T_m [m]
L_{m0}	:	Deep water wave length based on $\frac{g}{2\pi}T_{m0}^2$ [m]
L_p	:	Wave length based on T_p [m]
L_{p0}	:	Deep water wave length based on $\frac{g}{2\pi}T_{p0}^2$ [m]
m_{-1}	:	The minus first spectral moment [m^{2}s]
m_0	:	The zero'th spectral moment [m^2]

N	:	Number of waves [-]
N_{window}	:	Number of subseries [-]
P	:	Power obtained as potential energy by overtopping per unit time [W] or [W/m]
P_n	:	Power obtained as potential energy by overtopping per unit time in individual reservoirs n [W] or [W/m]
P'	:	Non-dimensionalized power obtained as potential energy by overtopping per unit time defined as $P' = \frac{P}{P_{wave}}$ [-]
P_{occur}	:	Probability of occurrence [-]
P_{ot}	:	Probability of overtopping [-]
P_{V_w}	:	Probability of a certain overtopping volume in a wave V_w given that overtopping occurs [-]
P_{wave}	:	The power that is passing through a vertical cross section of the water column, perpendicular to the wave direction with unit width [W] or [W/m]
p^+	:	Excess pressure caused by wave [N/m^2]
q	:	Average wave overtopping discharge per width [m^3/s/m]
q_n	:	Average wave overtopping discharge per width of the nth reservoir [m^3/s/m]
$q_{meas}(t)$	:	Measured wave overtopping discharge time series per width [m^3/s/m]
$q_{sim}(t)$	:	Simulated wave overtopping discharge time series per width [m^3/s/m]
q_{window}^i	:	Average wave overtopping discharge per width within a subseries T_{window} long [m^3/s/m]
Q	:	Dimensionless average overtopping discharge defined as $\frac{q}{\sqrt{gH_s^3}}$ where nothing else is stated [-]
r_{rc}	:	Radius of curved part of slope, circular curved slope [m]
R	:	Dimensionless freeboard defined as $\frac{R_c}{H_s}$ where nothing else is stated [-]
R^2	:	Square of the Pearson product moment correlation coefficient [-]
R_c	:	Crest freeboard [m]
R_c, n	:	Crest freeboard of the n'th reservoir [m]
r_l	:	Large radius in ellipse (used in description of elliptic shape of slope side walls) [m]
Ru	:	Run-up level [m]
Ru_{max}	:	Maximum run-up level [m]
$Ru_{2\%}$	:	Run-up level exceeded by 2 % of irregular waves [m]
s	:	Wave steepness defined as $\frac{H}{L}$ [-]
s_{m0}	:	Deep water wave steepness defined as $\frac{H_s}{L_{m0}}$
S_η	:	Spectral density of wave elevation [m^2/s]
t	:	Time [s]

T	:	Wave period [s]
T_e	:	Energy transport wave period, calculated as $T_e = \frac{m_{-1}}{m_0}$ [s]
T_m	:	Average period [s]
T_{m0}	:	Deep water average period [s]
T_{window}	:	Size of subseries [s]
u	:	Horizontal particle velocity component [m/s]
T_p	:	Spectral peak period [s]
V_w	:	Overtopping volume in a wave per width [m^3/m]
w_c	:	Distance between side walls at slope crest [m]
w_{d_r}	:	Distance between side walls at slope draft [m]
x	:	Coordinate in the direction the wave is traveling [m]
z	:	Vertical distance to the MWL [m]
z_1	:	Lower boundary of reservoir [m]
z_2	:	Upper boundary of reservoir [m]
α	:	Slope angle [°]
α_m	:	Optimal slope angle used in λ_α [°]
β	:	Fitting coefficient in λ_α
Δz	:	Vertical distance between reservoir crests [m]
η	:	Wave elevation [m]
η_c	:	Wave crest elevation [m]
η_{ws}	:	Hydraulic efficiency for a single wave condition defined as $\frac{P}{P_{wave}}$ [-]
η_{hydr}	:	Overall hydraulic efficiency defined as $\frac{\sum_{m=1}^{5} P^m P_{occur}^m}{\sum_{m=1}^{5} P_{wave}^m P_{occur}^m}$ [-]
γ	:	Peak enhancement factor [-]
γ_b	:	Reduction coefficients taking the influence of berm into account [-]
γ_h	:	Reduction coefficients taking the influence of shallow foreshore into account [-]
γ_r	:	Reduction coefficients taking the influence of roughness into account [-]
γ_w	:	Specific weight of water defined as $\gamma_w = \rho_w g = 10{,}016\ kg/(m^2 s^2)$
γ_β	:	Reduction coefficients taking the influence of angle of wave attack into account [-]
κ	:	Fitting coefficient in λ_{d_r}
λ_{d_r}	:	Correction factor describing the influence of limited draft on the average overtopping discharge [-]
λ_m	:	Correction factor describing the influence of various geometry modifications on the average overtopping discharge [-]
λ_s	:	Factor for correction of the average overtopping discharge for small dimensionless crest free boards R [-]
λ_α	:	Correction factor describing the influence of varying slope angle on the average overtopping discharge [-]

θ_n : Angle of the n'th reservoir front [°]

ρ_w : Density of water $\rho_w = 1{,}020 \; kg/m^3$

ξ : Surf similarity parameter defined as $\xi = \dfrac{\tan \alpha}{\sqrt{\frac{H}{L}}}$ [-]

ξ_p : Surf similarity parameter defined as $\xi_p = \dfrac{\tan \alpha}{\sqrt{\frac{H_s}{L_p}}}$ [-]

ξ_{p0} : Surf similarity parameter defined as $\xi_{p0} = \dfrac{\tan \alpha}{\sqrt{\frac{H_s}{L_{p0}}}} = \dfrac{\tan \alpha}{\sqrt{2\pi \frac{H_s}{gT_p^2}}}$ [-]

x

List of Abbreviations

AAU	:	Aalborg University
MWL	:	Mean water level
SWL	:	Still water level
WEC	:	Wave energy converter
WD	:	Wave Dragon
PP	:	Power Pyramid

Summary

Wave Overtopping of Marine Structures —
Utilization of Wave Energy

During the past 50, years tools for predicting wave overtopping of sea defense structures have continuously been refined. However, developers of wave energy converters have raised questions about how to predict the overtopping of structures with layouts significantly different from those of sea defense structures. Optimization of structures utilizing wave overtopping for the production of electrical power has been ongoing throughout the last decade.

It has been established that the information available in the existing literature is insufficient to describe overtopping of such structures. The present thesis describes investigations conducted against this background.

The development of guidelines for calculating overtopping discharges for a wide variety of slope layouts is presented. Both structures with single and multi level reservoirs are examined. All geometries have been subjected to a wide range of sea states. Overtopping slope layouts resulting in substantial energy content in the overtopping discharges have been pointed out.

The influence of various geometrical parameters, such as slope shape, shape of guiding walls, draft and crest freeboard, on the overtopping discharges has been investigated. The effect of using overtopping reservoirs at multiple levels has also been quantified. The emphasis is generally on optimizing the overtopping with respect to maximizing the potential energy in the overtopping water.

Based on the experimental data, expressions for predicting wave overtopping discharges, and vertical distribution of overtopping above the slope, are proposed. The overall hydraulic efficiency of wave energy converters, based on the overtopping principle, can be 20 - 35 % when a single reservoir is used, and up to 45 - 50 % for a structure with reservoirs at 4 levels.

Summary in Danish

Bølgeoverskyl af marine konstruktioner —
Udnyttelse af bølgeenergi

Igennem det sidste halve århundrede er der blevet arbejdet med udvikling af metoder til beregning af bølgeoverskyl af kystbeskyttelsesbygværker, og som følge heraf er disse metoder kontinuerligt blevet forbedret. Indenfor de seneste år har udviklere af bølgeenergianlæg af overskylstypen ønsket at beregne bølgeoverskyl af konstruktioner som adskiller sig væsentlig fra kystbeskyttelsesbygværker, samt at optimere disse konstruktioner således at energimængden i bølgeoverskyllet maksimeres. Det er fundet at den information der foreligger i litteraturen ikke er tilstrækkelig til at svare på disse spørgsmål. Dette er grundlaget for de undersøgelserne der præsenteres i nærværende rapport.

Formålet med det udførte arbejde har været, at tilvejebringe retningslinier for hvorledes overskylsmængder kan beregnes for en bred vifte af geometriske udformninger af overskylsskråninger, med reservoirer i både et enkelt og flere niveauer, når disse udsættes for en forskellige søtilstande, samt at udpege udformninger, som resulterer i et stort energiindhold i det overskyllende vand.

I studiet er det undersøgt hvorledes forskellige geometriske parametre, så som skråningsform, formen af ledevægge, dybdegående og fribordshøjde influerer på overskylsraten. Effekten af at anvende reservoirer i flere niveauer er også undersøgt. Generelt er vægten i undersøgelserne lagt på at optimere overskyllet med hensyn til at maksimere den potentielle energi i det overskyllende vand.

Baseret på de eksperimentielle data, er der opstillet udtryk til beregning af overskylsraten, samt den lodrette fordeling af overskyllet over skråningen. Det er fundet, at en overordnet hydraulisk effektivitet af bølgeenergianlæg af overskylstypen på 20 - 35 % kan opnås, når der anvendes et enkelt reservoir. En effektivitet på 45 - 50 % kan opnås for anlæg med reservoirer i 4 niveauer.

CHAPTER 1

Introduction

Research into wave overtopping of coastal structures has been the subject of numerous investigations over the past 50 years. Since then the overtopping prediction tools for typical sea defense structures have continuously been refined. The term wave overtopping is used here to refer to the process where waves hit a sloping structure, run up the slope, and eventually, if the crest level of the slope is lower than the highest run-up level, overtop the structure. The wave overtopping discharge is thus defined as overtopping volume $[m^3]$ pr. time $[s]$ and structure width $[m]$.

The motivation for predicting the overtopping of structures has until now been linked to the design of structures protecting mankind and objects of value against the violent force of the surrounding sea. Typically, rubble mound or vertical wall breakwaters have been used for the protection of harbors, and dikes and offshore breakwaters have been used for the protection of beaches and land. All these structures are designed to avoid overtopping or at least reduce it to a minimum, as overtopping can lead either to functional or structural failure of structures. Here functional failure refers to cases where for example large wave overtopping discharges might damage persons, ships, the structure it self or equipment on it, or generate waves behind the structure (in case water is present there), which again is hazardous to the maneuvering or mooring of ships. An example of such conditions is shown in figure 1.1. Structural failure refers to cases where the overtopping discharge is heavy enough to damage the lee side of the breakwater or dike, which ultimately can lead to the collapse of the structure.

Figure 1.1: *Wave run-up and overtopping at Zeebrugge breakwater during (mild) storm conditions (from OPTICREST project, awww.rug.ac.be/opticrest).*

1.1 Concept of utilizing wave overtopping in WEC's

The work described in this thesis has an unusual background, as it was motivated by questions raised by developers of wave energy converters (WEC) utilizing wave overtopping for production of electrical power. Motivated by the fact that a number of the wave energy projects supported by the Danish Wave Energy Program utilize wave overtopping, a project was formulated to investigate overtopping with respect to optimization of the amount of potential energy obtained in the overtopping water.

Not only have the vast majority of the overtopping investigations in the literature focused on structural designs that minimize the amount of overtopping, but a number of the proposed wave energy devices utilizing overtopping are floating structures, which means that the structures are not extending all the way to the seabed, but have a limited draft. It has therefore been established that only very limited information is available in the literature on how to estimate overtopping of such structures. Furthermore, some of the proposed wave energy devices utilizing overtopping are using reservoirs at more than one level, which also raises the question of the vertical distribution of the overtopping discharge.

Using this background, physical model studies have been conducted to investigate how a wide range of different geometrical parameters influence the overtopping volume when the structure is subjected to heavily varying wave conditions. Furthermore, the study investigates how these new results fit into the results reported in the literature.

1.2 Development state of WEC's utilizing wave overtopping

Under the Danish Wave Energy Programme a number of WEC's have been suggested and tested. Among these WEC's are devices like the Wave Dragon (WD), Wave Plane, Sucking Sea Shaft, Power Pyramid (PP) and others. Furthermore, a number of devices have been proposed – and some built – internationally. All these devices have in common that they utilize wave energy by leading overtopping water to one or more reservoirs placed at a level higher than the mean water level (MWL). The potential energy obtained in the overtopping water is then converted to electrical energy by leading the water from the reservoir back to the sea via a low head turbine connected to a generator.

Below a selection of WEC's that utilize overtopping is presented. The devices are categorized in two groups, coast based and floating structures.

1.2.1 Coast based devices

Among the few WEC's that have been built and tested is the Norwegian TAP-CHAN (TAPered CHANnel). This device is equipped with the same machinery as a low-pressure hydroelectric power station with a reservoir and a Kaplan turbine. The reservoir is fed by waves trapped by a broad channel opening that reaches into the sea. Towards the reservoir, the channel is tapered and bent in such a way that the waves pile up and spill over the channel margin. In figure 1.2 the plant in Toftestallen, Norway is shown. The plant was designed for a power output of 350 kW (which was slightly exceeded during operation) and began operating in 1985. However, it is no longer in operation because of insufficient financial resources for maintenance.

Planning of a larger TAPCHAN project on the Indonesian Island of Java was also undertaken (see figure 1.2). The Java plant was designed for power production of 1.1 MW. The construction was scheduled to start in winter 1998, but due to general financial problems in the region the project has not yet been realized (www.open.ac.uk/StudentWeb/t265/update/wave.htm).
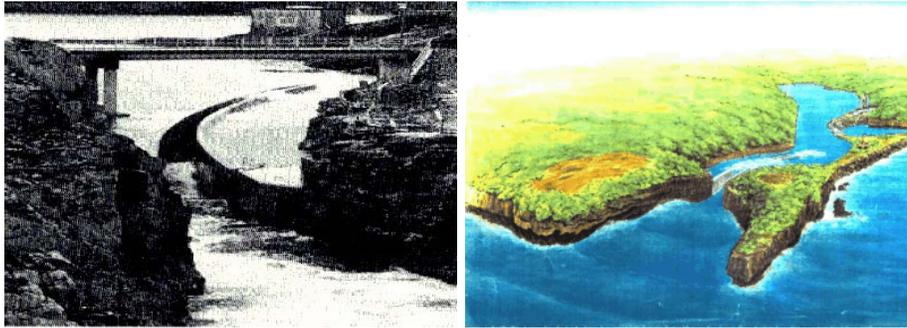
Figure 1.2: Left: Picture from TAPCHAN at Toftestallen, Norway.
Right: Artist's impression of Indonesian plant at Java.
(From www.oceanor.no/projects/wave_energy.)

Other coast or beach based structures are being planned and/or installed in Mexico and Chile.

Studies have also been performed on a variation of this coast based approach, where overtopping water is not used to produce power, but to re-circulate water in harbors (in a project called Kingston harbor pump). This approach can be useful at locations where only a small tide exists and therefore only insufficient flushing of the harbors occurs. As the coast based overtopping devices work best in areas with small tidal ranges this can be a very useful application.

1.2.2 Floating devices

The coast based devices are most applicable in coastal regions with deep water close to a rocky coast line. Therefore, for countries where the coast generally consists of gentle sloped beaches, such as Denmark, the coast based devices are not appropriate, as the waves lose the majority of their energy content through bottom friction and wave breaking before they reach the shore. Thus, a number of floating WEC's utilizing wave overtopping have been proposed. The fact that these devices are floating not only makes it possible to move them to regions with larger wave energy density, but also solves problems associated with tide and enables relatively easy control of the crest level of the slope.

Among the first devices to use this approach was the Sea Power WEC from Sweden. This device has been tested in prototype scale (see figure 1.3).

In Denmark one of the WEC's which has been most developed is the Wave Dragon (WD). The WD combines ideas from TAPCHAN and Sea Power and is

Figure 1.3: Left: Picture from sea test of Sea Power, Sweden. Right: Artist's impression of Sea Power. (From www.seapower.se.)

a floating structure equipped with wave reflectors that focus the waves towards the slope (see figure 1.4). The WD has so far undergone substantial model testing of both the hydraulic performance of the structure and the performance of the turbines. A "near-prototype" size model of the WD (1:4.5 length scale compared with a North Sea version of the device) is currently being constructed for deployment in the sheltered water of Nissum Bredning in north-western Denmark, scheduled to begin operating in early 2003.

Another Danish device, called Power Pyramid (PP), utilizes wave overtopping of more than one reservoir placed at different levels. This principle is also being applied by another Danish project called the Wave Plane and a Norwegian project called Seawave Slot-cone Generator (www.seawave-power.no).

1.3 Purpose of study

In light of the outlined state of development of the WEC's cited, the author has carried out a generic study of wave overtopping of marine structures as a Ph.D. project at Hydraulics & Coastal Engineering Laboratory, AAU. This work aims is to provide guidelines for how to calculate overtopping discharges for a wide variety of geometric layouts of overtopping slopes when subjected to a broad range of sea states and to point out overtopping slope layouts resulting in large energy content in the overtopping discharges.

The study has investigated how different geometric parameters such as profile shape, shape of guiding walls, shape of cross section, draft (especially with regard to floating structures) and crest freeboard influence the overtopping discharges,

5
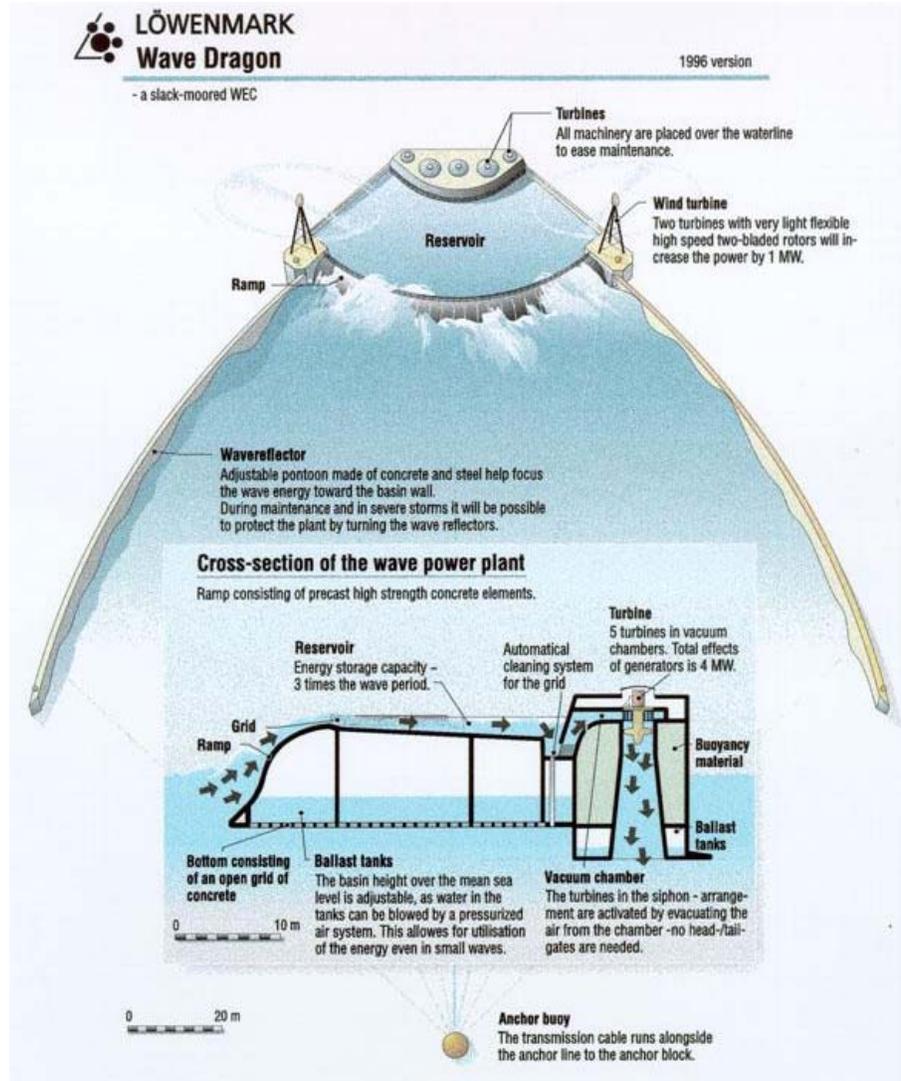
Figure 1.4: Sketch of the working principle of the Wave Dragon. (Illustration by Marstrand.)

and the emphasis is on optimizing the overtopping with respect to maximizing the potential energy in the overtopping water. This has been achieved through studies of the literature, theoretical considerations and model tests in wave tank and flume. By using the model tests, the influence of the geometric parameters has been evaluated. The variation in the overtopping discharges over time has also been evaluated, as this influences the efficiency and the demand for a reservoir of a certain WEC. Also the vertical distribution of overtopping has been investigated, and the geometrical layout of multi level reservoirs has been optimized.

It is expected that the findings of this study will be useful for the inventors and developers of WEC's of the overtopping type. In Denmark WEC's of the overtopping type, such as Wave Dragon, the Wave Plane and the Power Pyramid, will be obvious users of the results.

CHAPTER 2

State of the Art

This chapter provides a summary of the present state of knowledge concerning wave overtopping. When possible, this presentation focuses on studies where large amounts of overtopping are observed and where more generic layouts of the structure are investigated (overtopping of linear smooth slopes rather than site–specific rubble mound breakwaters).

The first section of this chapter presents an overview of the recent overtopping investigations. Later on, the effects of wave climate, wind, structure geometry and other topics relevant to the current study are presented.

2.1 Overview of recent overtopping investigations

When investigating wave overtopping of marine structures it is evident that the discharge depends not only on environmental conditions such as wave height, wave period and water level, but also on the geometrical layout and material properties of the structure. Thus, there are almost infinite possible combinations. Therefore, although a lot of investigations related to wave overtopping have been conducted, none of these cover all situations. Each of the investigations typically covers one or a few specific cases, which are then conducted by means of physical model tests in the laboratories (typically small scale models). Such investigations usually lead to an empirical relationship between the environmental conditions, geometrical layout and material properties of the structure and the overtopping discharge.

Authors	Structures	Overtopping model	Dimensionless overtopping discharge Q	Dimensionless freeboard R
Owen (1980), Owen (1982a)	Impermeable smooth, rough, straight and bermed slopes	$Q = ae^{-bR}$	$\frac{q}{gH_s T_{m0}}$ $(= \frac{q\sqrt{\frac{s_{m0}}{2\pi}}}{\sqrt{gH_s^3}})$	$\frac{R_c}{H_s}\sqrt{\frac{s_{m0}}{2\pi}}\frac{1}{\gamma}$
Bradbury and Allsop (1988)	Rock armoured impermeable slopes with crown walls	$Q = aR^{-b}$	$\frac{q}{gH_s T_{m0}}$	$(\frac{R_c}{H_s})^2\sqrt{\frac{s_{m0}}{2\pi}}$
Aminti and Franco (1988)	Rock, cube and Tetrapod double layer armor on rather impermeable slopes with crown walls (single sea state)	$Q = aR^{-b}$	$\frac{q}{gH_s T_{m0}}$	$(\frac{R_c}{H_s})^2\sqrt{\frac{s_{m0}}{2\pi}}$
Ahrens and Heimbaugh (1988b)	7 different seawall/revetment designs	$Q = ae^{-bR}$	$\frac{q}{\sqrt{gH_s^3}}$	$\frac{R_c}{(H_s^2 L_{p0})^{\frac{1}{3}}}$
Pedersen and Burcharth (1992)	Rock armored rather impermeable slopes with crown walls	$Q = aR$	$\frac{qT_{m0}}{L_{m0}^2}$	$\frac{H_s}{R_c}$
Van der Meer and Janssen (1995)	Impermeable, smooth, rough straight and bermed slopes	$Q = ae^{-bR}$	$\frac{q}{\sqrt{gH_s^3}}\sqrt{\frac{s_{p0}}{\tan\alpha}}$ for $\xi_{p0} < 2$ $\frac{q}{\sqrt{gH_s^3}}$ for $\xi_{p0} \geq 2$	$\frac{R_c}{H_s}\frac{\sqrt{s_{p0}}}{\tan\alpha}\frac{1}{\gamma}$ for $\xi_{p0} < 2$ $\frac{R_c}{H_s}\frac{1}{\gamma}$ for $\xi_{p0} \geq 2$

Table 2.1: Models for average overtopping discharge formulae, partly based on Table VI-5-7 in Burcharth and Hughes (2000).

Tables 2.1 and 2.2 present recent overtopping investigations based on model tests of various coastal structures exposed to irregular waves, along with the resulting overtopping discharge predictions formulae.

Authors	Structures	Overtopping model	Dimensionless overtopping discharge Q	Dimensionless freeboard R
Franco et al. (1995), Franco and Franco (1997)	Vertical wall breakwater with and without perforated front	$Q = ae^{-bR}$	$\dfrac{q}{\sqrt{gH_s^3}}$	$\dfrac{R_c}{H_s}\dfrac{1}{\gamma}$
Pedersen (1996)	Rock armored permeable slopes with crown walls	$Q = R$	$\dfrac{qT_{m0}}{L_{m0}^2}$	$3.2 \cdot 10^{-5}\dfrac{H_s^{\frac{5}{2}}\tan\alpha}{R_c^3 A_c B}$
Hedges and Reis (1997)	Impermeable smooth, rough, straight and bermed slopes (Data from Owen[1982a])	$Q = a(1-R)^b$ for $0 \le R < 1$ $Q = 0$ for $R \ge 1$	$\dfrac{q}{\sqrt{gRu_{max}^3}}$	$\dfrac{R_c}{Ru_{max}}$
Hebsgaard et al. (1998)	Rubble mound structures with and without super structure, armor layer of rounded stones, quarry rocks, Antifer, Accropode and Dolos units.	$Q = ae^{-bR}$	$\dfrac{q}{ln(s_{p0})\sqrt{gH_s^3}}$	$\dfrac{R_c^*}{H_s}\dfrac{1}{\gamma}$ (R_c^* dependent on slope angle and crest width)
Schüttrumpf et al. (2001)	Impermeable smooth 1:6 slope (for no freeboard ($R_c = 0$) and without overtopping ($R_c > R_{max}$))	$Q = ae^{-bR}$ (a dependent on ξ_{m0})	$\dfrac{q}{\sqrt{2gH_s^3}}$	$\dfrac{R_c}{1.5\xi_{m0}H_s}$

Table 2.2: Models for average overtopping discharge formulae, partly based on Table VI-5-7 in Burcharth and Hughes (2000), continued.

A comprehensive overview of overtopping of coastal structures in general is also available in Burcharth and Hughes (2000), where more details on some of the prediction formulae from tables 2.1 and 2.2 also can be found.

In the current study the results presented by Van der Meer and Janssen (1995) are used for comparison. The study by Van der Meer and Janssen (1995) is based on a large number of both small and large scale model tests and includes a number of tests with geometries usable in the current study (straight and impermeable slopes).

In Van der Meer and Janssen (1995) the expressions in the overtopping model depend on ξ_{p0}. However, slopes that are typically utilized in WEC's of the

overtopping type result in ξ_{p0} larger than 2. This is reasonable, since according to Van der Meer and Janssen (1995), the overtopping discharge is reduced if the slope angle α is changed so ξ_{p0} is smaller than 2 for a fixed wave situation. Thus, the overtopping model used further on in this report is

$$\frac{q}{\sqrt{gH_s^3}} = 0.2e^{-2.6\frac{R_c}{H_s}\frac{1}{\gamma_r\gamma_b\gamma_h\gamma_\beta}} \tag{2.1}$$

According to Van der Meer and Janssen (1995) this expression is valid for $\xi_{p0} \geq 2$. The coefficients γ_b, γ_h, γ_r and γ_β are introduced to take into account the influence of a berm, shallow foreshore, roughness and angle of wave attack, respectively. All these coefficients are in the range 0.5 to 1.0, meaning that when maximizing overtopping, the coefficients should be 1.0, which is the case for no berm, no shallow foreshore, smooth slope (no roughness and impermeable) and head-on waves. This will also be the case in the current study.

2.2 Effect of wave climate

The overtopping discharge is, as can be seen from tables 2.1 and 2.2, completely dependent on the wave climate as given by the significant wave height, the water level (through the crest freeboard), and also in many cases, the wave peak or mean period. However, various studies have also shown some dependency on other parameters related to the wave climate. These dependencies are considered in the following.

2.2.1 Oblique waves

Several investigations have shown that the overtopping discharge decreases when the angle of wave attack increases (0° head-on waves). The effect of oblique wave attack is included in the overtopping expressions by Van der Meer and Janssen (1995) through the reduction factor γ_β for sloping structures.

2.2.2 Directional spreading

Franco et al. (1995a) comment on the effect of directional spreading on overtopping discharge on both slopes and vertical walls. For slopes the effect of directional spreading is minimal for head-on waves but results in faster decay for increasing angle of attack compared with long crested waves. For vertical

12

wall structures the directional spreading reduces the overtopping discharge significantly even for head-on waves. The reduction in overtopping discharge for multi directional and oblique waves is also reported by Sakakiyama and Kajima (1997).

2.2.3   Spectral shape

Typically, the model tests performed in overtopping investigations utilize standard wave spectra such as TMA or JONSWAP (Hasselmann et al. [1973]). These spectra apply to offshore conditions or conditions with simple foreshores.

In order to take more complicated situations into account, Van der Meer and Janssen (1995) incorporate double-peaked spectra in their overtopping formulae by splitting the spectra into two, identifying the peak periods for each of the two parts and combining these into an equivalent peak period.

Hawkes (1999) comments on swell and bimodal seas, and states that they possibly represent the worst case (here worst case refers to most overtopping) sea states with regard to mean overtopping discharge. The prediction methods by Owen (1980) and Hedges and Reis (1998a) work well for wind sea overtopping, while Van der Meer and Janssen (1994) are realistic, but less consistent. Owen's (1980) method overpredicts swell overtopping by a factor of 5, as the predicted overtopping discharge increases indefinitely for increasing wave periods. Hedges and Reis' (1998a) and Van der Meer and Janssen's (1994) methods incorporate separate formulae for plunging waves, where overtopping is strongly dependent on wave period, and for surging waves, where it is much less dependent. According to Hawkes (1999), Hedges and Reis' (1998a) method seems the most promising.

Schüttrumpf et al. (2001) performed large scale model tests with natural spectra from field measurements which are multi peaked due to the influence of the foreshore. Schüttrumpf et al. (2001) concluded that the peak period is of no use when describing run-up and overtopping, and have proposed to use the mean period instead, as it appears in table 2.2.

2.3   Effect of wind

According to Jensen and Juhl (1987) the influence of wind is practically negligible in situations with extreme "green water" overtopping. However, for small discharges, i.e. "spray-carry-over" conditions, wind velocity is an important factor. Besley (1999) states that there is an increase in discharges due to wind for mean overtopping discharge larger than 10^{-3} $m^3/s/m$.

13

Based on model tests, Ward et al. (1997) state that wind effects are more pronounced on steeper slopes. However, as it is not practically achievable to satisfy both Froude (gravity waves) and Reynolds (friction effect from wind) scaling laws in a single model (it would require a centrifuge in order to scale gravity or the use of a "super fluid" to change viscous effects in the model), the wind effects found in the study are not scalable.

Wind effects were also found by J. A. Gonzales-Escriva and De Rouck (2002) for strong wind speeds. Based on model tests, J. A. Gonzales-Escriva and De Rouck (2002) found that overtopping at logarithmic scale is proportional to the square of the wind.

2.4 Effect of structure geometry

The overtopping discharge is, as seen from tables 2.1 and 2.2, also dependent on the structure geometry. The most important parameter is the crest freeboard. However, a number of other parameters describing the structure geometry also influence the overtopping discharge. These parameters are considered in the following.

2.4.1 Surface roughness and permeability

Obviously, introducing surface roughness and permeability of the slope will reduce the overtopping discharges compared with an impermeable and smooth slope. Both Van der Meer and Janssen (1995) and Owen (1980) have given reduction factors to take this into account.

2.4.2 Crest width

Both Juhl and Sloth (1995) and Hebsgaard et al. (1998) have incorporated the effect of the width of the crest on the overtopping discharge by modifying the used crest level in the expression for the overtopping discharge, depending on the crest width. As would be expected, an increasing crest width results in decreasing overtopping discharges.

2.4.3 Slope angle and shape

The dependency of the slope angle is typically included in the prediction formulae via ξ_{p0}, e.g., in Van der Meer and Janssen (1995). However, according to Van der Meer and Janssen (1995) the dependency of ξ_{p0} disappears for surging waves.

Other authors have made various statements regarding the influence of slope angle and shape that are relevant to the present study.

Le Méhauté et al. (1968) also quote Grantham (1953) who stated that maximum run-up occurs for a given incident wave for slope angle $\alpha = 30°$.

In TACPAI (1974) there is a statement that a convex slope increases run-up.

Josefson (1978) performed a study of a WEC utilizing overtopping. In this study a number of model tests were carried out using regular waves. From the results of the tests the following was concluded:

- For maximization of obtained power, overtopping times crest freeboard (maximum efficiency), the slope angle increases with an increase in wave steepness.

- Introduction of concave edge on upper part of slope results in a reduction in efficiency.

- Introduction of converging walls on slope results in a reduction in efficiency.

- A combination of the two modifications results in a slight increase in efficiency.

According to CIRIA/CUR (1991) the slope angle becomes less important as crest heights are lower and larger overtopping discharges occur.

Kofoed and Nielsen (1997) investigated overtopping in connection with an evaluation of the WEC WD. In this investigation the overtopping slope had a limited draft ($d_r/d = 0.3$) as the WD is a floating structure. Tests were performed with different slope angles α (linear slopes, $\alpha = 35°$, $40°$, $45°$ and $50°$) and it was found that the optimal slope angle is around $40°$. However, for slope angles between $35°$ and $50°$ no significant variation in overtopping discharges was found. The results of the tests with $\alpha = 40°$ were fitted to an overtopping model like the one used by Van der Meer and Janssen (1995) for $\xi_{p0} \geq 2$ (see table 2.1). This resulted in coefficients a and b that differed from the coefficients given by Van der Meer and Janssen (1995) and also were dependent of the peak period T_p. These differences were due the tests having been performed with a limited draft, which was not the case for Van der Meer and Janssen (1995).

15

Furthermore, a limited number of variations on the slope geometry were tested by Kofoed and Nielsen (1997), but it was concluded that none of the tested slope geometries were superior to a linear slope in terms of maximizing the overtopping discharges.

2.4.4   Low crest level

Oumeraci et al. (1999) investigated overtopping of dikes with very low crest freeboards (R_c down to zero) caused by high water levels. Their results agreed well with those of Van der Meer and Janssen (1995) for relative crest freeboards in the range tested by Van der Meer and Janssen (1995). However, for relative crest freeboards R ($R = \frac{R_c}{H_s}$) close to zero the tests by Oumeraci et al. (1999) show that the expression given by Van der Meer and Janssen (1995) (eq. 2.1) overpredicts the average overtopping discharge. These data are also used by Schüttrumpf et al. (2001) to establish the overtopping expressions for no freeboard condition, as referred to in table 2.2.

2.4.5   Multiple crest levels

Kofoed and Frigaard (2000a) carried out some preliminary investigations into a wave energy device utilizing wave overtopping by leading the overtopping water to reservoirs at different levels in order to capture the water at the level reached and thereby achieve higher efficiency. The results of this investigation showed that the use of three reservoirs at different levels instead of one resulted in 38 - 53 % more potential energy in the overtopping water.

2.5   Effect of floating structure

Martinelli and Frigaard (1999b) performed laboratory tests with a floating model of the WD. These tests indicated that the overtopping discharge was reduced by up to 50 % because of the movement, compared with tests using a fixed model. However, the reduction of the overtopping discharge due to a floating structure is highly dependent on the structure itself. The tests showed that movement should be minimized in order to make the reduction as small as possible.

From model tests with a model of the WEC PP, Kofoed (2002) found almost no difference in overtopping discharge when comparing with results from tests performed with a fixed model. These results are also presented in section 4.9.

2.6 Overtopping discharge levels

Under random wave attack, overtopping discharges vary with up to several orders of magnitude from one wave to another, meaning that wave overtopping is a very non-linear function of wave height and wave period. This time variation is difficult to measure and quantify in the laboratory and hence overtopping discharges are most often given in terms of average discharge.

To assess admissible overtopping discharges for different objects, several researchers have studied the impact of overtopping water volumes on different obstacles placed on top of an overtopped structure. Goda (1971), ?) and Goda (1985) developed the guidelines given in figure 2.1 based on prototype investigations consisting of wave climate measurements and expert impressions of the impact of overtopping volumes on different objects situated on top of breakwaters. These guidelines have been adopted by the Japanese code of practice and by the Dutch/English *"Manual on the use of Rock in Hydraulic Engineering"* (CIRIA/CUR [1991]) on which the illustration in figure 2.1 is based.

When designing sea defense structures the controlling hydraulic response is often the wave overtopping discharge. In figure 2.1 critical overtopping discharges are shown for typical structure types when considering sea defense structures. In the figure the discharge levels of overtopping typical for wave energy devices are also indicated.

As is obvious from the figure, the overtopping discharges considered when utilizing the overtopping for energy production are far from the range desired for sea defense structures. Thus, the focus of overtopping investigations carried out for sea defense structures typically is on smaller overtopping discharges than what would be of interest for WEC's of the wave overtopping type.

2.7 Horizontal distribution of overtopping

Jensen and Juhl (1987) presented an expression describing the horizontal distribution of overtopping in the form $q(x) = q_0 10^{\frac{x}{\beta}}$ where q is the intensity at a distance x, q_0 is the intensity for $x = 0$ and β is a constant and equal to the distance for which the overtopping intensity decreases by a factor of 10.

In model tests performed by Lab. (2000) the general spatial distribution of the overtopping discharge was measured in four areas behind the crest. Each area had a length (in the direction perpendicular to the structure) similar to the crest freeboard. In the first area the overtopping discharge was 80 % of the total. For the next three areas the overtopping discharge were 16, 3 and 1 % of the total, respectively.

17
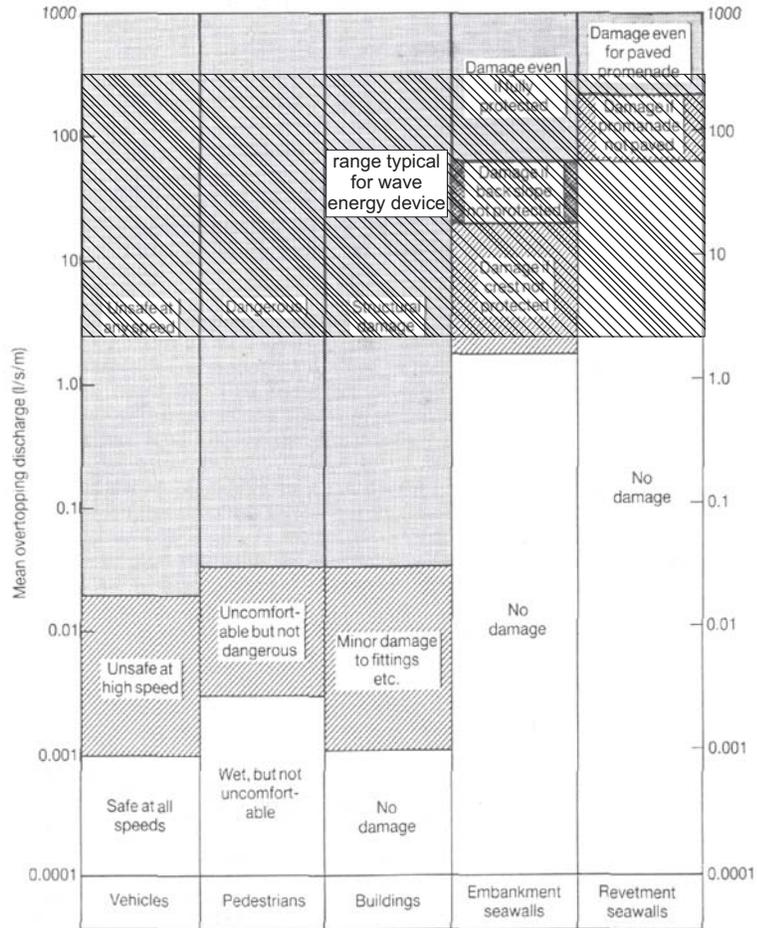
Figure 2.1: *Criteria for critical overtopping discharges (from CIRIA/CUR [1991]). A typical range of overtopping discharge for a WEC based on the wave overtopping principle has been added to the figure.*

2.8 Distribution of overtopping from individual waves and variation in time

Van der Meer and Janssen (1995) present an expression for the probability of overtopping as well as the probability of a certain overtopping volume in a wave, given that overtopping occurs. This expression has been used by Martinelli and Frigaard (1999a) for simulating the variation in time of overtopping discharge of a WEC, which is also described in section 3.8. Here the simulation procedure is also verified experimentally (also presented in Kofoed and Burcharth [2000]). Also Franco et al. (1995a), Besley (1999) and Jensen and Juhl (1987) present a similar expression for the distribution of wave overtopping discharge of individual waves.

2.9 Theoretical and numerical calculations

Kikkawa et al. (1968) presented an overtopping expression based on a weir analogy. The expression was verified by model tests with regular waves. Based on this model Oezhan and Yalciner (1991) introduced an analytic model for solitary wave overtopping of a sea dike.

Another method based on wave energy considerations is used by Umeyama (1993) to formulate the wave overtopping discharge on a vertical barrier, and the model is compared with model tests.

The recent years many attempts have been made to numerically model wave overtopping.

Kobayashi and Wurjanto (1989) performed numerical modeling of regular wave overtopping of impermeable coastal structure on sloping beach.

Hiraishi and Maruyama (1998) presented a numerical model for calculation of overtopping discharges for a vertical breakwater in multi directional waves. The basic assumption is that the overtopping discharge can be described by a weir expression as suggested by Kikkawa et al. (1968).

Hu et al. (2000) presented a 2-D numerical model for calculation of overtopping using non-linear shallow water equations. However, even this very recent study was primarily validated using regular waves.

It seems that even with the data power available today, the task of numerical modeling of wave overtopping processes is still too demanding. However, once the computational power is sufficient, methods like the ones mentioned above,

as well as other methods, based on, e.g., Volume of Fluids, probably will be able to predict overtopping discharges also in irregular and 3-D waves. This will likely make it possible to study the overtopping process in greater detail than is possible in physical model tests. Again, this will make it easier to design structures that better fulfil their purpose than do the structures of today.

2.10 Scale effects on overtopping

Scale effects in overtopping tests are considered by Weggel (1976). His conclusions indicate that mainly the run-up is influenced by scale effects, which means that if the run-up is corrected for scale effects, if any, the calculated overtopping discharges will be correct. Generally, scale effects are only significant for thin layers of run-up/overtopping, i.e., for run-up levels smaller than or close to the crest level, and thus for small overtopping discharges.

Grüne (1982) reports field measurements of run-up on two dikes. Here it emerges that the run-up is generally larger than commonly used formulae. The same tendency is found by B. Van de Walle and Frigaard (2002) from full scale measurements on the Zeebrugge breakwater in Belgium. B. Van de Walle and Frigaard (2002) compare full scale run-up measurements with measurements from small scale model tests performed with wave conditions reproducing the full scale conditions.

2.11 Accuracy of overtopping discharge predictions

Douglass (1986) reviewed and compared a number of methods for estimating irregular wave overtopping discharges. He concludes that calculated overtopping discharges, using empirically derived equations, should only be considered within a factor of 3 of the actual overtopping discharge. The methods considered deal with overtopping of coastal defense structures, and so the typical crest freeboards are relatively high and the overtopping discharges low. Under such conditions the overtopping discharge depends on relatively few and relatively large overtopping events, which again means that the overtopping discharge becomes very sensitive to the stochastic nature of irregular waves. It must be expected that the uncertainty of the overtopping discharge estimation must be expected to be reduced as the crest freeboard is reduced, since more and more of the waves overtops the structure.

2.12 Scope of the thesis

In chapter 1 an introduction to the thesis as well as a statement of its purpose was provided. The current chapter gives an overview of the state of the art of the main thesis topic, namely wave overtopping of marine structures. As indicated in this chapter a number of subjects within the main topic need further investigation in order to enable reliable estimation of the overtopping discharge, and thereby also the energy output, of WEC's based on the wave overtopping principle. The remaining part of the thesis provides results of investigations covering a few of these subjects.

Chapter 3 deals with overtopping of a single level reservoir. Model tests have been carried out in order to provide information of the dependency on the overtopping discharge on varying slope angle, crest freeboard and draft for a linear slope. Furthermore, modifications of slope profile and side walls of the slope are tested in the search for a slope geometry which could enhance the overtopping and thereby increasing in captured energy. The results of the model tests conducted are incorporated into the overtopping expression given by Van der Meer and Janssen (1995) by application of correction factors. Finally, the time dependency of the overtopping discharge is evaluated and compared with an empirical prediction model.

Chapter 4 deals with overtopping of multiple level reservoirs. Initially, model tests using eight reservoir levels are conducted in order to provide information about the vertical distribution of the overtopping discharge. Based on these tests, an expression describing the vertical distribution is presented. This expression is used in a numerical optimization of number and vertical placement of reservoirs, and the results are then presented. Furthermore, the results of model tests with a smaller number of levels are presented. Here, the dependency of the overtopping discharge on horizontal placement and the geometry of the reservoir fronts is investigated. Finally, the results of tests using a floating model with multiple level reservoirs are presented.

Chapter 5 concludes the thesis.

CHAPTER 3

Overtopping of Single Level Reservoir

In this chapter the conditions for model tests performed with overtopping of a single level reservoir are described. First, the purpose of the tests is explained, followed by an account of the sea states used and the geometric parameters investigated. The model test setup is presented, and the results are presented and compared with data from the literature. The results are incorporated into existing an overtopping expression by applying correction factors. Finally, the time variation of the overtopping discharge is evaluated and compared with an empirical expression.

3.1   Purpose of model study

The influence of the overtopping discharge and the obtained potential energy of the following geometrical parameters are investigated during the model tests (see figure 3.1):

- Slope angle.
- Crest freeboard.
- Draft.
- Slope shape.
- Shape of guiding walls.
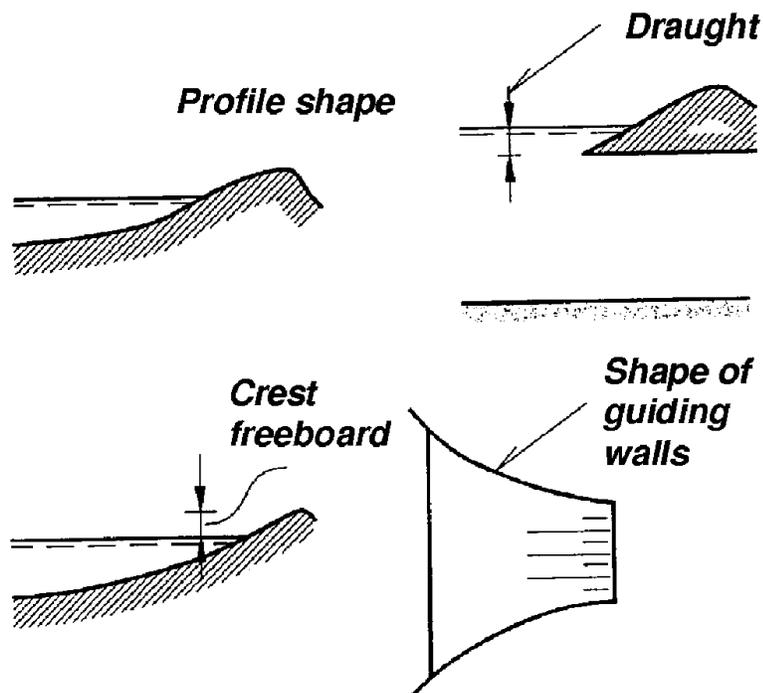
Figure 3.1: Investigated geometric parameters.

All model tests are performed in a wave basin and the modeled structures are subjected to irregular 2-D waves. The model tests are performed using fixed structures and a constant water depth of 0.5 m. Although the models used in the tests do not represent any specific prototype structures, a length scale of 1:50 seems appropriate. This results in a prototype water depth of 25 m.

The amount of overtopping of the structure depends on wave parameters such as:

- Wave type, regular/irregular.

- Wave height.

- Wave period.

- Spectral shape.

- Wave groupiness.

- Angle of wave attack.

- Directional spreading.

Furthermore, overtopping depends on the geometric parameters defining the structure (as mentioned above) and also on surface roughness and permeability of the structure. This model study focuses on the influence of the geometry rather than covering a large number of different wave parameters. Thus, such parameters as spectral shape, wave groupiness, angle of wave attack and directional spreading are not tested, and only wave situations consisting of irregular 2-D waves typical of the North Sea west of Denmark are used.

It is commonly accepted that the introduction of surface roughness and permeability decreases the amount of overtopping, and therefore only smooth and non-permeable structures are tested in this study. As the point of departure, tests are performed with a linear profile. For this type of structure the influence of the slope angle, the crest freeboard and the draft on the overtopping discharge is investigated and compared with existing expressions from the literature. The motivation for testing slope geometries with limited draft is that a number of the suggested overtopping based WEC's are floating, and it is thus important to know how large a draft it is feasible to use for this type of structure. For hereby-found suitable values (in terms of obtained amount of potential energy in the overtopping water volume) of crest freeboard, angle of slope and draft, tests are performed with structures modified as follows:

- Slope with horizontal plate added at the slope bottom.

- Slope with convex upper part.

- Slope with concave upper part.

- Converging leading walls (linear).

- Converging leading walls (curved).

Knowledge of the influence of a range of geometrical parameters on the overtopping discharge is obtained from the conducted tests. The range of geometrical parameters considered here is larger than that considered for structures normally used in coastal engineering.

3.2   Sea states used in model tests

Irregular 2-D waves have been used in all the model tests conducted. The irregular waves are generated using the parameterized JONSWAP-spectrum (Hasselmann et al. [1973]):

$$S_\eta(f) \quad = \quad \frac{1.4}{\gamma}\frac{5}{16}H_s^2 f_p^4 f^{-5}\gamma^\delta(-\frac{5}{4}(\frac{f_p}{f})^4) \tag{3.1}$$

$$\delta \quad = \quad e^{(-\frac{(f-f_p)^2}{2\sigma_f^2 f_p^2})} \tag{3.2}$$

where

$$\sigma_f \quad = 0.10 \text{ for } f \le f_p$$
$$\sigma_f \quad = 0.50 \text{ for } f > f_p$$

The spectral enhancement factor γ has been set to 3.3, corresponding to the Danish part of the North Sea.

All of the tested slope geometries have been subjected to a wide range of wave conditions – in total 37 sea states for each of the tested geometries. The sea states have been selected so that the great majority of sea states that occurs over time in the Danish area of the North Sea are covered. The focus is on the sea states that occur often, and less on extreme sea states that command the attention of researchers dealing with coastal defense structures such as breakwaters or dikes.

The selected sea states are presented in table 3.1, where the significant wave height H_s and the wave peak period T_p are provided along with the resulting peak wave steepness s_p and surf similarity parameter (Iribarren number) ξ_{p0}, depending on the slope.

T_p [s]		H_s [m]								
		0.5	1.0	2.0	3.0	4.0	5.0	6.0	7.0	8.0
4	s_p [%]	**2.0**	**4.0**	**6.0**						
	ξ_{p0}, $\alpha = 20°$	2.6	1.8	1.3						
	ξ_{p0}, $\alpha = 30°$	4.1	2.9	2.0						
	ξ_{p0}, $\alpha = 40°$	5.9	4.2	3.0						
	ξ_{p0}, $\alpha = 50°$	8.4	6.0	4.2						
	ξ_{p0}, $\alpha = 60°$	12.2	8.7	6.1						
6	s_p [%]	**0.9**	**1.8**	**3.6**	**5.4**	**7.2**	**8.9**			
	ξ_{p0}, $\alpha = 20°$	3.9	2.7	1.9	1.6	1.4	1.2			
	ξ_{p0}, $\alpha = 30°$	6.1	4.3	3.1	2.5	2.2	1.9			
	ξ_{p0}, $\alpha = 40°$	8.9	6.3	4.5	3.6	3.1	2.8			
	ξ_{p0}, $\alpha = 50°$	12.6	8.9	6.3	5.2	4.5	4.0			
	ξ_{p0}, $\alpha = 60°$	18.4	13.0	9.2	7.5	6.5	5.8			
8	s_p [%]		**1.1**	**2.1**	**3.2**	**4.3**	**5.4**	**6.4**	**7.5**	**8.6**
	ξ_{p0}, $\alpha = 20°$		3.6	2.6	2.1	1.8	1.6	1.5	1.4	1.3
	ξ_{p0}, $\alpha = 30°$		5.8	4.1	3.3	2.9	2.6	2.4	2.2	2.0
	ξ_{p0}, $\alpha = 40°$		8.4	5.9	4.8	4.2	3.8	3.4	3.2	3.0
	ξ_{p0}, $\alpha = 50°$		11.9	8.4	6.9	6.0	5.3	4.9	4.5	4.2
	ξ_{p0}, $\alpha = 60°$		17.3	12.2	10.0	8.7	7.7	7.1	6.5	6.1
10	s_p [%]			**1.5**	**2.3**	**3.1**	**3.8**	**4.6**	**5.4**	**6.1**
	ξ_{p0}, $\alpha = 20°$			3.2	2.6	2.3	2.0	1.9	1.7	1.6
	ξ_{p0}, $\alpha = 30°$			5.1	4.2	3.6	3.2	2.9	2.7	2.6
	ξ_{p0}, $\alpha = 40°$			7.4	6.1	5.2	4.7	4.3	4.0	3.7
	ξ_{p0}, $\alpha = 50°$			10.5	8.6	7.4	6.7	6.1	5.6	5.3
	ξ_{p0}, $\alpha = 60°$			15.3	12.5	10.8	9.7	8.8	8.2	7.7
12	s_p [%]			**1.2**	**1.8**	**2.4**	**3.0**	**3.6**	**4.2**	**4.8**
	ξ_{p0}, $\alpha = 20°$			3.9	3.2	2.7	2.4	2.2	2.1	1.9
	ξ_{p0}, $\alpha = 30°$			6.1	5.0	4.3	3.9	3.5	3.3	3.1
	ξ_{p0}, $\alpha = 40°$			8.9	7.3	6.3	5.6	5.1	4.8	4.5
	ξ_{p0}, $\alpha = 50°$			12.6	10.3	8.9	8.0	7.3	6.8	6.3
	ξ_{p0}, $\alpha = 60°$			18.4	15.0	13.0	11.6	10.6	9.8	9.2
14	s_p [%]				**1.5**	**2.0**	**2.5**	**3.0**	**3.5**	**4.0**
	ξ_{p0}, $\alpha = 20°$				3.7	3.2	2.8	2.6	2.4	2.3
	ξ_{p0}, $\alpha = 30°$				5.8	5.1	4.5	4.1	3.8	3.6
	ξ_{p0}, $\alpha = 40°$				8.5	7.3	6.6	6.0	5.6	5.2
	ξ_{p0}, $\alpha = 50°$				12.0	10.4	9.3	8.5	7.9	7.4
	ξ_{p0}, $\alpha = 60°$				17.5	15.2	13.6	12.4	11.5	10.7

Table 3.1: Sea states used in the model tests.

The duration of each of the sea states has been 30 minutes in model scale, corresponding to approx. 3.5 hours in full scale – or 1,100 to 3,600 waves, depending on the peak period. This means that each of the tested slope geometries has been subjected to about 70,000 waves.

3.3 Geometric parameters investigated

The geometries have been placed in three categories. First, a number of linear slopes have been tested. Second, tests with a number of modifications to the slope profile were carried out and, finally, modifications to the side walls of the slope were applied.

3.3.1 Linear slopes

The tests with linear slopes have been performed with the slope geometries given in table 3.2.
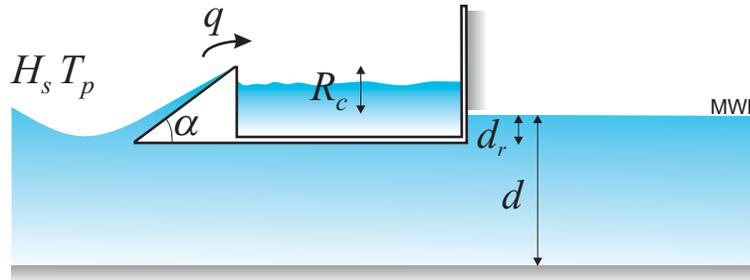
Figure 3.2: Geometric parameters used for linear slopes.

Geometry	α [°]	$\frac{R_c}{d}$ [-]	$\frac{d_r}{d}$ [-]
AA01	**20** (1:2.8)	0.16	0.32
AA02	**30** (1:1.7)	0.16	0.32
AA03	**40** (1:1.2)	0.16	0.32
AA04	**50** (1:0.8)	0.16	0.32
AA05	**60** (1:0.6)	0.16	0.32
AB01	40 (1:1.2)	**0.04**	0.32
AB02	40 (1:1.2)	**0.10**	0.32
AB03	40 (1:1.2)	**0.22**	0.32
AB04	40 (1:1.2)	**0.30**	0.32
AC01	40 (1:1.2)	0.16	**0.20**
AC02	40 (1:1.2)	0.16	**0.50**
AC03	40 (1:1.2)	0.16	**0.72**
AC04	40 (1:1.2)	0.16	**1.00**

Table 3.2: Geometric parameters describing the model setup in the tests with a linear slope.

These geometries have been selected so the influence of slope angle α, crest freeboard R_c and draft d_r can be evaluated.

In the tests where the influence of the slope angle is investigated, the crest freeboard and draft have been fixed to values that are considered reasonable for a slope in a WEC of the overtopping type – and likewise for the tests where the influences of crest freeboard and draft, respectively, are investigated. In particular, the choice of $\alpha = 40°$ for tests with varying crest freeboard and draft is based on results from Kofoed and Nielsen (1997).

3.3.2 Modifications of the slope profile

The tests with modifications of the slope profile have been done with the slope geometries shown in table 3.3.

In the modifications of the slope profile a linear slope with specifications given for geometry BA04 (table 3.3) is used as reference. The choice of this linear slope layout as a reference is based on the results of the tests with the linear slope layouts shown in table 3.2, which indicated that a slope angle $\alpha = 30°$ is optimal (see section 3.5.1). Furthermore, for all these geometries $\frac{d_r}{d}$ is set to 0.4 and $\frac{R_c}{d}$ is set to 0.1, which is also based on the results shown in section 3.5.1

Figure 3.3: Geometrical parameters used for modified slopes.

A series of tests with a horizontal plate added at the draft of the slope (geometries BA01 to BA03) have been carried out to investigate whether the overtopping discharge can be increased by trying to prevent excess pressure at the draft of the slope from "escaping" under the slope. The layouts of these slopes are shown in figure B.15 to B.19 in appendix B.2.2.

A series of tests with a convex deflection of the top of the slope (geometries CA01 to CC01) have been motivated by some of the results of the studies referred to in chapter 2. Furthermore, the idea of deflecting the slope at the top, in order

Geometry	Description	α [°]	$\frac{h_{hp}}{d_r}$ [-]	$\frac{r_{rc}}{d_r}$ [-]	c_{rc} [°]
BA01	Horizontal plate	30	0.500		
BA02	Horizontal plate	30	0.250		
BA03	Horizontal plate	30	0.125		
BA04	Reference setup	30			
CA01	Convex slope	30		1.875	28
CA02	Convex slope	30		3.755	28
CA03	Convex slope	30		5.630	28
CB01	Convex slope, diff. angle	35		2.795	31
CC01	Convex slope, elliptic	45			
DA01	Concave slope	30		1.365	30

Table 3.3: Geometrical parameters describing the model setup in tests of modifications of the slope profile. For all these geometries $\frac{d_r}{d} = 0.4$ and $\frac{R_c}{d} = 0.1$.

to extract as much of the kinetic energy as possible, seems reasonable as up-rush velocity is lower near the crest than near the MWL. The layouts of these slopes are shown in figure B.21 to B.29 in appendix B.2.3. Slope geometry CC01 is a layout suggested by the inventor of the WEC WD, Erik Friis-Madsen, Löwenmark.

A concave deflection of the top of the slope (geometry DA01) has also been tested. The layout of this slope is shown in figure B.31 in appendix B.2.4.

3.3.3 Modifications of the side walls of the slope

A series of tests with modifications of the side walls of the slope have been conducted with the slope geometries shown in table 3.4.

Geometry	Description	$\frac{w_c}{w_{d_r}}$ [-]	$\frac{r_l}{d_r}$ [-]
EA01	Linear converging walls	0.848	
EA02	Linear converging walls	0.696	
EA03	Linear converging walls	0.536	
EA04	Linear converging walls	0.368	
FA02	Curved converging walls	0.696	0.475

Table 3.4: Geometrical parameters describing the model setup in tests of modifications of the side walls of the slope.

In the series of tests with modifications of the side walls, the linear slope denoted geometry BA04 in table 3.3 is again used as reference.

The series of tests with linear converging walls (geometries EA01 to EA04) have been carried out to investigate whether the overtopping discharge can be improved by "compressing" the overtopping water as it comes up the slope in order to force it higher than it would go without the converging walls. The layouts of these guiding walls are shown in figure B.33 in appendix B.3.1. In the tests with curved converging walls (geometry FA02) the idea is the same as for the linear converging walls. The layout of the guiding walls is shown in figure B.38 in appendix B.3.2.

3.4 Model test setup

The model tests have been carried out in the deep water 3-D wave tank at the Hydraulics & Coastal Engineering Laboratory, AAU, using a length scale of 1:50. This wave tank is 8.5 x 15.7 m and is equipped with a 3-D wavemaker with 10 segments of the piston type. In the current setup a 0.5 m wide flume was built in the wave tank, as shown in figure 3.4 and in the photos in figure 3.5. Conducting the model tests in the wave tank and the purpose-built flume has some advantages over conducting the model tests in a regular wave flume. Because the majority of the tested geometries have limited draft, the reservoir where the overtopping water is collected had to be placed to the side of the tested model. The model and the reservoir takes up quite a lot of space and is therefore easier to fit into the wave tank than into a regular flume. Furthermore, in the wave tank there is plenty of space for passive wave absorption (gravel beaches are used) and the risk of re-reflection of waves reflected from the tested structure is minimal, as these waves diffract when they exit the flume and are absorbed by the gravel beaches. This means that even though no active wave absorption system is applied, there is very good control of the waves to which the tested models are exposed.

In the model test setup, two measuring systems have been deployed – a wave measuring system and an overtopping measuring system.

3.4.1 Wave measurements

The wave measuring system consist of two arrays of wave gauges – one in front of the tested structure and one behind it. Each of the arrays consists of four wave gauges of the resistance type placed on the center line of the flume. The gauges are placed at a distance of 0.15 m between 1. and 2. gauge, 0.25 m between 2. and 3. gauges, and 0.60 m between 3. and 4. gauge.

31
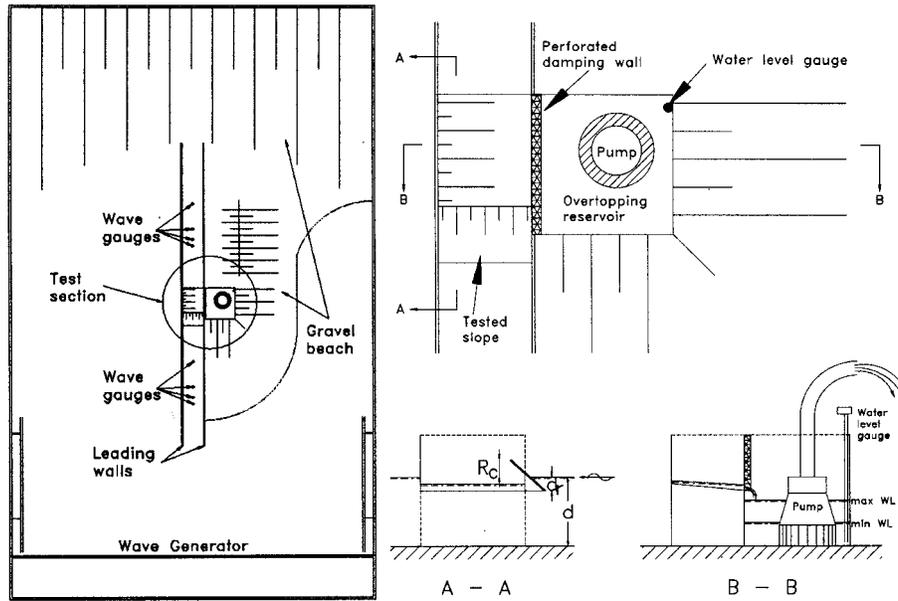
Figure 3.4: Sketch of the model test setup.

Placing four gauges at the chosen distances enables the use of the SIRW method developed by Frigaard and Brorsen (1995) for separation of incident and reflected irregular waves. The SIRW method has advantages compared with other separation methods in that it enables a separation of incident and reflected waves in the time domain. In order to achieve a good output from the SIRW method, wave records from two wave gauges with a distance in the range of 5 to 45 % of the recorded wave length are needed. Thus, by deploying four wave gauges with different distances it is possible, for each of the 37 wave situations, to use a suitable pair of wave gauges for the SIRW analysis. (By combining the wave gauges within an array the following distances are available: 0.15, 0.25, 0.40, 0.60, 0.85 and 1.00 m. These distances cover the tested wave situations.)

The incident wave time series calculated using the SIRW method is then applied to further wave analysis. For all the conducted model tests, both time and frequency domain analyses of the incident wave in front of the tested structure are conducted. In the time domain analysis the statistical distribution of the wave heights is found by zero down crossing and parameters, as significant wave height H_s, are calculated on this basis. In the frequency domain analysis the wave spectrum is found as well as parameters like the wave peak period T_p and the spectral estimate of the significant wave height H_{m0}.

32
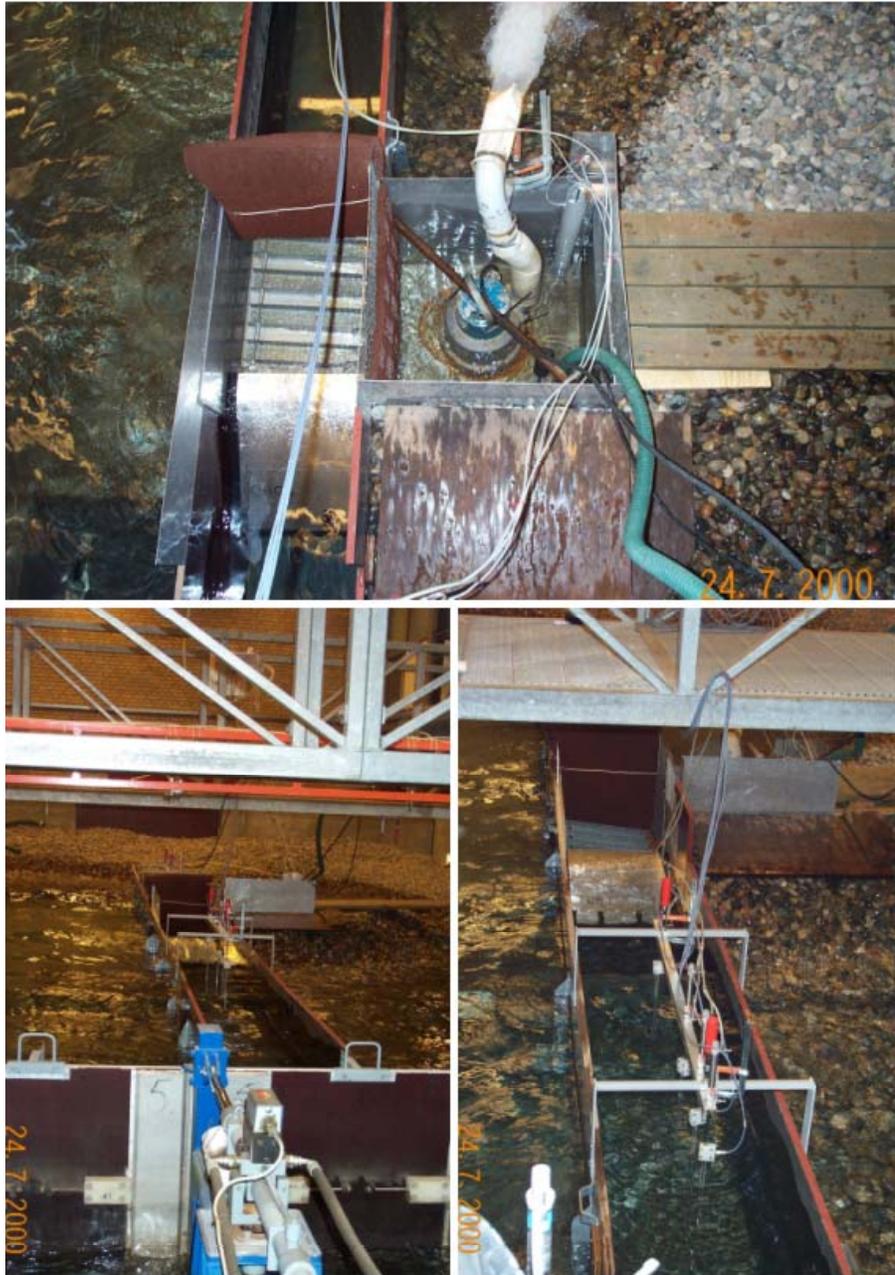
Figure 3.5: Photos from the model test setup.

In further analysis of the overtopping, the spectral estimate of the significant wave height H_{m0}, found from the frequency domain analysis, is used rather than the H_s.

3.4.2   Overtopping measurements

In the model tests conducted, the range of the overtopping discharge has been very wide due to the large number of wave conditions and geometries tested. Therefore, the design of the overtopping measuring system is a compromise between being able to measure very large and very small amounts of overtopping.

The chosen measuring system is shown in figure 3.4. The system consists of a reservoir, a pump and a water level gauge. The reservoir is placed beside the overtopping slope in order to allow free passage under the slope, as in most cases it is not extending to the bottom. Between the slope and the reservoir there is a perforated damping wall to decrease the amount of disturbance on the water surface in the reservoir, as this causes noise in the water level measurements and thereby also on the overtopping discharge time series. The water level gauge and the pump are connected to a PC that monitors and records the water level in reservoir. Once a preset maximum water level is reached, the pump is activated for a fixed time period (3 s in the used setup, model scale) and the pumped volume of water is then derived from a calibration of the pump (approx. 100 l in the used setup, model scale).

Based on the measured water level in the reservoir, the overtopping volume, and thereby also the discharge, during a test can be found. Furthermore, as the water level in the reservoir is measured continuously, the overtopping discharge time series during each test can be calculated by differentiation (see figure 3.6). When performing the differentiation, the signal from the water level gauge is corrected by adding a section of the water level time series measured during the calibration of the pump at the time where the pump is emptying the reservoir. This is done in order to calculate the overtopping discharge time series. In order to compensate for the disturbances created by the pumping the piece of time series is 12 s long (model scale). A continuous overtopping discharge time series is thus obtained. Though, in spite all efforts it has not been possible to make a perfect correction, which means that the time series of the overtopping discharge is not completely correct at the time of pumping. This can also be seen from figure 3.6. It appears that the overtopping discharge is sometimes negative. Of course, negative discharge cannot occur, but this effect results from the problems at the time of pumping (the large negative peaks) and the fact that disturbances in the water level measurements occur due to small waves in the reservoir. However, if the average overtopping discharge is calculated even for very small time frames (down to the order of 10 s, model scale) these will be
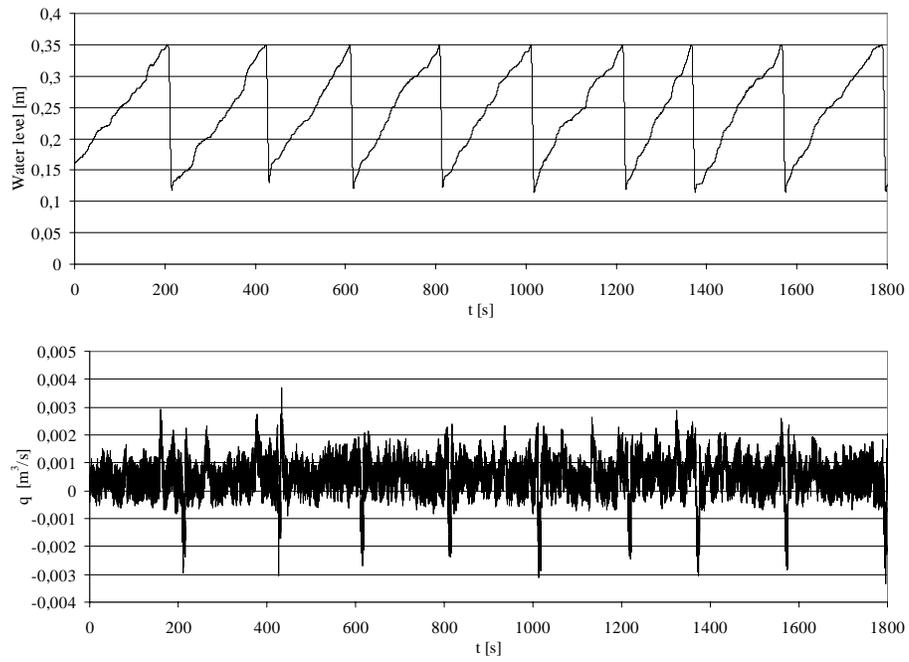
Figure 3.6: An example of a measured water level time series measured in the reservoir (top) and the corresponding time series of the derived overtopping discharge.

correct also if pumping occurs within the time frame. Another reason for not using time frame sizes smaller than those in the order of 10 waves is that the measured water level in the reservoir is delayed and smoothed by the distance from the slope and the reservoir, and the perforated damping wall.

The majority of the analyses conducted concern average overtopping discharges. In these analyses the average overtopping discharges q are typically made dimensionless by division by the factor $\sqrt{gH_{m0}^3}$. The dimensionless average overtopping discharge is named Q, and also a dimensionless crest freeboard R is defined as $R = \frac{R_c}{H_{m0}}$ (in both cases H_{m0} is calculated for the incident waves). Thus the parameters are made dimensionless as specified by Van der Meer and Janssen (1995), except H_{m0} is used as the significant wave height H_s.

3.5 Results of model tests with linear slopes

The following sections present the results of the model tests conducted.

In appendix B the results of each of the tests conducted are given in terms of average overtopping discharges. In the figures in the appendix, the dimensionless average overtopping discharge Q (defined as $Q = \frac{q}{\sqrt{gH_{m0}^3}}$) is plotted as a function of the dimensionless crest freeboard R (defined as R_c/H_{m0}) for each of the tested geometries. The following analyses are based on these results.

In this section the results of the model tests with linear slopes are presented and analyzed. In appendix B.1 the basic results are shown in figures B.1 to B.13.

3.5.1 Varying slope angle

The test series with varying slope angle α shows that the average overtopping discharge is slightly dependent an α, cf. figure 3.7.

A correction factor λ_α is introduced to take this dependency on the slope angle into account. By fitting a number of expressions emerges that eq. 3.3 describes the dependency well. In figure 3.8 the effect of introducing λ_α is shown. It can be seen that the R^2 (square of the Pearson product moment correlation coefficient) is thereby increased from 0.84 to 0.89.

The expression for the correction factor λ_α is

$$\lambda_\alpha = \cos^\beta(\alpha - \alpha_m) \tag{3.3}$$
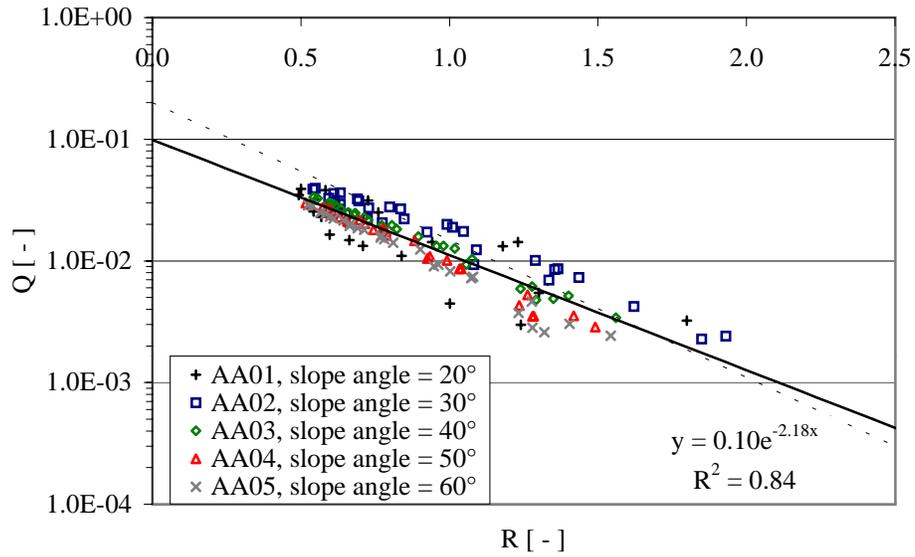
Figure 3.7: Results of tests with test geometries with varying α (test series AA). The dimensionless average overtopping discharge Q is plotted as a function of the dimensionless crest freeboard R. The dotted line represents eq. 2.1 and the solid line is an exponential fit with all the data points shown.
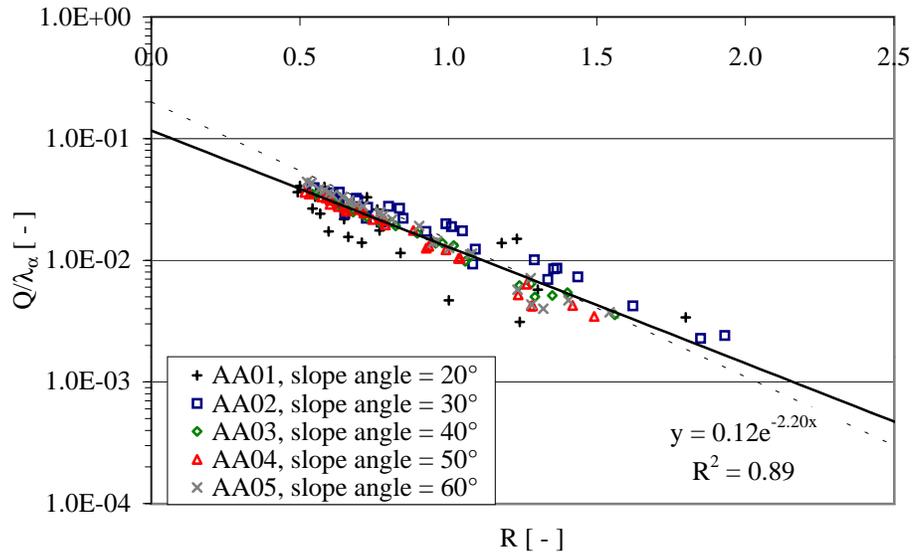
Figure 3.8: Results of tests with test geometries with varying α (test series AA). The dimensionless average overtopping discharge Q divided by the correction factor λ_α is plotted as a function of the dimensionless crest freeboard R. The dotted line represents eq. 2.1 and the solid line is an exponential fit with all the data points shown.

where $\alpha_m = 30°$ is the optimal slope angle and $\beta = 3$ is a coefficient, both found by best fit. The expression for λ_α in eq. 3.3 is formulated so it is 1 for the optimal slope angle (in terms of maximum overtopping) and decreases when the difference between the optimal and actual slope angle increases.

3.5.2 Varying crest freeboard

The test series with varying crest freeboard R_c shows that the average overtopping discharge is very well described by an exponential expression like the one suggested by Van der Meer and Janssen (1995) (see table 2.1), cf. figure 3.9.
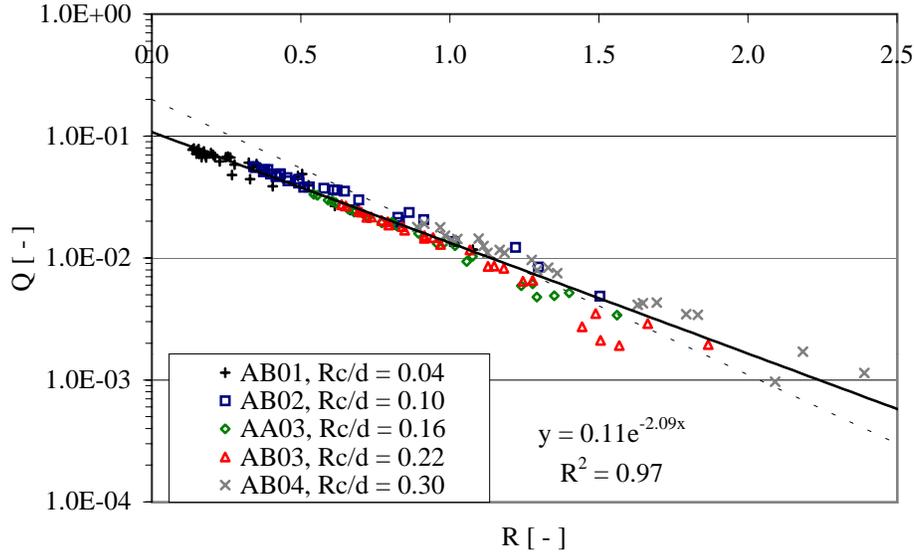
Figure 3.9: Results of tests with test geometries with varying R_c (test series AB). The dimensionless average overtopping discharge Q is plotted as a function of the dimensionless crest freeboard R. The dotted line represents eq. 2.1 and the solid line is an exponential fit with all the data points shown.

From figure 3.9 it can be seen that the correlation coefficient R^2 is as high as 0.97, indicating a very good fit.

3.5.3   Varying draft

The test series with varying draft d_r shows that the average overtopping discharge is dependent on d_r, cf. figure 3.10.
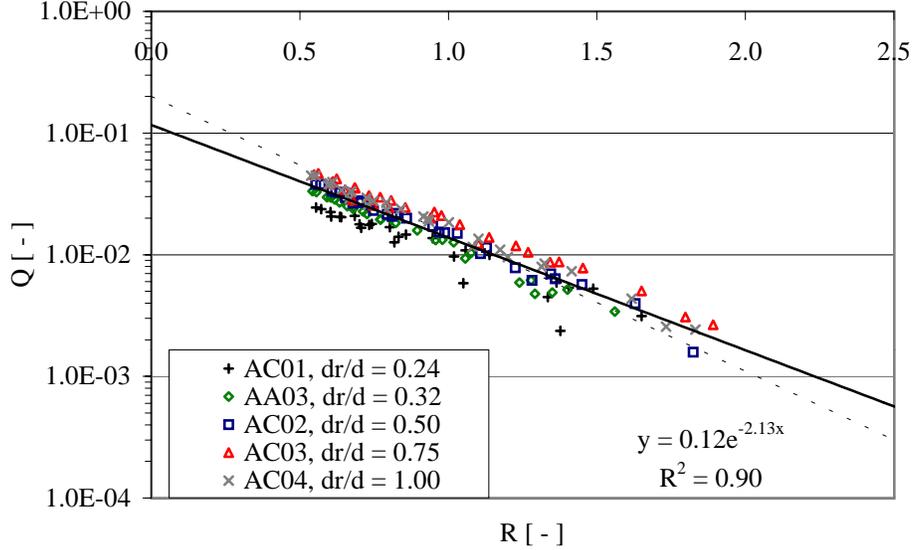
Figure 3.10: *Results of tests with test geometries with varying d_r (test series AC). The dimensionless average overtopping discharge Q is plotted as a function of the dimensionless crest freeboard R. The dotted line represents eq. 2.1 and the solid line is an exponential fit with all the data points shown.*

It is apparent that the overtopping increases with increasing draft. This is not surprising as the amount of energy passing under the slope is decreasing with increasing draft. In order to take this effect into account a correction parameter λ_{d_r} is introduced:

$$\lambda_{d_r} = 1 - \kappa \frac{\sinh(2k_p d(1 - \frac{d_r}{d})) + 2k_p d(1 - \frac{d_r}{d})}{\sinh(2k_p d) + 2k_p d} \tag{3.4}$$

where k_p is the wave number based on L_p and κ is a coefficient controlling the degree of influence of the limited draft. κ is found to be 0.4 by best fit.

The expression taking the dependency of the draft into account is based on the ratio between the time averaged amount of energy flux integrated from the draft

up to the surface E_{f,d_r} and the time averaged amount of energy flux integrated from the seabed up to the surface $E_{f,d}$.

$$
\begin{aligned}
\frac{E_{f,d_r}}{E_{f,d}} &= \frac{\int_{-d_r}^{0} p^+ u \; dz}{\int_{-d}^{0} p^+ u \; dz} \\
&= 1 - \frac{\sinh(2kd(1 - \frac{d_r}{d})) + 2kd(1 - \frac{d_r}{d})}{\sinh(2kd) + 2kd}
\end{aligned}
\tag{3.5}
$$
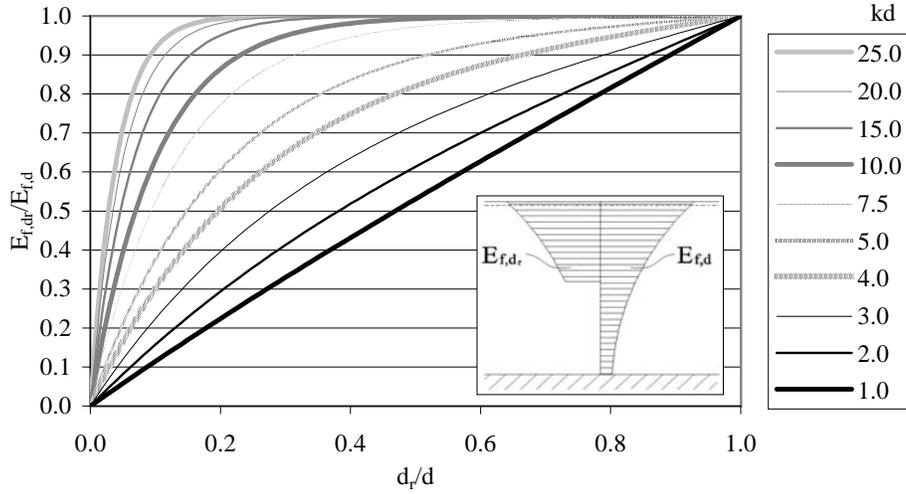
Figure 3.11: The ratio given in eq. 3.5 as a function of the relative draft $\frac{d_r}{d}$ for various values of kd.

In figure 3.11 eq. 3.5 is plotted as a function of the relative draft $\frac{d_r}{d}$ for various values of kd.

In the derivation of eq. 3.5 linear wave theory is used. Because of the limitations of the linear wave theory eq. 3.5 cannot completely describe the effect of limited draft on overtopping. Using λ_{d_r} equal to eq. 3.5 would lead to an estimation of zero overtopping for $d_r = 0$, which obviously is not the case for all combinations of H_s and R_c. Therefore, the coefficient $\kappa = 0.4$ is introduced and the expression for λ_{d_r} given by eq. 3.4 is obtained.

The result of applying λ_{d_r} is shown in figure 3.12.
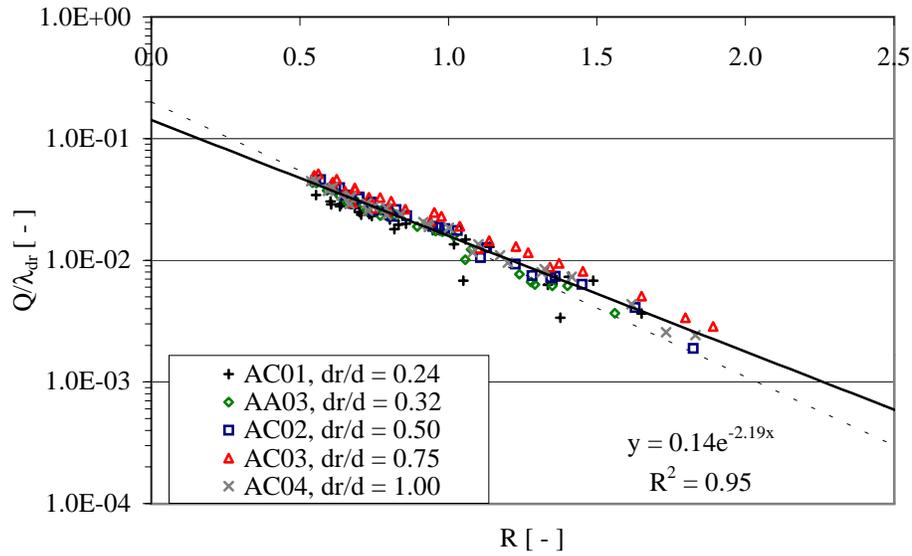
Figure 3.12: Results of tests with test geometries with varying d_r (test series AC). The dimensionless average overtopping discharge Q divided by the correction factor λ_{d_r} is plotted as a function of the dimensionless crest freeboard R. The dotted line represents eq. 2.1 and the solid line is an exponential fit with all the data points shown.

As seen from figures 3.10 and 3.12 the correlation coefficient R^2 is hereby increased from 0.90 to 0.95.

3.5.4 Comparison with Van der Meer and Janssen (1995)

In figure 3.13 the results from the tests with linear slopes are plotted together with results given by Van der Meer and Janssen (1995) and Oumeraci et al. (1999). The data from Van der Meer and Janssen (1995) include both data from tests with straight slopes and data from tests with slopes with a berm, foreshore, rough surface, short-crested and oblique waves. For tests with slopes with a berm, foreshore, rough surface, short-crested and oblique waves the data have been corrected using the appropriate reduction factors given by Van der Meer and Janssen (1995). The data from Oumeraci et al. (1999) include data from 1:3, 1:4 and 1:6 slopes subjected to both 2-D and 3-D waves. Again the reduction factors given by Van der Meer and Janssen (1995) have been applied when appropriate. For the data from Van der Meer and Janssen (1995) and Oumeraci et al. (1999) the correction factors λ_α and λ_{d_r} are 1.

Figure 3.13 shows that for R larger than approx. 0.75 the expression given by Van der Meer and Janssen (1995) (eq. 2.1) fits the data very well. However, when R decreases from 0.75 to 0 discrepancies increases. Based on these observations, it is proposed that the expression by Van der Meer and Janssen (1995) be modified by a correction factor λ_s in addition to the factors λ_α and λ_{d_r} introduced in the previous sections:

$$\lambda_s = \begin{cases} 0.4\sin(\frac{2\pi}{3}R) + 0.6 & \text{for } R < 0.75 \\ 1 & \text{for } R \geq 0.75 \end{cases} \tag{3.6}$$

Introduction of λ_s results in a very good fit for all the data (indicated by a correlation coefficient $R^2 = 0.97$), including the range where R is close to 0. This is shown in figure 3.14.

Thus, using this background a new overtopping expression for non-breaking waves can be formulated:

$$Q = \frac{q}{\lambda_\alpha \lambda_{d_r} \lambda_s \sqrt{gH_s^3}} = 0.2e^{-2.6\frac{R_c}{H_s}\frac{1}{\gamma_r \gamma_b \gamma_h \gamma_\beta}} \tag{3.7}$$

where λ_α, λ_{d_r} and λ_s are defined by eq. 3.3, 3.4 and 3.6, respectively, and γ_r, γ_b, γ_h and γ_β, are defined as given in Van der Meer and Janssen (1995).

In the following analyses eq. 3.7 is used as the definition of Q.
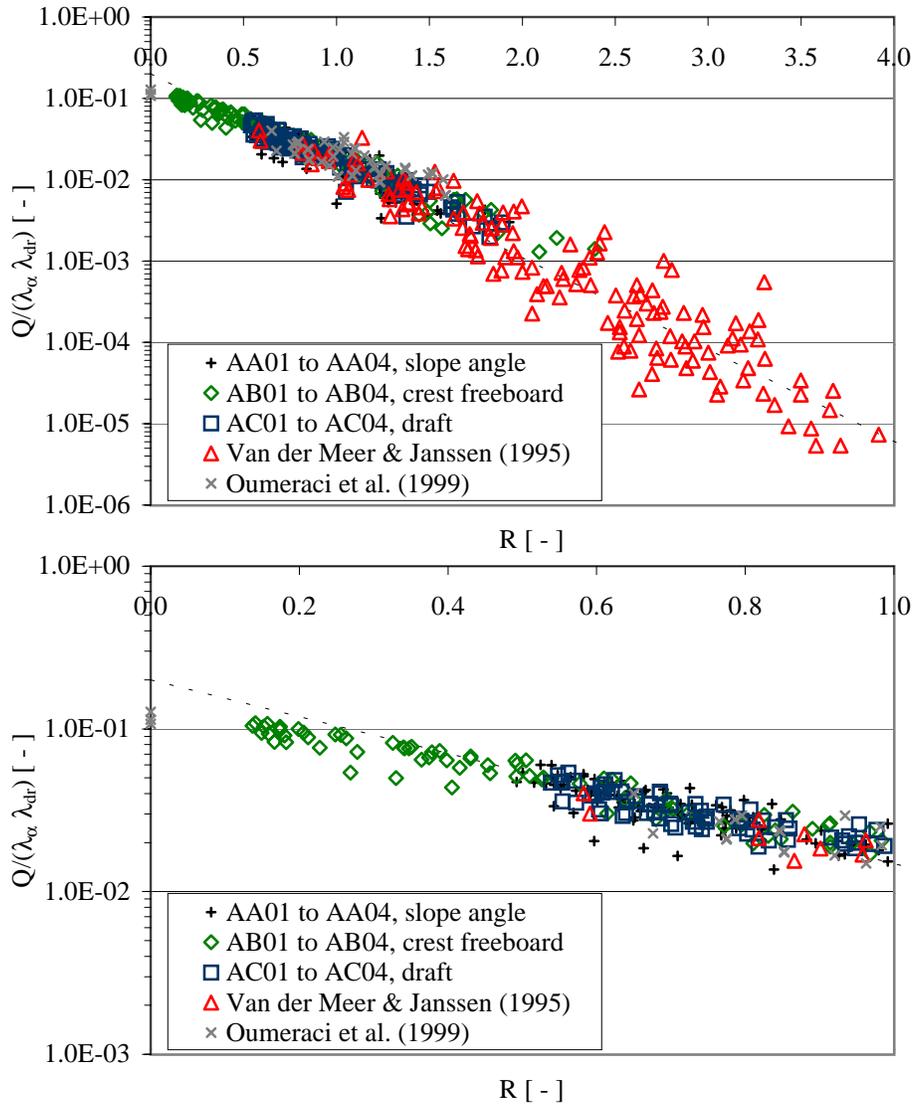
Figure 3.13: The experimental data from the tests with linear slopes plotted together with the overtopping data given in Van der Meer and Janssen 1995 for $\xi_p > 2$, and data reported by Oumeraci et al. (1999). The dotted line represents eq. 2.1. The lower graph is a zoom of the upper graph.
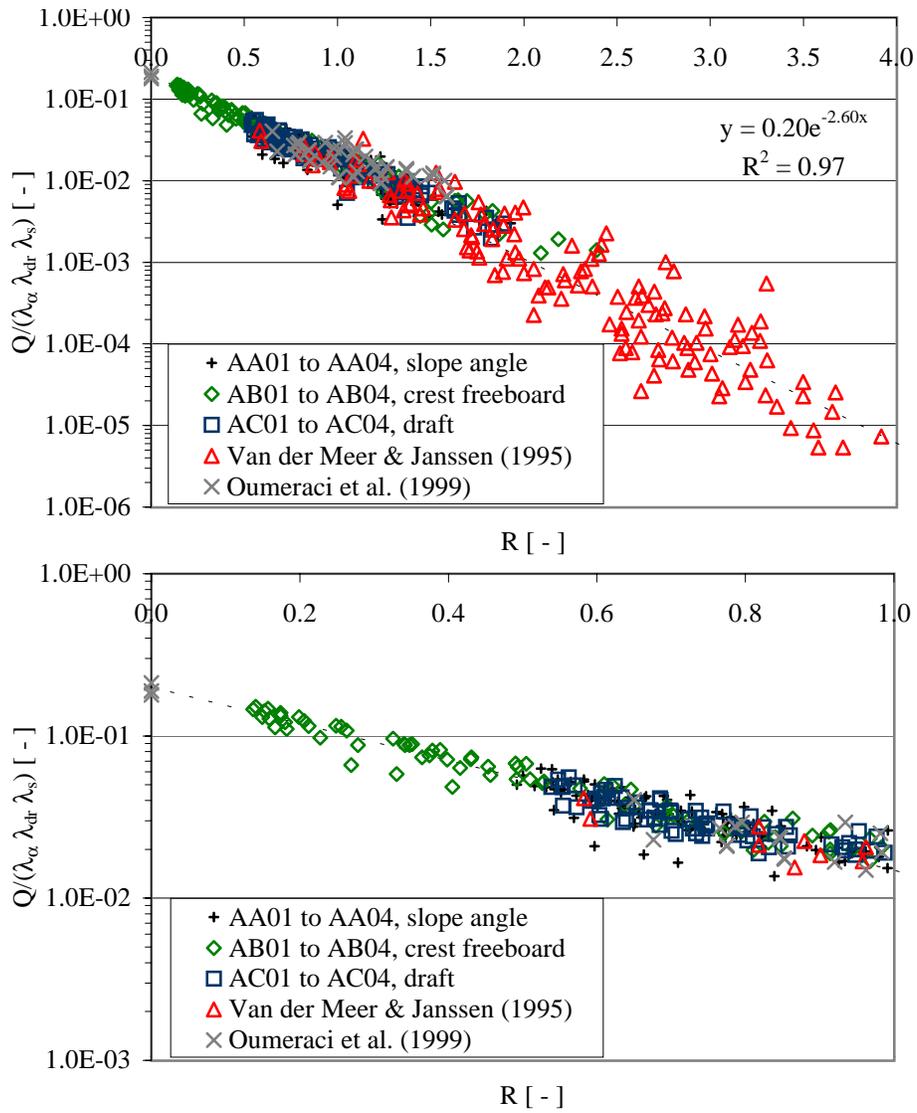
Figure 3.14: The experimental data from the tests with linear slopes plotted together with the overtopping data given in Van der Meer and Janssen 1995 for $\xi_p > 2$, and data reported by Oumeraci (1999). λ_s has been introduced. The dotted line represents eq. 2.1. The lower graph is a zoom of the upper graph.

45

3.5.5   Choice of setup for further tests

An investigation of the average efficiency of different test slope layouts is carried out in order to choose the basic geometrical parameters for the following model tests of modifications of the slope. The parameters are determined by calculating how much potential energy is obtained from each of the tested linear slopes over a year and comparing this with the amount of energy present in the waves.

In this investigation five sea states are considered. These sea states are typical of the Danish part of the North Sea and describe the conditions that apply 85 % of the time. The sea states are given by Bølgekraftudvalgets Sekretariat (1999) and are shown in table 3.5, where P_{occur} denotes the probability of occurrence and P_{wave} is the power that passes through a vertical cross section of the water column, perpendicular to the wave direction with unit width. The significant wave height H_s that applies the remaining 15 % of the time is either smaller than 0.5 m ($\sim$14 %) or larger than 5.5 m ($\sim$1 %). It is assumed in both cases that no potential energy is captured under these conditions, which makes the calculated amounts of captured energy conservative.

H_s [m]	T_p [s]	P_{occur} [%]	P_{wave} [kW/m]
1.0	5.6	47.6	2.5
2.0	7.0	21.4	13.6
3.0	8.4	9.6	35.0
4.0	9.8	4.1	69.3
5.0	11.2	1.7	123.7

Table 3.5: Sea states typical of the Danish part of the North Sea. The probability and power flux for each of the wave situations are given. The given sea states cover conditions that apply 85 % of the time.

In table 3.5 the wave power flux is based on wave energy transport per m wavefront P_{wave} [W/m] calculated by

$$P_{wave} = \frac{\rho g^2}{64\pi} T_e H_s^2 \tag{3.8}$$

where $T_e = \frac{m_{-1}}{m_0}$ is the energy transport wave period, m_{-1} and m_0 is the minus first and zero spectral moment, Falnes (1993).

The power obtained in terms of potential energy in the overtopping water is calculated as

$$\begin{aligned} P &= qR_c g\rho_w \\ &= \sqrt{gH_{m0}^3}Ae^{-B\frac{R_c}{H_{m0}}}R_c g\rho_w \end{aligned} \qquad (3.9)$$

The power P [W/m] is calculated for each of the sea states by using the co-efficients A and B fitted to the results of the tests of each of the geometries. The coefficients used are shown in the graphs in appendix B.1, figures B.1 to B.13. The average power P over a year is found weighing the power for each wave situation with the probability of occurrence of the wave situation. Thus, the weighed average ratio between P and P_{wave}, η_{hydr} (also called the hydraulic efficiency), can be calculated for each of the tested linear slopes. These ratios are plotted in figure 3.15 as functions of slope angle, relative crest freeboard and relative draft.

From the first graph in figure 3.15 the choice of slope angle $\alpha = 30°$ is obvious. The choice of crest freeboard is not as obvious, but bearing in mind that turbines perform better with larger than lower head (at least in the low head range in which all WEC's of the overtopping type operate) results in the choice of a relative crest freeboard $\frac{R_c}{d} = 0.10$. When choosing the draft, the consideration of getting as much overtopping as possible would lead to extending the slope all the way to the bottom. However, from a cost-benefit point of view, this is not optimal. Therefore, a relative draft $\frac{d_r}{d} = 0.4$ is chosen, as the benefit of going deeper, in terms of obtained power, is smaller than the loss of power that results from going less deep.

In conclusion the reference and starting point of the models tested in the following is a linear slope with a slope angle $\alpha = 30$ °, a relative crest freeboard $\frac{R_c}{d} = 0.10$ and a relative draft $\frac{d_r}{d} = 0.4$.

Comments on calculated efficiencies

From figure 3.15 it can be seen that the ratio between the amount of potential energy in the water overtopping a structure like the tested ones (with a limited draft) and the energy present in the waves averaged over time (η_{hydr}) can be as high as 20 - 25 % for a structure in the Danish part of the North Sea. This is obtained from geometry AB01 and AB02 where $\alpha = 40°$, $\frac{d_r}{d} = 0.32$ and $\frac{R_c}{d} = 0.04$ and 0.10, respectively. For the selected reference linear slope, it is likely that an even higher η_{hydr} is obtained.

To put these results into perspective, theoretical considerations concerning regular wave overtopping of string are presented in appendix A. From this it can
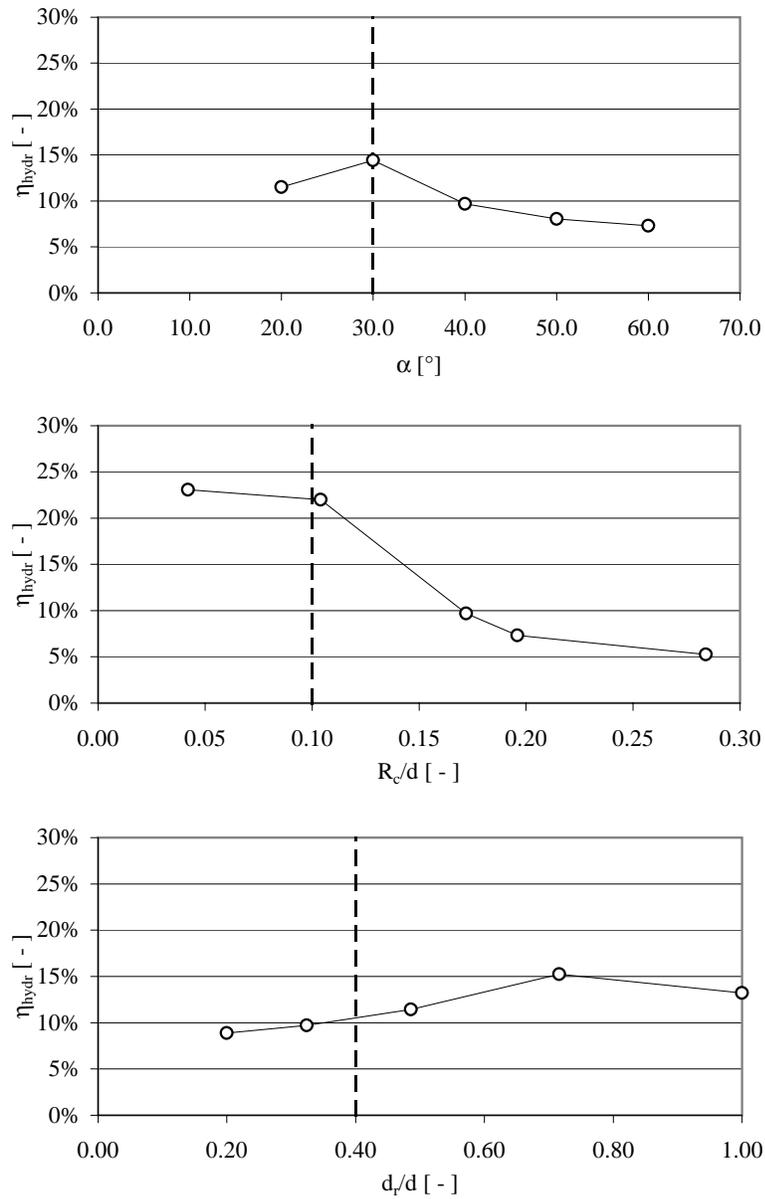
Figure 3.15: The efficiency η_{hydr} of the tested linear slopes plotted as functions of slope angle, relative crest freeboard and relative draft. The vertical broken line indicates the choices for the further model tests.

be seen that if only the potential energy present in a regular wave is considered (this is what is meant by overtopping of a string), the maximum efficiency η_{hydr} is 11.5 % for shallow water and 23.1 % for deep water. Compared with the results above these are rather small values, considering that the values stated above are overall efficiencies for a number of irregular wave situations. However, by placing a slope in the waves, part of the kinetic energy that is present in the waves is converted into potential energy in the overtopping waves, which adds significantly to the efficiencies.

It should be noted that the potential energy used when calculating η_{hydr} is the amount of potential energy present in the overtopping water at the time it passes over the crest of the slope. This means that unless the water level behind the slope is kept right at the crest of the slope at all times, some of the potential energy is lost and the efficiency is thus decreased.

3.6 Results of model tests with modifications of the slope profile

In this section the results of the model tests with modifications of the slope profile are presented and analyzed. In appendix B.2 the basic results are shown in figures B.14 to B.39. In the following the dimensionless overtopping discharge Q is defined as $\frac{q}{\lambda_\alpha \lambda_{d_r} \lambda_s \sqrt{gH_s^3}}$ as it was found in section 3.5.4, eq. 3.7.

3.6.1 Horizontal plate at slope bottom

In the test series BA, horizontal plates with different lengths have been placed at the slope bottom. The effect of these horizontal plates on the overtopping discharge can be seen in figure 3.16.

From figure 3.16 it can be seen that the effect of adding a horizontal plate at the slope bottom depends very much on the length of the plate. The longest horizontal plate (BA01) results in almost exactly the same overtopping discharges as without (BA04), while a plate with half the length (BA02) results in an increase of 7 %, but a plate with a quarter of the length (BA03) results in a decrease of the overtopping discharge of 9 %. This indicates that it is favorable to use a plate with a length of 25 % of the slope draft, but it seems appropriate to conduct additional tests with horizontal plates with lengths in this range in order to find the optimal length.
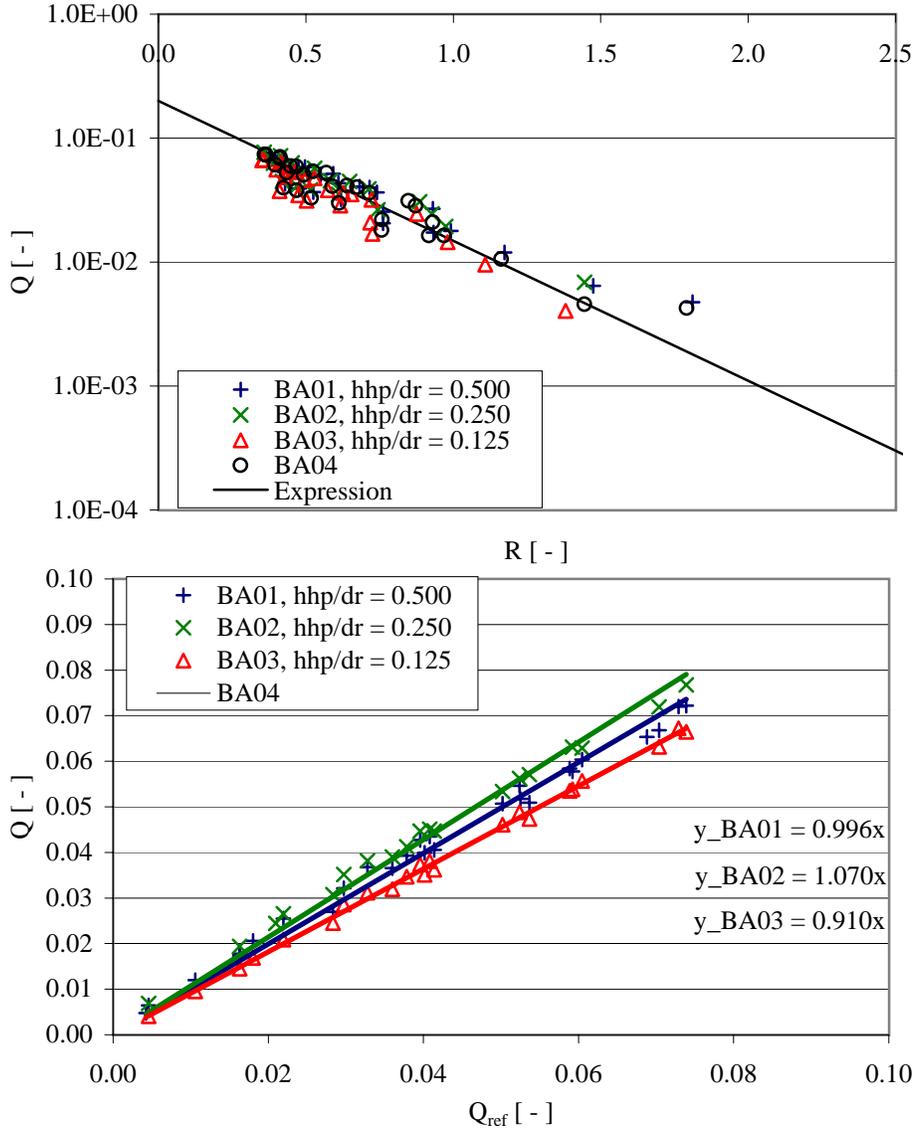
Figure 3.16: Results of tests with horizontal plate at slope bottom (test series BA). In the upper graph the dimensionless average overtopping discharge Q is plotted as a function of the dimensionless crest freeboard R. The line represents eq. 3.7. In the lower graph the results of the tests with horizontal plate at slope bottom (Q) are compared with the corresponding results of reference test BA04 (Q_{ref}).

3.6.2 Convex top of slope

In the test series CA the upper part of the slope has been given a convex deflection but the slope angle below the deflection remains unchanged. The effect of these deflections on the overtopping discharge can be seen in figure 3.17.

From figure 3.17 it can be seen that no increase in the overall overtopping discharge is obtained by introducing a convex deflection with an unchanged slope angle below the deflection. In fact, in the example where the largest radius of the convex part was used (CA03) an overall reduction of almost 11 % was found, whereas the two smaller convex deflections had no effect (less than 2 %).

A series of tests with a convex deflection, but with a changed slope angle of 35° (CB01), have also been conducted. The effect of this change is shown in figure 3.18.

From figure 3.18 it can be seen that this modification results in an overall increase of the overtopping discharge of 4 %.

A test series has also been conducted on a slope with a convex upper part of an elliptical shape (test series CC). This slope geometry has been suggested by the inventor of WD, Erik Friis-Madsen, and the cross section of the slope on WD has been modified to a shape similar to the one tested in test CC01. The results of the tests are shown in figure 3.19.

From figure 3.19 it can be seen that this modification results in an overall increase of the overtopping discharge of 18 %. Given this background it seems reasonable to do further tests of slopes with an elliptic shape in order to determine whether this is the optimal shape or an even better one can be found.

3.6.3 Concave top of slope

A test series with a concave slope top (test series DA) has been conducted. The results of these tests are shown in figure 3.20.

From figure 3.20 it can be seen that introducing the concave slope top reduces the overall overtopping discharges by more than 11 %. This result agrees with the results reported by Josefson (1978), referred to in section 2.

51
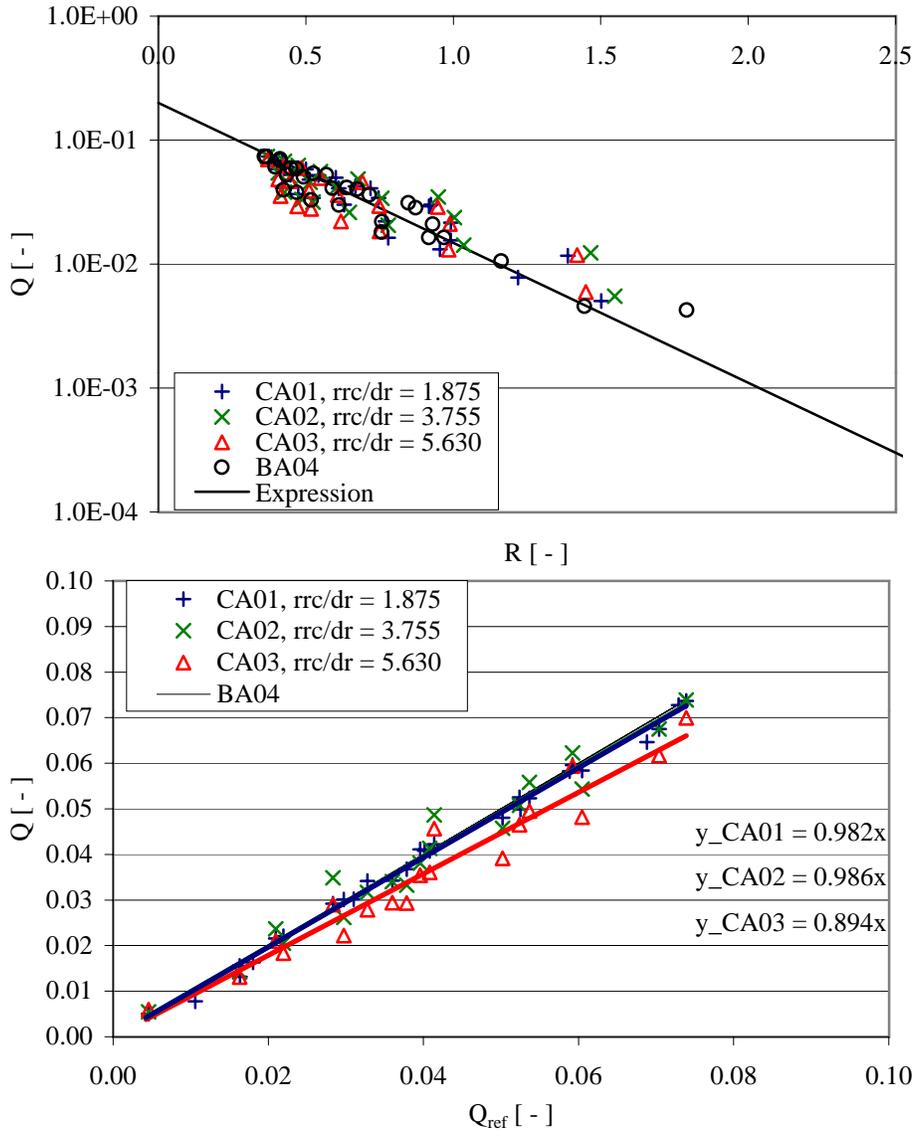
*Figure 3.17: Results of tests with convex top of the slope (test series CA). In the upper graph the dimensionless average overtopping discharge Q is plotted as a function of the dimensionless crest freeboard R. The line represents eq. 3.7. In the lower graph the results of the tests with convex top of the slope (Q) are compared with the corresponding results of reference test BA04 (Q_{ref}).*
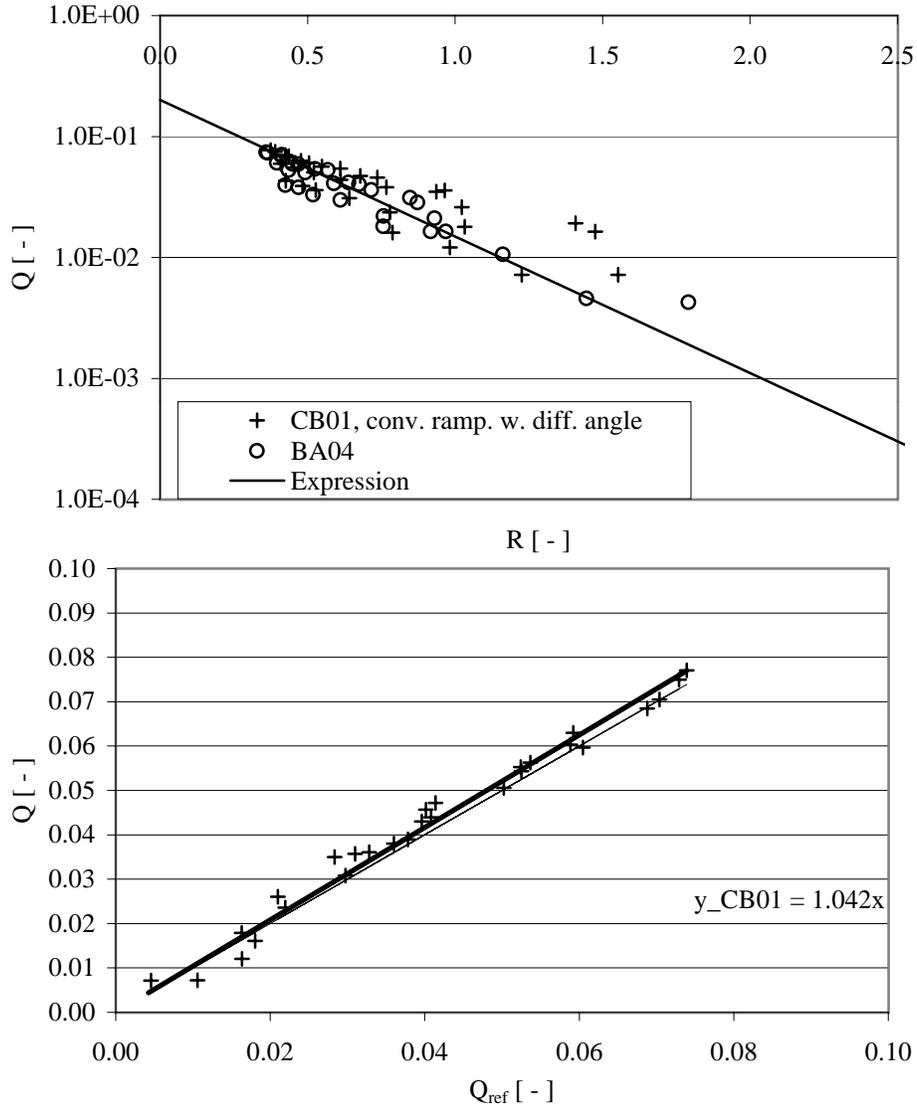
Figure 3.18: Results of tests with convex top of the slope with a slope angle $\alpha = 35°$ (test series CB). In the upper graph the dimensionless average overtopping discharge Q is plotted as a function of the dimensionless crest freeboard R. The line represents eq. 3.7. In the lower graph the results of the tests with convex top of the slope with a slope angle $\alpha = 35°$ (Q) are compared with the corresponding results of reference test BA04 (Q_{ref}).
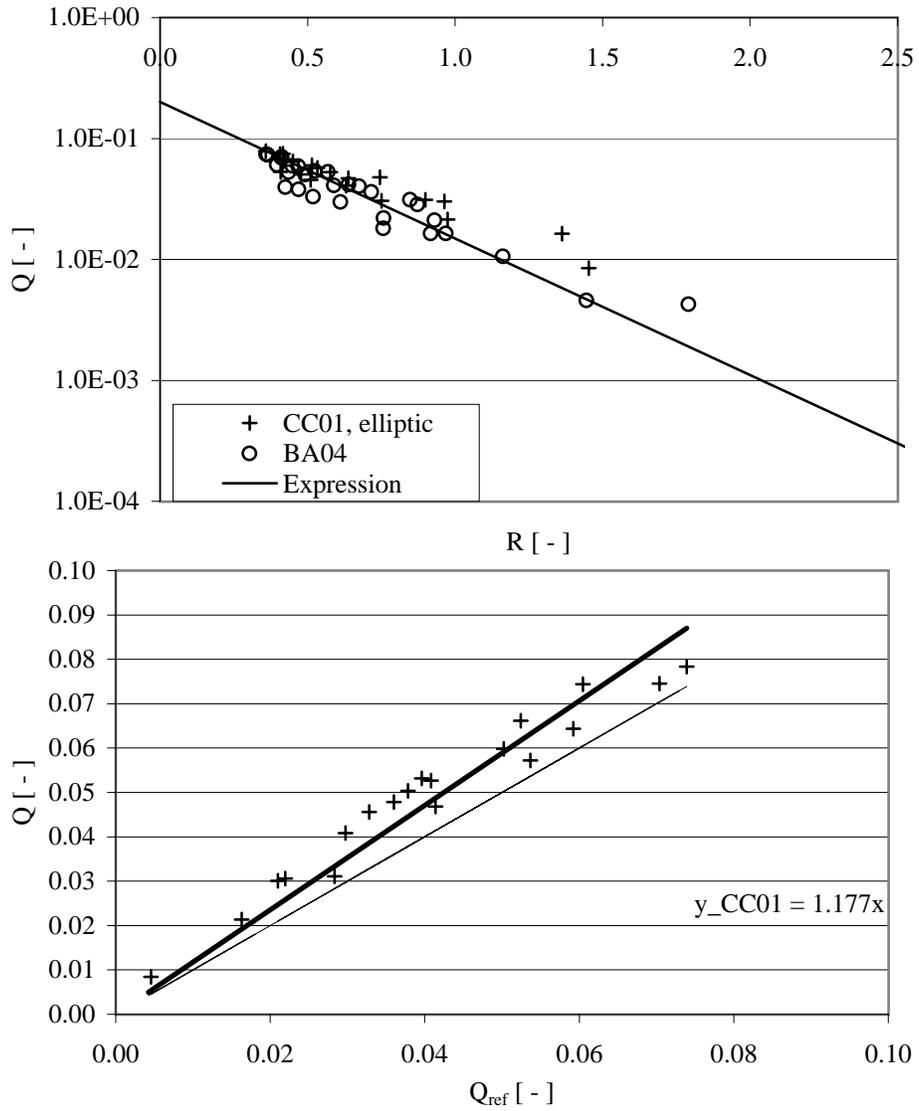
Figure 3.19: Results of tests with convex top of the slope with an ellip-tic shape (test series CC). In the upper graph the dimen-sionless average overtopping discharge Q is plotted as a function of the dimensionless crest freeboard R. The line represents eq. 3.7. In the lower graph the results of the tests with convex top of the slope with an elliptic shape (Q) are compared with the corresponding results of refer-ence test BA04 (Q_{ref}).
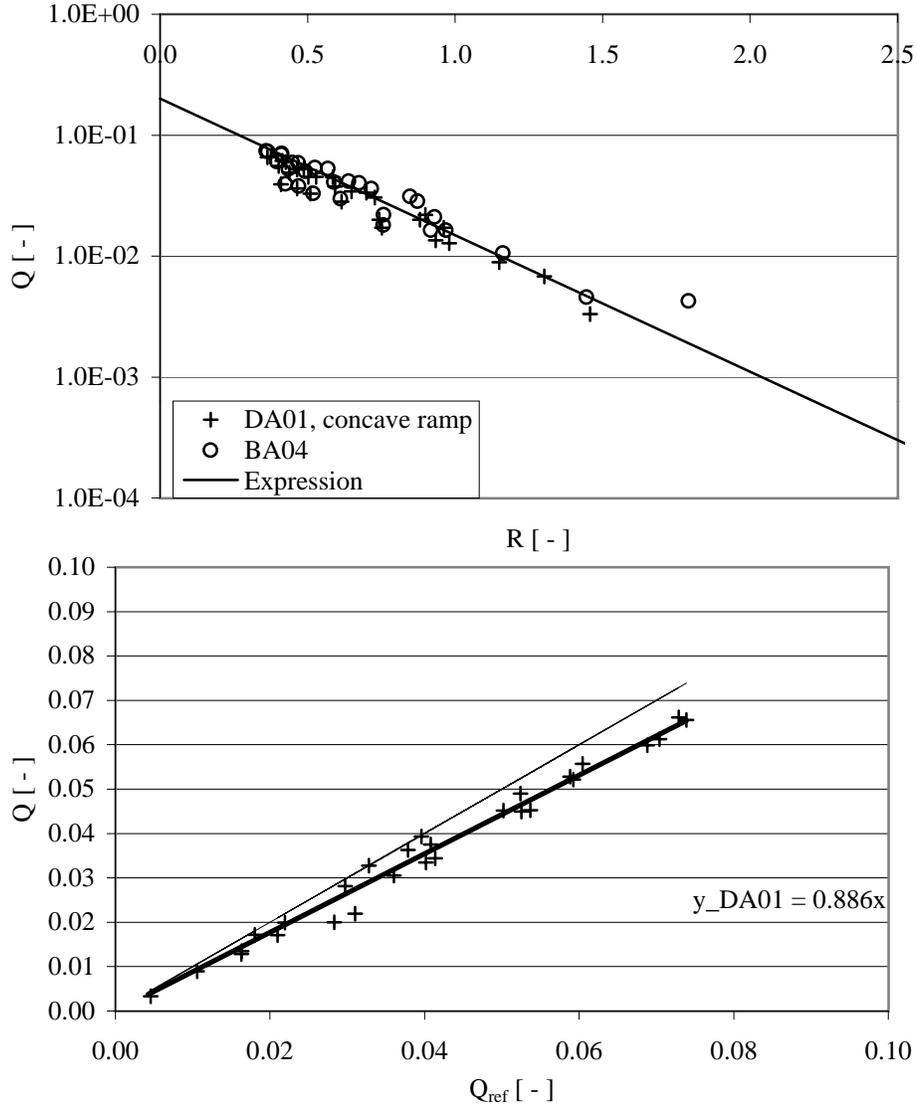
*Figure 3.20: Results of tests with concave top of the slope (test series DA). In the upper graph the dimensionless average overtopping discharge Q is plotted as a function of the dimensionless crest freeboard R. The line represents eq. 3.7. In the lower graph the results of the tests with concave top of the slope (Q) are compared with the corresponding results of reference test BA04 (Q_{ref}).*

3.7 Results of model tests with modifications of the side walls of the slope

In this section the results of the model tests with modifications of the slope profile are presented and analyzed. In appendix B.3 the basic results are shown in figures B.34 to B.39.

3.7.1 Linear converging guiding walls

A series of tests have been conducted with four different layouts of linear converging walls (test series EA). The results of these tests are shown in figure 3.21.

Figure 3.21 shows that a positive effect can be obtained by using linear converging walls with an opening ratio relatively close to 1.0 (opening ratios 0.848 and 0.696 results in an increase in the overall overtopping of 15 and 4 %, respectively). In contrast, smaller opening ratios result in reductions in the overall overtopping discharge (opening ratios of 0.536 and 0.368 result in reductions of 5 and 24 %, respectively). At this point the converging guiding walls begin to reflect the waves rather than compressing them. It therefore seems reasonable to perform additional tests with opening ratios in the range from 0.7 to 1.0, in order to find the optimal opening ratio by testing a slope with linear guiding walls.

3.7.2 Curved converging guiding walls

A series of tests has been conducted with curved converging walls (test series FA). The results are shown in figure 3.22.

From figure 3.22 it can be seen that there is no noticeable effect from using curved guiding walls instead of linear ones.

3.7.3 Summary of the results from tests with modifications of the slope profile

In order to provide a tool for calculating the average overtopping discharges for the tested modified slope profiles, a new correction factor λ_m is introduced in the overtopping expression eq. 3.7, which thus becomes:

$$\frac{q}{\lambda_m \lambda_\alpha \lambda_{d_r} \lambda_s \sqrt{gH_s^3}} = 0.2e^{-2.6\frac{R_c}{H_s}\frac{1}{\gamma_r \gamma_b \gamma_h \gamma_\beta}} \tag{3.10}$$
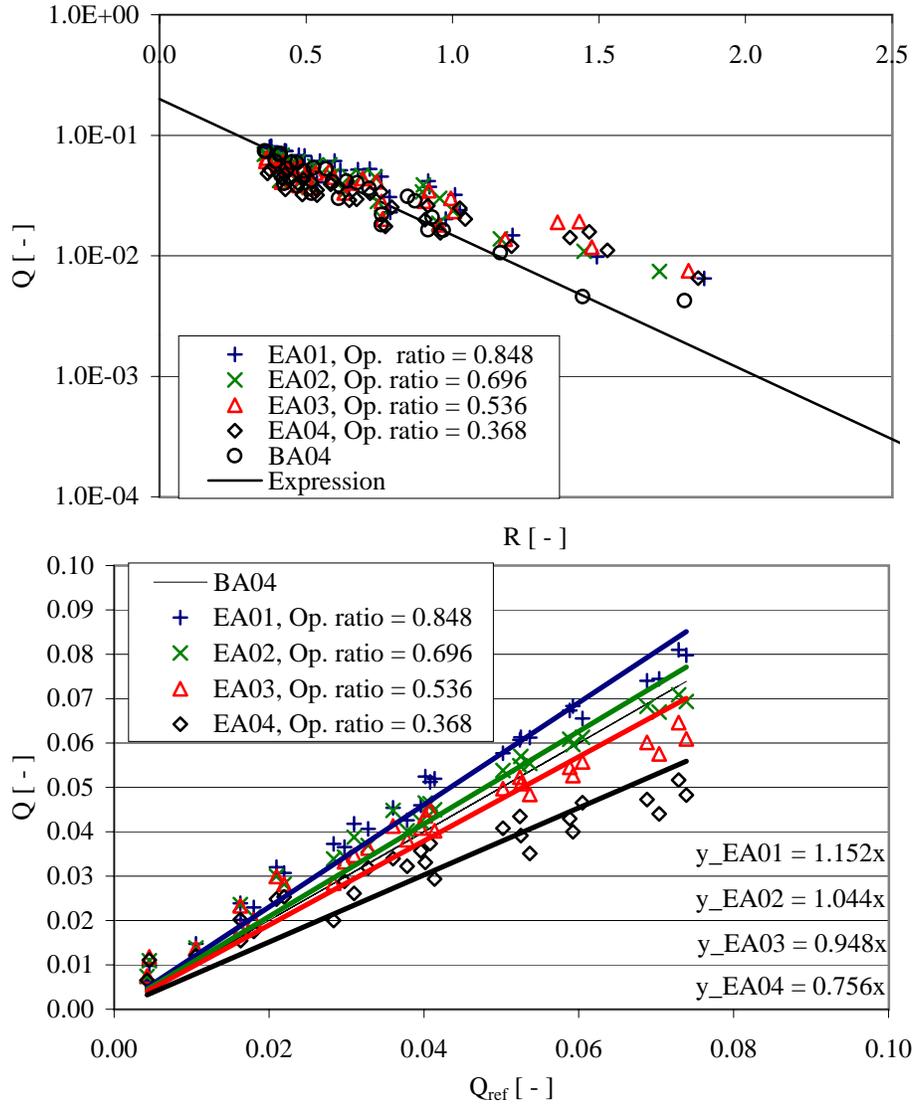
Figure 3.21: Results of tests with linear guiding walls (test series EA).
In the upper graph the dimensionless average overtopping
discharge Q is plotted as a function of the dimensionless
crest freeboard R. The line represents eq. 3.7. In the lower
graph the results of the tests with linear guiding walls (Q)
are compared with the corresponding results of reference
test BA04 (Q_{ref}).
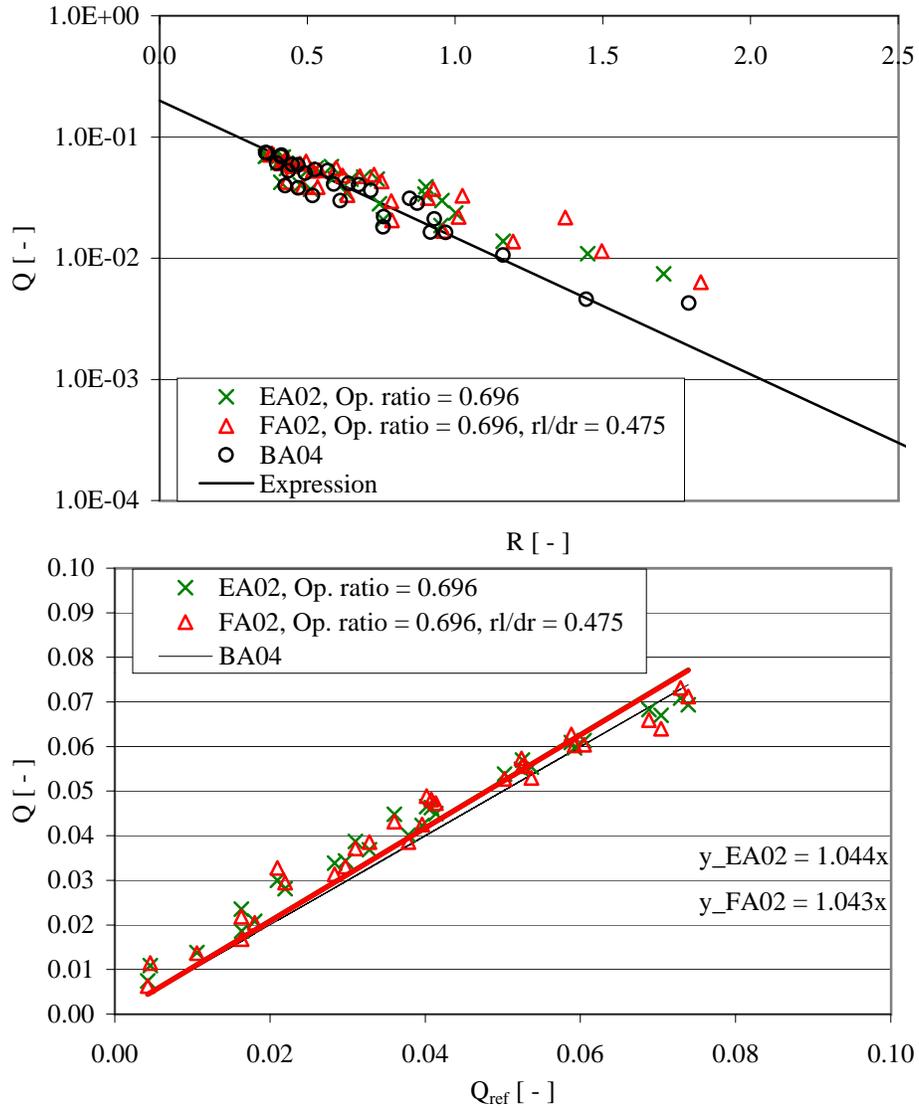
Figure 3.22: Results of tests with curved guiding walls (test series FA). In the upper graph the dimensionless average overtopping discharge Q is plotted as a function of the dimensionless crest freeboard R. The line represents eq. 3.7. In the lower graph the results of the tests with curved guiding walls (Q) are compared with the corresponding results of reference test BA04 (Q_{ref}).

The λ_m values for the tested modifications are shown in table 3.6.

Session name	Description	λ_m [-]
BA01	Horizontal plate	1.00
BA02	Horizontal plate	1.07
BA03	Horizontal plate	0.91
BA04	Reference setup	1.00
CA01	Convex slope	0.98
CA02	Convex slope	0.99
CA03	Convex slope	0.89
CB01	Convex slope, diff. angle	1.04
CC01	Convex slope, elliptic	1.18
DA01	Concave slope	0.87
EA01	Linear converging walls	1.15
EA02	Linear converging walls	1.04
EA03	Linear converging walls	0.95
EA04	Linear converging walls	0.76
FA02	Curved converging walls	1.04

Table 3.6: Correction factors λ_m to be used in eq. 3.10.

In appendix B, figures B.15 to B.38, the layouts of the geometries listed in table 3.6 are shown.

It should be noted that tests have not been performed with combinations of the geometries given in table 3.6. Thus, whether or not more than one λ_m can be applied at the same time has not been tested. However, if more than one λ_m can be applied at the same time, an increase in the overtopping discharge (and thereby also in the obtained energy of the overtopping water) of up to 45 % could be obtained by applying a horizontal plate (BA02, $\lambda_m = 1.07$), an elliptic convex slope (CC01, $\lambda_m = 1.18$) and converging side walls (EA01, $\lambda_m = 1.15$).

3.8 Time dependency of overtopping discharges

In this section an empirical model for time variation of overtopping discharge is verified through a comparison with two of the tests conducted. The motivation for this is that little or no knowledge is presently available regarding the time variation of overtopping discharge for slope layouts typical of WEC's of the overtopping type. It is important to know how the irregular nature of sea waves influences the variation of the overtopping discharge; this information is needed in order to optimize the reservoir size and the control strategy for the turbines utilizing the energy in the overtopping water, so that the loss of energy in reservoir and turbines is minimized.

As seen in chapter 2 the focus in the literature so far has been on mean overtopping discharge for sea defense structures like seawalls, breakwaters and dikes. In some cases also the probability of an overtopping event, as well as the distribution of the largest overtopping volumes (e.g., the mean overtopping volume from the 1/250 largest overtopping events) has also been investigated. However, the primary objective of these studies has been to investigate extreme overtopping events for sea defense structures designed to avoid or at least limit the amount of overtopping. Therefore the studies cannot in general be expected to cover the parameter ranges relevant to WEC's, where the maximum potential energy of overtopping volumes is generally desired. Thus, in the present study attention is especially directed to situations with small values of the relative crest freeboard R (smaller than, say, 0.75). The equations given by Van der Meer and Janssen (1995) have been developed for breakwaters and dikes that typically have larger values of R (see also section 3.5.4). Martinelli and Frigaard (1999a) presented an empirical model for prediction of time variation of overtopping. This model is based on formulae by Van der Meer and Janssen (1995).

3.8.1 Empirically based model

Martinelli and Frigaard's (1999a) empirical model for calculating the overtopping discharge is based on Van der Meer and Janssen's (1995) expression for probability of overtopping P_{ot}:

$$P_{ot} = e^{-(\frac{1}{1.21}\frac{H_s}{R_c})^{-2}} \tag{3.11}$$

Furthermore, the following expression (also given by Van der Meer and Janssen [1995]) for the probability P_{V_w} of a certain overtopping volume in a wave V_w, given that overtopping occurs, is used to calculate the volume of an overtopping wave:

$$
\begin{aligned}
P_{V_w} &= 1 - e^{-(\frac{V_w}{a})^{\frac{3}{4}}} \;,\; a = 0.84\frac{qT_m}{P_{ot}} \\
V_w &= 0.84\frac{qT_m}{P_{ot}}(-ln(1 - P_{V_w}))^{\frac{3}{4}}
\end{aligned}
\tag{3.12}
$$

In order to calculate a time series of overtopping volumes, the following procedure is used:

- P_{ot} is calculated using eq. 3.11.

- q is calculated using an overtopping formula or, as in this investigation, is simply taken from a model test.

- For a chosen number of waves N (each assumed to be T_m long), the following calculations are used:

  A random number p between 0 and 1 is drawn for each wave.

  If $p > P_{ot}$ then V_w^i is set to 0, else V_w^i is calculated using eq. 3.12.

- The obtained series of V_w^i 's (V_w^1 to V_w^N) is then converted into a discharge time series $q_{sim}(t)$ in order to enable a comparison with a measured discharge time series from the model tests $q_{meas}(t)$.
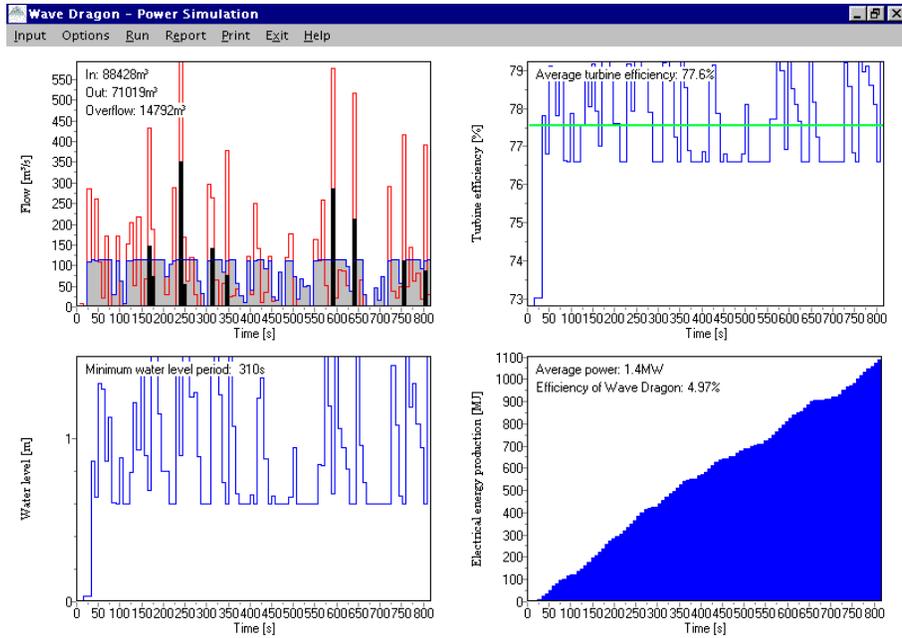
Figure 3.23: An example of a simulation performed using the empirical model WDpower.

Figure 3.23 shows an example of the results of a simulation using the empirical model (implemented in the PC program WDpower utilized in the development of WD by Jakobsen and Frigaard [1999]). Based on such simulations it is possible to test turbine configurations and control strategies (see Madsen and Frigaard [2000]).

3.8.2 Test results and comparison with empirical model

The comparison of the simulated and measured overtopping discharge $q_{sim}(t)$ and $q_{meas}(t)$, respectively, is conducted by comparing the results of an analyses done in the following way for each of the discharge time series:

- The discharge time series is divided into N_{window} sub-series each T_{window} long.

- For each of the sub-series the average discharge values q^i_{window} (for $i = 1$ .. N_{window}) are obtained.

- Each of the values q^i_{window} is normalized by the average discharge of the whole time series q ($\frac{q^i_{window}}{q}$), and the average (which should be 1) and the standard deviation of these values are calculated.

If the probability distribution of $\frac{q^i_{window}}{q}$ of the two time series is the same, it can be concluded that the simulation method is able to predict overtopping time series for slopes with low freeboards.

Two model tests have been selected for the evaluation of the simulation method. The geometry BA04 is used and the wave situations are characterized by $H_s = 4.0$ and 8.0 m, respectively, both with a $T_p = 8.0$ s. This results in relative crest freeboards $R = 0.61$ and 0.37, respectively.

For each of the two tests chosen for this analysis, the comparison is made using a window size corresponding to $\frac{T_{window}}{T_m} = 60$ (assuming $\frac{T_p}{T_m} = 1.13$). The results of this are shown in figure 3.24.

Furthermore, the analyses have been done using different values for T_{window} for the test with $R = 0.61$. The results of this are shown in figures 3.25 and 3.26.

R	$\frac{T_{window}}{T_m}$	St. dev. $(\frac{q^i_{window}}{q})$ for $q_{meas}(t)$	St. dev. $(\frac{q^i_{window}}{q})$ for $q_{sim}(t)$	Ratio
0.61	300	0.12	0.10	1.20
0.61	120	0.17	0.16	1.06
0.61	60	0.26	0.20	1.30
0.61	30	0.39	0.28	1.39
0.61	10	0.57	0.50	1.14
0.37	60	0.17	0.19	0.89

Table 3.7: Standard deviations of $\frac{q^i_{window}}{q}$ ($i = 1$ .. N_{window}) for $q_{meas}(t)$ and $q_{sim}(t)$ and the ratios between these.
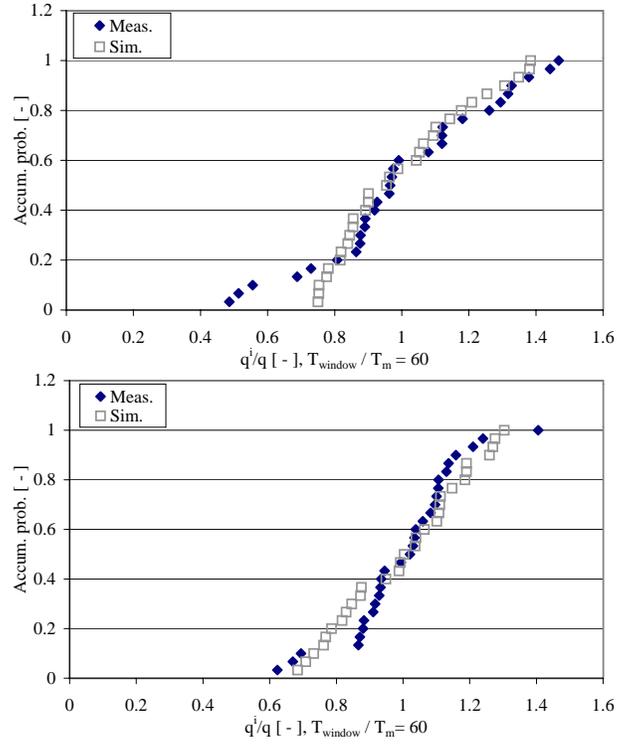
Figure 3.24: Results for the two tests with $R = 0.61$ (top) and 0.37 (bottom). The accumulated probability density for $\frac{q^i_{window}}{q}$ is plotted for $q_{meas}(t)$ and $q_{sim}(t)$, respectively.
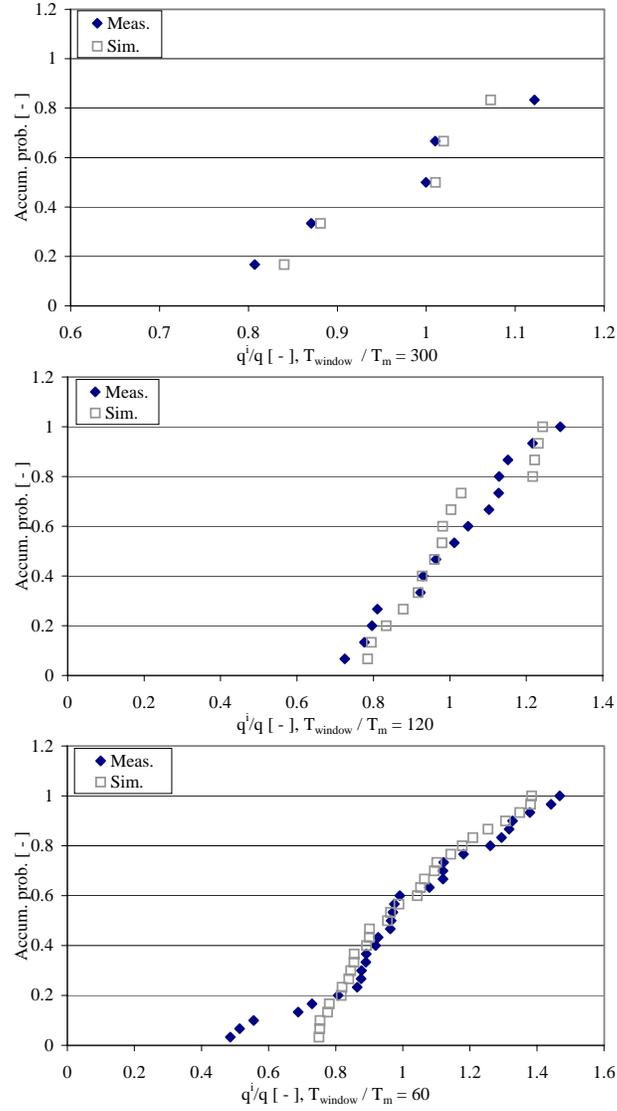
Figure 3.25: Results for the $R = 0.61$ where different T_{window} have been applied ($\frac{T_{window}}{T_m} = 300$ [top], $\frac{T_{window}}{T_m} = 120$ [middle] and $\frac{T_{window}}{T_m} = 60$ [bottom]). The accumulated probability density for $\frac{q^i_{window}}{q}$ is plotted for $q_{meas}(t)$ and $q_{sim}(t)$, respectively.
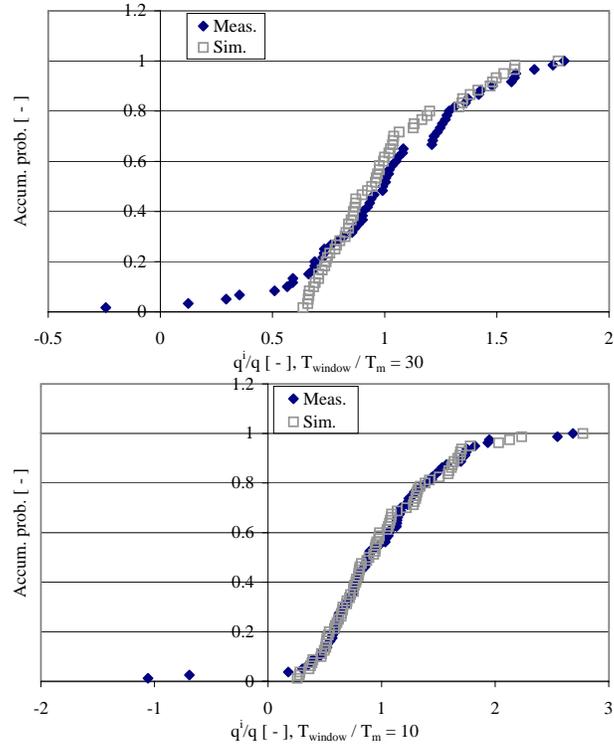
Figure 3.26: Results for the $R = 0.61$ where different T_{window} have been applied ($\frac{T_{window}}{T_m} = 30$ [top] and $\frac{T_{window}}{T_m} = 10$ [bottom]). The accumulated probability density for $\frac{q^i_{window}}{q}$ is plotted for $q_{meas}(t)$ and $q_{sim}(t)$, respectively.

In table 3.7 the standard deviations of $\frac{q_{window}^i}{q}$ (i = 1 .. N_{window}) for $q_{meas}(t)$ and $q_{sim}(t)$ are shown along with the ratio between these. From the presented results the following can be observed:

- For the tests with $R = 0.61$ and 0.37 with $\frac{T_{window}}{T_m} = 60$ (figure 3.24) it can be seen that good agreement between the analysis of $q_{meas}(t)$ and $q_{sim}(t)$ exists. However, from table 3.7, it can be seen that for the test with R $= 0.61$ the standard deviation for $q_{meas}(t)$ is 30 % larger than for $q_{sim}(t)$, whereas for the test with $R = 0.37$ the standard deviation for $q_{meas}(t)$ is 11 % smaller than for $q_{sim}(t)$. For the simulation of overtopping for the evaluation of turbine configuration, etc., in a WEC, these deviations are considered acceptable. From results of the test with $R = 0.61$ and varying T_{window} (figures 3.25 and 3.26) it can be seen that the standard deviation for $q_{meas}(t)$ is larger (6 - 39 %) than for $q_{sim}(t)$ for all values of T_{window}. Thus, the tendency is in general the same as that seen for $\frac{T_{window}}{T_m} = 60$.

- For the test with $R = 0.61$ and $\frac{T_{window}}{T_m} = 30$ and 10 (figure 3.26) it can be seen that q_{window}^i for a few sub-series is negative. This supports that the limit of how small a value of T_{window} for which the analysis is reasonable is approx. 10 waves.

- For both $q_{meas}(t)$ and $q_{sim}(t)$ it can be seen from table 3.7 that the standard deviation of $\frac{q_{window}^i}{q}$ decreases for increasing T_{window}.

CHAPTER 4

Overtopping of Multi Level Reservoirs

In this chapter the conditions for the study of overtopping of multi level reservoirs are described. First, the purpose of the model tests conducted is described, followed by an account of the geometric parameters investigated and the sea states used, and the model test setup is presented. The first part of the model tests has been conducted to provide the basis for an expression describing the vertical distribution of overtopping above a slope. Based on the expression found, a numerical study is performed to estimate the effect of using more reservoirs on the obtained amount of potential energy in the overtopping water.

Furthermore, model tests have been conducted using multi level reservoirs with a front mounted on each reservoir, and the results are presented and compared with previous results.

Finally, model tests with a floating multi level WEC are presented, and the effect of adjusting the crest freeboard to the sea states is studied.

4.1 Background and purpose

Preliminary investigations of the WEC PP showed that a considerable increase in energy from the overtopping water could be obtained by using reservoirs at multiple levels, Kofoed and Frigaard (2000a). The first version of the PP is presented in figure 4.1.

Figure 4.1: The first version of the Power Pyramid in action.

Based on the results found by Kofoed and Frigaard (2000a), is was decided to investigate the PP concept further. The primary aim of the investigations has been to quantify the effect of using more reservoirs and to optimize the geometric layout of the structure so the maximum captured energy is obtained.

The investigations have been divided into four stages:

- Establishing an expression describing the vertical distribution of overtopping over a slope.

- Optimization of number and vertical placement of reservoirs.

- Optimization of horizontal placement of reservoirs and reservoir front geometries.

- Performance of floating WEC with multi level reservoirs.

The first and third stages involve model tests conducted using a fixed structure, as described in the next section. The second stage is conducted numerically, using the results from the first stage. The last stage involves model tests using a floating model.

4.2   Geometries tested

All of the geometries in the model tests use an overtopping slope with the angle $\alpha = 35°$.

The geometries tested in a fixed model test setup are described in this section (corresponding pictures and drawings of the geometries are shown in appendix C). The conditions for the model tests performed with the floating model are provided in section 4.9.

4.2.1 Tests with 8 reservoirs, no fronts

The first part of the model tests involves 8 reservoirs without fronts mounted on them. A total of 4 series of model tests (20 tests in total) have been performed, each series consisting of 5 tests as shown in section 4.3.

The geometric parameters describing the setup in each of the test series are shown in table 4.1. $R_{c,1}$ denotes the crest freeboard of the lowest of the reservoirs (reservoir 1).

Test series	d [m]	d_r [m]	$R_{c,1}$ [m]
A1	21.0	8.1	0.9
A2	20.4	7.5	1.5
A3	19.8	6.9	2.1
B	19.8	9.9	2.1

Table 4.1: Tested parameters for the model setup with 8 reservoirs, no fronts.

All these model tests are conducted with a vertical distance between the individual reservoirs $\Delta z = 1.35$ m. Thus, the crest freeboard of the individual reservoirs is given by $R_{c,n} = R_{c,1} + (n-1)\Delta z$, when Δz is constant. This is the case in all the model tests conducted.

The principal layout of the geometries tested is shown in figure 4.2, as well as the geometric parameters describing it.

4.2.2 Tests with 4 reservoirs, no fronts

A total of 9 series of model tests (45 tests in total) have been conducted using 4 reservoirs without fronts mounted on them. These 9 series have all been performed with $\Delta z = 1.00$ m, $d = 21.4$, $d_r = 11.5$ and $R_{c,1} = 0.5$ m. The purpose of the 9 series of tests has been to study the effect of varying the horizontal placement of the reservoirs. The variation of geometric parameters for the 9 series of tests is shown in table 4.2 in terms of horizontal distance from the line defined by the slope and crest of the reservoirs n, $h_{w,n}$.
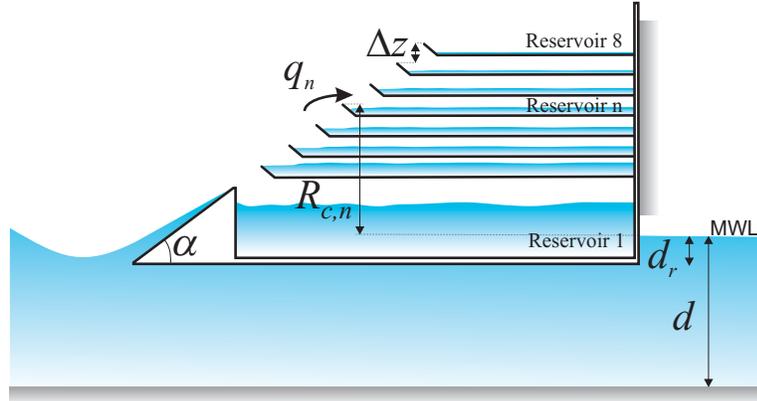
Figure 4.2: Geometric parameters used for multi level reservoirs.

Withdrawal		Test series	$h_{w,2}$	$h_{w,3}$	$h_{w,4}$
	-0.60	C4	-0.60	-1.20	-1.80
Linear	-0.30	C9	-0.30	-0.60	-0.90
	0.00	C3	0.00	0.00	0.00
	0.60	C1	0.60	1.20	1.80
	0.60	C6	0.60	1.20	1.80
	-0.30	C8	-0.30	-0.90	-1.80
Progressive	0.30	C5	0.30	0.90	1.80
	0.60	C2	0.60	1.80	3.60
	0.90	C7	0.90	2.70	5.40

Table 4.2: Tested parameters for the model setup with 4 reservoirs, no fronts.

In figure 4.3 the principal layout of the tested geometries is shown as well as the geometric parameter describing it.
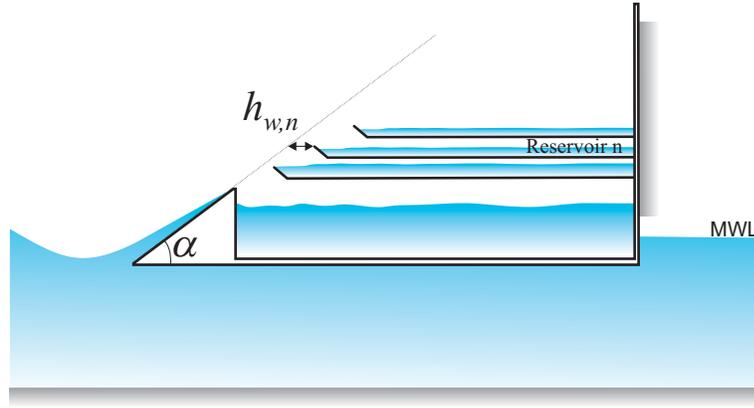
Figure 4.3: Definition of the geometric parameter $h_{w,n}$, horizontal distance from the line defined by the slope and crest of the reservoirs n.

In table 4.2 the series of tests is divided in two. In the first part the horizontal distance from the line defined by the slope and crest of the reservoirs is defined by a linear withdrawal of the reservoirs. This means $h_{w,n}$ increases linearly relative to the reservoir number, e.g., $h_{w,4} = h_{w,3} + 0.60 \ m = 1.80 \ m$. In the second part the horizontal distance from the line defined by the slope and crest of the reservoirs is defined by a progressive withdrawal of the reservoirs. This means $h_{w,n}$ increases progressively relative to the reservoir number, e.g., $h_{w,4} = h_{w,3} + 3 \cdot 0.60 \ m = 3.60 \ m$.

Negative values of the withdrawal thus result in horizontal positions of the reservoir' crest in front of the line defined by the slope.

4.2.3 Tests with 4 reservoirs, with fronts

A total of 16 series of model tests (80 tests in total) have been conducted with 4 reservoirs with fronts mounted on them. The first 12 series has been conducted with the geometric parameters shown table 4.3, where the horizontal opening between reservoir m and n is denoted $h_{l \ n,m}$ and the angle of the n'th reservoir front is denoted θ_n, see also figure 4.4. The purpose of these 12 series of tests has been to study the effect of varying the horizontal placement of the reservoirs with fronts mounted on them.

71

Test series	$R_{c,1}$ [m]	Δz [m]	$h_{l\ n,m}$ [m]	θ_n [°]
D1	0.50	1.00	0.60	50
D2	0.50	1.00	1.20	50
D3	0.50	1.00	1.20	20
E1	1.00	1.33	0.60	50
E2	1.00	1.33	1.20	50
E3	1.00	1.33	1.80	50
E4	1.00	1.33	0.60	35
E5	1.00	1.33	1.20	35
E6	1.00	1.33	1.80	35
E7	1.00	1.33	0.60	20
E8	1.00	1.33	1.20	20
E9	1.00	1.33	1.80	20

Table 4.3: Tested parameters for the model setup with 4 reservoirs with fronts, tests D1 - E9.
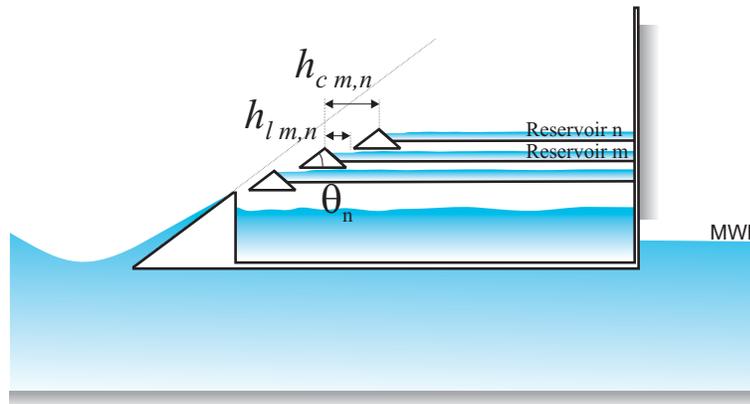
Figure 4.4: Definition of the geometric parameter $h_{l\ m,n}$, horizontal opening between reservoir m and n, and θ_n, angle of the n'th reservoir front.

The second part of the tests using 4 reservoirs with fronts mounted on them is conducted with geometrical setups chosen to find an optimal configuration based on the results of previous tests. These geometries are more complex than the previous ones, and are defined by the parameters presented in table 4.4.

Test series	$R_{c,1}$ [m]	Δz [m]	$h_{l\ 1,2}$ [m]	$h_{l\ 2,3}$ [m]	$h_{l\ 3,4}$ [m]	θ_2 [°]	θ_3 [°]	θ_4 [°]
F1	1.00	1.33	1.20	0.90	0.60	20	35	35
F2	1.00	1.00	1.20	0.90	0.60	20	35	50
F3	1.25	1.00	1.20	0.90	0.60	50	50	35
F4	0.75	1.00	1.20	2.75	2.75	35	20	35

Table 4.4: Tested parameters for the model setup with 4 reservoirs with fronts, tests F1 - F4.

Drawings and pictures of these 4 geometries can be seen in appendix C.3, figures C.9 to C.12.

4.3   Sea states used in model tests

The current study focuses on the performance of the structures tested in terms of the average amount of energy obtained from the overtopping water over a longer period of time (e.g., a year) in Danish waters. Therefore, the structures have been subjected to wave conditions representing average sea states in the Danish part of the North Sea. These sea states are shown in table 4.5, along with their probability of occurrence P_{occur} and their energy contents P_{wave}.

H_s [m]	T_p [s]	P_{occur} [%]	P_{wave} [kW/m]
1.0	5.6	46.8	2.4
2.0	7.0	22.6	11.9
3.0	8.4	10.8	32.2
4.0	9.8	5.1	66.7
5.0	11.2	2.4	119.1

Table 4.5: Sea states typical of the Danish part of the North Sea. The probability and power flux for each of the sea states are provided. The shown sea states cover 85 % of the time.

The data shown in table 4.5 are slightly different from those in table 3.5, section 3.5.5. This is due to updates made to Bølgekraftudvalgets Sekretariat (1999) made in 2000. The average wave energy available on a yearly basis, based on table 4.5, is $P_{wave} = 13.54$ kW/m.

The model tests have been conducted using irregular 2-D waves generated from the parameterized JONSWAP spectrum, as shown in eq. 3.2. Each of the tests conducted consists of 1200 - 2300 irregular waves, depending on wave periods, corresponding to a little under 3 hours (30 min in model scale). In the model tests conducted each of the tested geometries has been subjected to the 5 sea states shown in table 4.5. The five tests of this kind are referred to as a series of tests.

4.4 Model test setup

In order conduct model tests with the described geometries, a flexible model setup was designed. The design of the model setup allowed for moving the deployed reservoirs around in order to enable testing of the various geometries within a limited time frame. The model was set up in a 25 x 1.5 m wave flume (using a water depth of approx. 0.75 m, model scale) at the Hydraulics & Coastal Engineering Laboratory, AAU, using a length scale of 1:30. The layout of the model test setup is shown in figure 4.5, along with photos from the setup.

The test section is placed between two guide walls. This part of the setup occupied only one third of the flume width. The test section can hold up to 8 overtopping reservoirs. Each reservoir is connected by a flexible hose to a tank behind the test section, where the amount of overtopping water is measured. The wave condition to which the section is subjected is measured by wave gauges in front of the test section between the guide walls.

4.4.1 Wave measurements

The wave measuring system consists of an array of wave gauges. The array comprises of 4 wave gauges of the resistance type placed on the center line of the flume. The gauges are placed at a distance of 0.15 m between gauges 1. and 2., 0.25 m between gauges 2. and 3., and 0.60 m between gauges 3. and 4..

Placing 4 gauges at the chosen distances enables separation of incident and reflected irregular waves for the wave conditions used. The separation of incident and reflected irregular waves here relies on the method developed by Funke and Mansard (1979) which uses 3 gauges at a time. Which 3 of the 4 gauges are used depends on the wave conditions.

The method developed by Funke and Mansard (1979) provides the frequency domain parameters as the wave peak period T_p and the spectral estimate of the significant wave height H_{m0}.
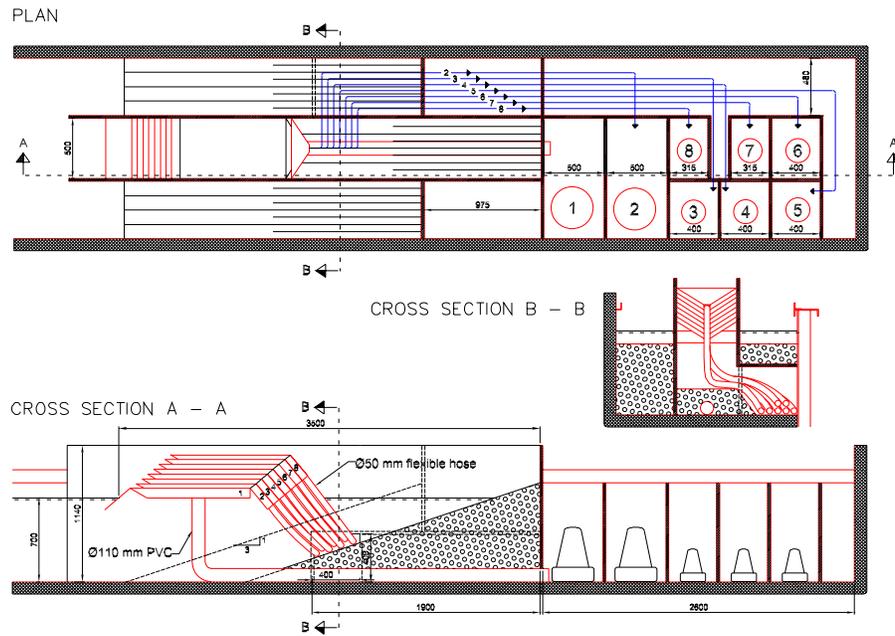
Figure 4.5: *Drawings and photos of the model test setup as constructed in the wave flume. Top: Plan view. Middle: Cross section A - A and B - B. Measures are in mm (model scale). Bottom, left: Model test setup before the flume is filled with water. Bottom, right: The model in action.*

In further analysis of the overtopping discharge, the spectral estimate of the significant wave height H_{m0} found from the frequency domain analysis is used instead of H_s.

4.4.2 Overtopping measurements

The overtopping measuring system deployed in the current model test setup is similar to the one used in the tests described in the previous chapter, except that here 8 tanks are used simultaneously, see figure 4.6. In the current test setup, there is a longer way for the overtopping water to travel before it ends up in the tank where it is measured than was the case in the test setup described in the previous chapter. However, in the current study only average overtopping discharges are of interest and therefore this does not constitutes a problem.

Figure 4.6: Tanks used for measuring overtopping of the 8 reservoirs with pumps and level gauges mounted.

4.5 Comparison of test results with results for single level reservoir

Before analyzing the test results further, it is essential to ensure consistency between the various model tests. This necessitates comparing the results of the model tests conducted using the fixed structure in the wave flume with

the overtopping expression provided in the previous chapter. The measured overtopping discharge for all the tests conducted with the fixed structure has thus been compared with the overtopping expression provided by eq. 3.10. For this purpose the overtopping of all the reservoirs has been summed up and related to the crest freeboard of the lowest reservoir. The results are shown in figure 4.7. The overtopping discharge is made dimensionless as suggested by eq. 3.10

$$Q = \frac{\sum_n^{no.\ of\ res.} q_n}{\lambda_m \lambda_\alpha \lambda_{d_r} \lambda_s \sqrt{gH_s^3}} \tag{4.1}$$

In the current setup $\lambda_m = 1$ and λ_α, λ_{d_r} and λ_s have been calculated according to the conditions.

Likewise, the crest freeboard is made dimensionless as

$$R = \frac{R_{c,1}}{H_s} \frac{1}{\gamma_r \gamma_b \gamma_h \gamma_\beta} \tag{4.2}$$

where $\gamma_r = \gamma_b = \gamma_h = \gamma_\beta = 1$ in the current setup.

The results of the comparison are provided in figure 4.7.

From the figure it can be seen that good agreement is found between the measured data and the predictions provided by eq. 3.10.

4.6 Vertical distribution of overtopping

In this section the results from the tests with 8 reservoirs with fronts are used to establish an expression describing the vertical distribution of the overtopping above the overtopping slope.

4.6.1 Expression for vertical distribution of overtopping

In Kofoed (2002) an expression for the dimensionless derivative of the overtopping discharge with respect to the vertical distance is described as

$$Q' = \frac{\frac{dq}{dz}}{\lambda_s \lambda_{d_r} \sqrt{gH_s}} = Ae^{-B\frac{z}{H_s}} \tag{4.3}$$
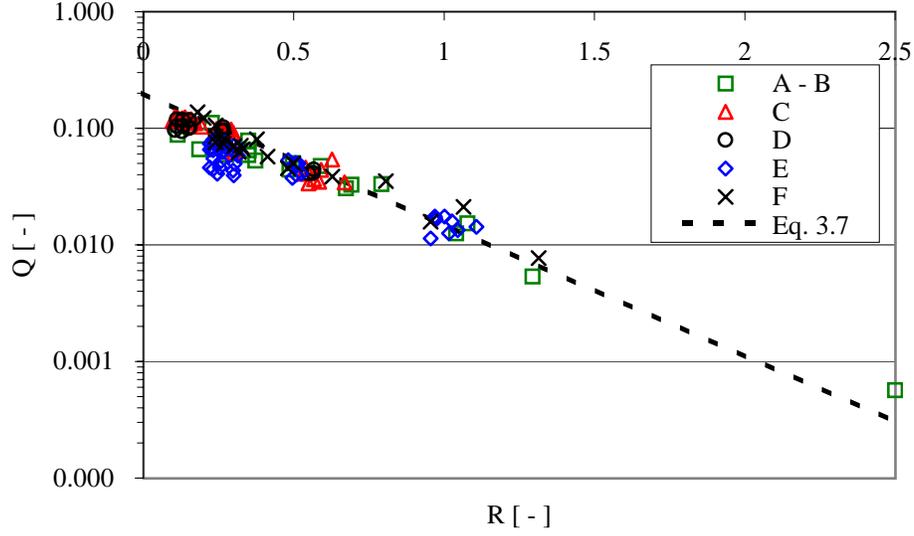
Figure 4.7: Non-dimensionalized total overtopping discharge (sum of all reservoirs) as a function of dimensionless freeboard, compared with eq. 3.10.

where

$$A\left(\frac{z}{H_s}\right) = \begin{cases} 1.50 & \frac{z}{H_s} < 0.8 \\ -1.59\frac{z}{H_s} + 2.79 & for \quad 0.8 \leq \frac{z}{H_s} < 1.5 \\ 0.79 & 1.5 \leq \frac{z}{H_s} \end{cases} \tag{4.4}$$

$$B\left(\frac{z}{H_s}\right) = \begin{cases} 3.00 & \frac{z}{H_s} < 0.8 \\ 0.29\frac{z}{H_s} + 2.77 & for \quad 0.8 \leq \frac{z}{H_s} < 1.5 \\ 3.20 & 1.5 \leq \frac{z}{H_s} \end{cases} \tag{4.5}$$

and z is the vertical distance to the MWL.

From Kofoed (2002) it can be established that eq. 4.3 gives a poor prediction of the overtopping discharge in reservoirs with a configuration significantly different from the setup used for establishing the expression. Kofoed (2002) performed a numerical calculation of the energy obtained using a reservoir configuration like C3 (see table 4.2). This resulted in an overall hydraulic efficiency η_{hydr} of 27.2 % defined as

$$\eta_{hydr} = \frac{\sum_{m=1}^{5} P^m P_{occur}^m}{\sum_{m=1}^{5} P_{wave}^m P_{occur}^m} \tag{4.6}$$

(m indicates the wave situation referring to table 4.5), while the result of the series of tests with C3 yielded $\eta_{hydr} = 12.6$ %. From a closer comparison of the calculation and measurements it is obvious that eq. 4.3 is imperfect because only the vertical distance to the MWL z is included in the expression, but not the crest freeboard of the lowest reservoir (the top of the impermeable slope) $R_{c,1}$. In the following an alternative to eq. 4.3 is established, based on the same data material.

Dimensional analysis demonstrates that

$$\frac{\frac{q}{\sqrt{gH_s^3}}}{\frac{z}{H_s}} = f_1(\frac{z}{H_s}, \frac{R_{c,1}}{H_s}) \tag{4.7}$$

This can be written as

$$\frac{\frac{dq}{dz}}{\lambda_{d_r}\sqrt{gH_s}} = f_2(\frac{z}{H_s}, \frac{R_{c,1}}{H_s}) \tag{4.8}$$

as it has been assumed that the influence of the limited draft can be included using λ_{d_r} as shown in eq. 3.4.

By regression analyses using the data from model tests A1 - B it can be established that an exponential expression for f_2 as eq. 4.9 results in a correlation coefficient $R^2 = 0.96$.

$$\frac{\frac{dq}{dz}}{\lambda_{d_r}\sqrt{gH_s}} = Ae^{B\frac{z}{H_s}}e^{C\frac{R_{c,1}}{H_s}} \tag{4.9}$$

The coefficients A, B, and C have been found to be 0.37, -4.5 and 3.5, respectively.

It should be noted that only data where $\frac{z}{H_s} < 2.5$ are included in the analysis. This choice was made because the overtopping discharges measured for $\frac{z}{H_s} > 2.5$ are very small and there is considerable scatter in these data, due to difficulties in measuring very small overtopping discharges. However, as the emphasis here is on the energy obtained in the overtopping water, and the amount of energy in water for $\frac{z}{H_s} > 2.5$ is negligible, this does not constitute a problem for the current application.

In order to check the performance of eq. 4.9, the expression has been used to calculate the overtopping discharge in the individual reservoirs in a configuration

79
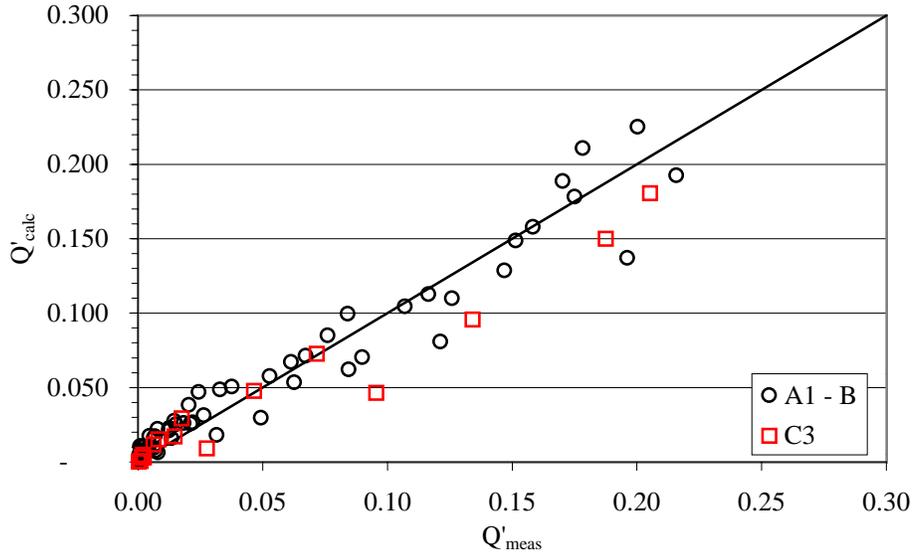
Figure 4.8: Comparison of measured and calculated values of Q' for test series A1 to B and C3. Q' is calculated as described in eq. 4.9.

like C3 and the results are compared with measurements from the model tests in figures 4.8 to 4.11.

In figure 4.8 eq. 4.9 is compared with the data used for the regression analysis (A1 - B), and the data included for validation (C3). As expected, the figure shows good agreement between the expression and the data set A1 - B. For data set C3 there is also good agreement for smaller values of Q'. However, it seems as though the expression underestimates the larger values of Q'.

Figure 4.9 shows how eq. 4.9 predicts the overtopping discharges q_n for the individual reservoirs as a function of sea states characterized by H_s. From the figure it can be seen, as from figure 4.8, that the overtopping discharge in the lowest reservoir is underestimated. For the other reservoirs, eq. 4.9 seems to give a good prediction of q_n. However, when focusing on the energy obtained from the overtopping water, errors in the overtopping discharge are of greater importance the higher the reservoir is placed. This is emphasized by figure 4.10 which shows how eq. 4.9 predicts the energy obtained P_n for the individual reservoirs as a function of sea states characterized by H_s.

From figure 4.10 it can be seen that although the largest errors were found in the overtopping discharge for the lowest reservoir, the errors for the higher reservoirs actually are more important when the focus is on the amount of energy obtained.
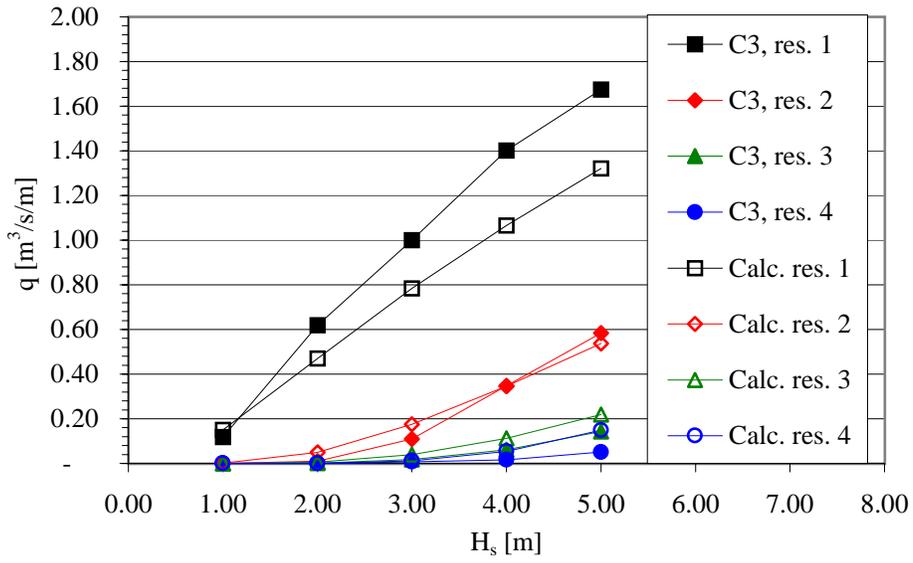
Figure 4.9: Comparison of measured and calculated values of the over-topping discharges for the individual reservoirs q_n for test series C3 as a function of the sea states characterized by H_s.
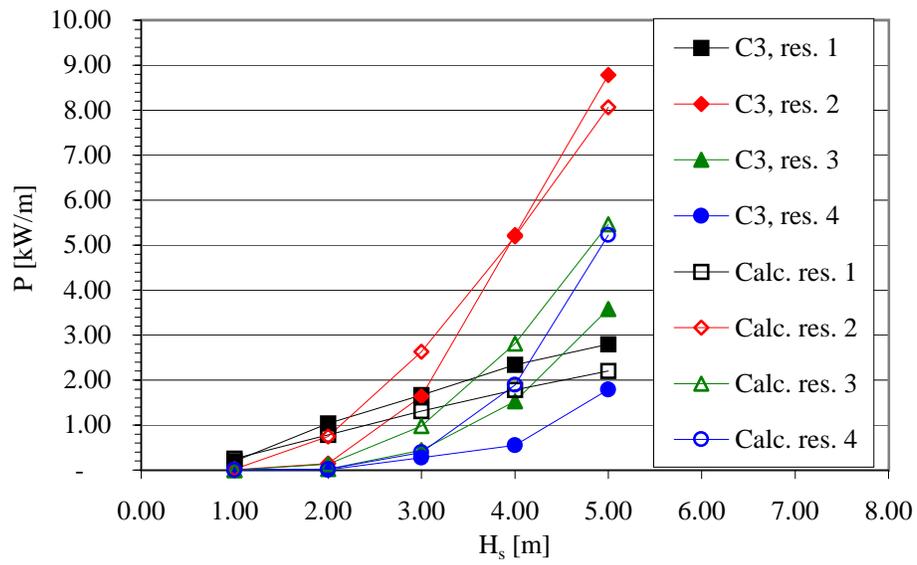
Figure 4.10: Comparison of measured and calculated values of the obtained energy in the individual reservoirs P_n for test series C3 as a function of the sea states characterized by H_s.

In figure 4.11 the hydraulic efficiency for each sea state η_{ws} (defined as $\frac{P}{P_{wave}}$) is given as a function of wave condition characterized by H_s.
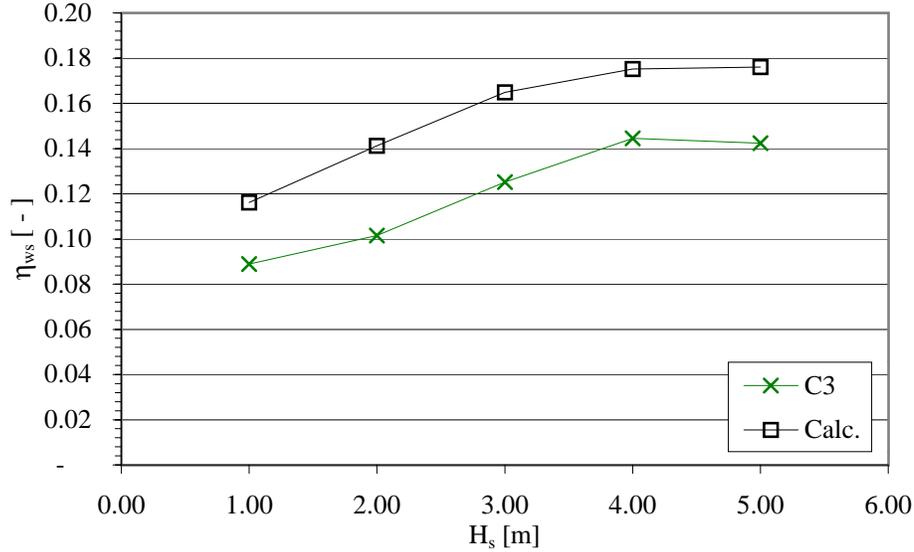
Figure 4.11: Comparison of measured and calculated values of the hydraulic efficiencies η_{ws} for test series C3 as a function of the sea states characterized by H_s.

From figure 4.11 it can be seen that η_{ws} is overestimated in the calculations based on eq. 4.9 for all wave conditions. However, figure 4.10 shows that this is not due to a systematic overestimation of the energy obtained in all reservoirs, but to combinations of over- and underestimations for different reservoirs for different sea states.

The overall hydraulic efficiency estimated through the calculations is found to be $\eta_{hydr} = 16.1$ %. The corresponding value found from the measurements for C3 is $\eta_{hydr} = 12.6$ %, whereas the calculation method used by Kofoed (2002) based on eq. 4.3 resulted in $\eta_{hydr} = 27.2$ %. It can therefore be concluded, although there still is a difference between calculated and measured values, that the expression in eq. 4.9 describes well the vertical distribution of the overtopping discharge. It is at least a considerable improvement over the expression by Kofoed (2002) given in eq. 4.3.

4.7 Numerical optimization of number and vertical placement of reservoirs

The expression describing the vertical distribution of the overtopping over the slope (found in the previous section [eq. 4.9]) has been used in a numerical optimization where the optimal vertical position for reservoir configurations with 1 to 5 reservoirs is established.

4.7.1 Calculation procedure

When calculating the overtopping discharge for the individual reservoir q_n in a system with multi level reservoirs, eq. 4.9 is used. Rewriting eq. 4.9 results in

$$\frac{dq}{dz} = \lambda_{d_r} \sqrt{gH_s} A e^{B\frac{z}{H_s}} e^{C\frac{R_{c,1}}{H_s}} \tag{4.10}$$

$$
\begin{aligned}
q_m(z_1, z_2) &= \int_{z_1}^{z_2} \frac{dq}{dz} dz \\
&= \int_{z_1}^{z_2} \lambda_{d_r} \sqrt{gH_s} A e^{B\frac{z}{H_s}} e^{C\frac{R_{c,1}}{H_s}} dz \\
&= \lambda_{d_r} \sqrt{gH_s^3} \frac{A}{B} e^{C\frac{R_{c,1}}{H_s}} \left(e^{B\frac{z_2}{H_s}} - e^{B\frac{z_1}{H_s}} \right)
\end{aligned}
\tag{4.11}
$$

where z_1 and z_2 denote the lower and upper boundary of the reservoir, respectively. Generally, $z_1 = R_{c,n}$ and $z_2 = R_{c,n+1}$ is used. However, for the top reservoir z_2 is in principle infinite, but can for practical calculations be set at some high value, e.g., two times z_1.

The energy contained in the overtopping water for each level P_n can thus be calculated as:

$$P_n(z_1, z_2) = q_n(z_1, z_2) z_1 \rho_w g \tag{4.12}$$

For WEC's of the overtopping type, the properties of the turbines/generators used to convert the potential energy in the water in the reservoirs into electrical energy is of major importance. Thus, these properties can also influence the optimal placement of the reservoirs. However, no research has been done on what turbines/generators are suitable for use in the PP project, and the impact of the turbines/generators is therefore difficult to include. In order to at least roughly include the impact of turbines/generators, a simplified model of the efficiency of the turbines/generators has been used in evaluating the reservoir configurations. The simplified turbine/generator characteristic used in the following is shown in

eq. 4.13 in terms of the turbine/generator efficiency η_{turb} as a function of the head, here given as the distance from the MWL, z in m.

$$\eta_{turb} = \begin{cases} \frac{z}{1.5} & for \quad 0 < z \leq 1.5 \\ 1 & for \quad z > 1.5 \end{cases} \tag{4.13}$$

This turbine/generator characteristic has been chosen based on the experience of Madsen and Frigaard (2000).

The total energy for a single wave situation P is calculated as the sum

$$P(H_s) = \sum_{n}^{no.\ of\ res.} P_n(z_1, z_2)\eta_{turb}(z_1) \tag{4.14}$$

To evaluate the performance of a setup of reservoirs, the overall hydraulic efficiency of the system η_{hydr} is calculated as shown in eq. 4.6.

4.7.2 Results of optimization

The results of the optimization are shown in table 4.6 in terms of the optimal vertical placements of reservoirs found ($R_{c,n}$'s) and the resulting overall hydraulic efficiency η_{hydr} for 1 to 5 reservoirs.

No. of reservoirs	$R_{c,1}$ [m]	$R_{c,2}$ [m]	$R_{c,3}$ [m]	$R_{c,4}$ [m]	$R_{c,5}$ [m]	η_{hydr} [%]	$\frac{\eta_{hydr}^{no.\ of\ res.}}{\eta_{hydr}^{1}}$ [-]
1	2.86					34.8	1.00
2	2.58	3.34				38.1	1.09
3	2.45	2.91	3.72			39.7	1.14
4	2.38	2.72	3.21	4.05		40.7	1.17
5	2.33	2.60	2.96	3.47	4.34	41.4	1.19

Table 4.6: Results of numerical optimization of placement of reservoirs for different numbers of reservoirs.

The results in table 4.6 are also shown in figure 4.12.

From table 4.6 and figure 4.12 it can be seen that the numerical optimization indicates that moving from 1 to 5 reservoirs results in an increase in η_{hydr} of 19 %. However, it should be noted that using eq. 4.9 for calculating the performance of a single level configuration might be carrying things too far. By way of
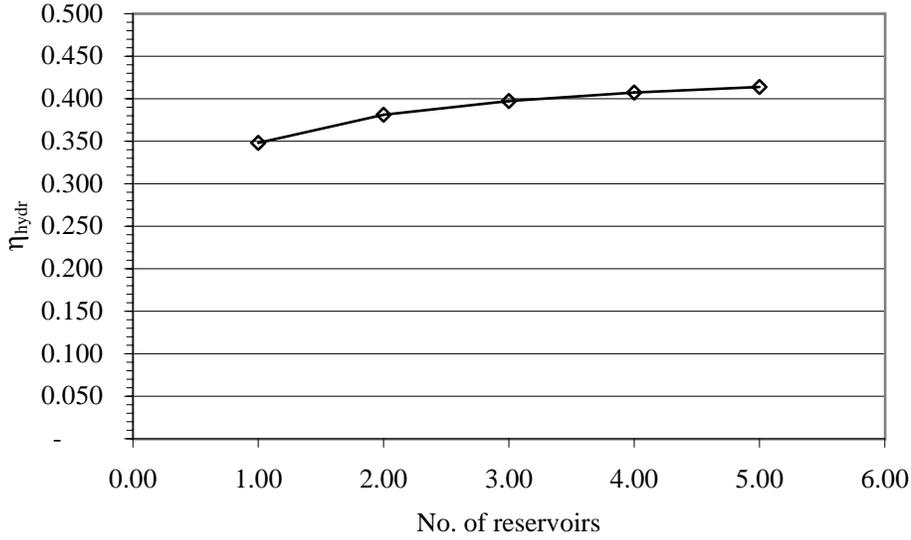
Figure 4.12: Graph of data shown in table 4.6

comparison, an optimization has been performed for a single level reservoir in a similar manner to that sketched in the previous section. In this instance, though, eq. 3.10 (the expression for overtopping discharge of a single reservoir found in the previous chapter) is used to calculate the overtopping discharge instead of the integration of eq. 4.9 given in eq. 4.11. This results in a $\eta_{hydr} = 28.7$ % for an optimal $R_{c,1} = 1.50$ m. If this is used as reference, moving from 1 to 5 reservoirs then results in an increase in η_{hydr} of 44 %.

In general terms the optimization shows that using 3 or more reservoirs placed around 3 m above the MWL with a Δz 0.3 to 0.8 m (depending on the number of reservoirs) results in a η_{hydr} around 40 %.

4.8 Optimization of reservoir configuration and front geometry

Model tests have been conducted to determine how the horizontal distance between the reservoirs and the geometry of fronts on reservoirs influence the amount of energy obtained. At first the effect of the horizontal distance between the reservoirs is studied without fronts on the reservoirs. Then combinations of various distances between reservoirs and varied front geometries are studied.

4.8.1 Model tests with varied horizontal distance between reservoirs

In figure 4.13 the results of tests using varying horizontal distance between the reservoirs without fronts are shown in terms of hydraulic efficiency for each wave condition η_{ws} as a function of the sea state. The data used for figure 4.13 can be found in table C.2, appendix C.2.
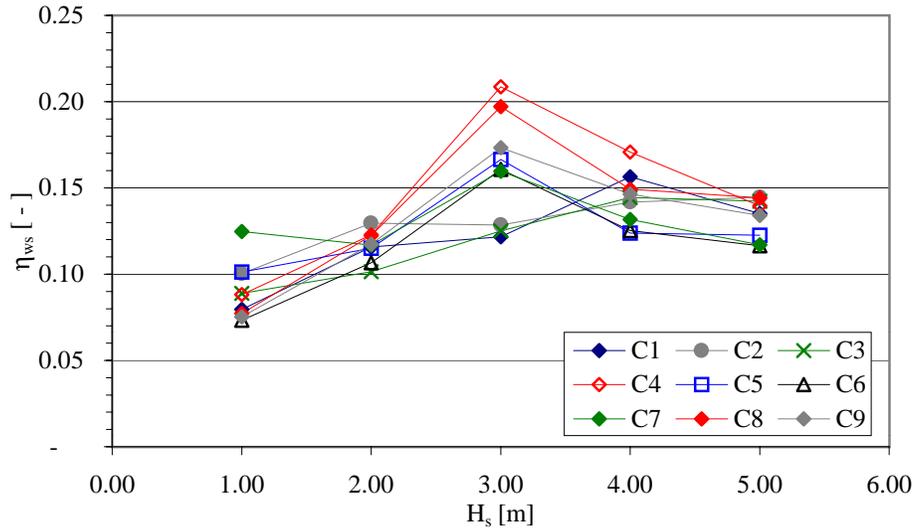
Figure 4.13: Hydraulic efficiency η_{ws} given as a function of the sea state, characterized by the significant wave height H_s, for model tests C1 - C9.

In figure 4.14 the results are presented as overall hydraulic efficiencies as a function of the horizontal withdrawal. The definition of horizontal withdrawal is given in section 4.2.2, table 4.2.

From figure 4.14 it can be seen that changing the horizontal placement can increase η_{ws} by 25 % (from 12.6 % for C3, reservoirs on the line defined by the slope, to 15.8 % for C4, reservoirs placed in front of the line defined by the slope). However, as the reservoirs are expected to be equipped with fronts it makes no sense to have negative withdrawal. In that case the fronts would be likely to cover the entry to the reservoir below.

87
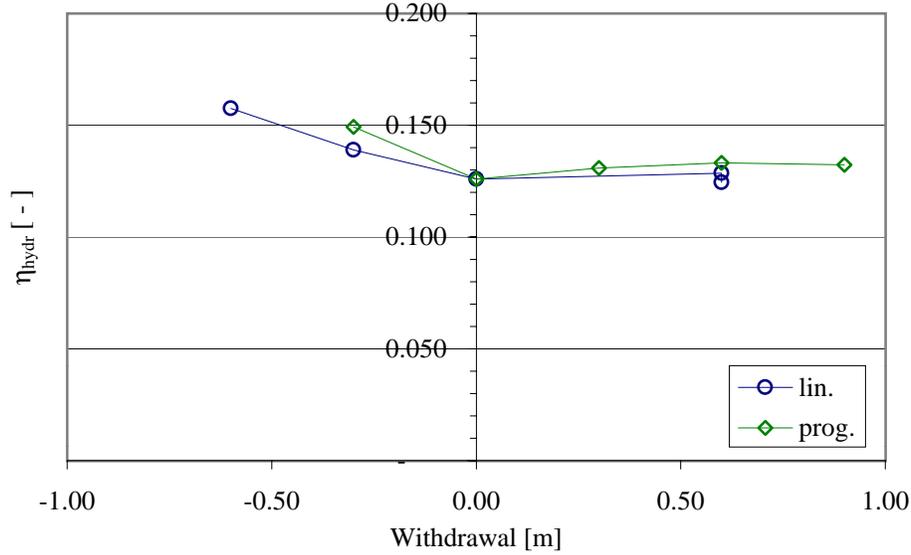
Figure 4.14: Overall hydraulic efficiency η_{hydr} shown as a function of the withdrawal as shown in table 4.2.

4.8.2 Model tests with various front geometries

The results of the model tests with various front geometries given in table 4.3 are shown in figures 4.15 to 4.19.

The results for D1 - D3 are shown in figure 4.15. The overall hydraulic efficiencies η_{hydr} for D1, D2 and D3 are 23.8, 21.6 and 23.7 %, respectively.

Based on the results of D1 - D3 the configurations E1 - E9 were selected in order to investigate more systematically the influence of the horizontal opening between the reservoirs $h_{l\ m,n}$ and the angle of the fronts of the reservoirs θ_n.

The results for E1 - E9 are shown in figure 4.16. The overall hydraulic efficiency η_{hydr} is given in table 4.7.

The results from table 4.7 are also presented in figures 4.17 and 4.18.

Furthermore, in figure 4.19, the overall hydraulic efficiency η_{hydr} is given as a function of the horizontal distance between the reservoir crests $h_{c\ m,n}$. The definition of $h_{c\ m,n}$ is also given in figure 4.4.
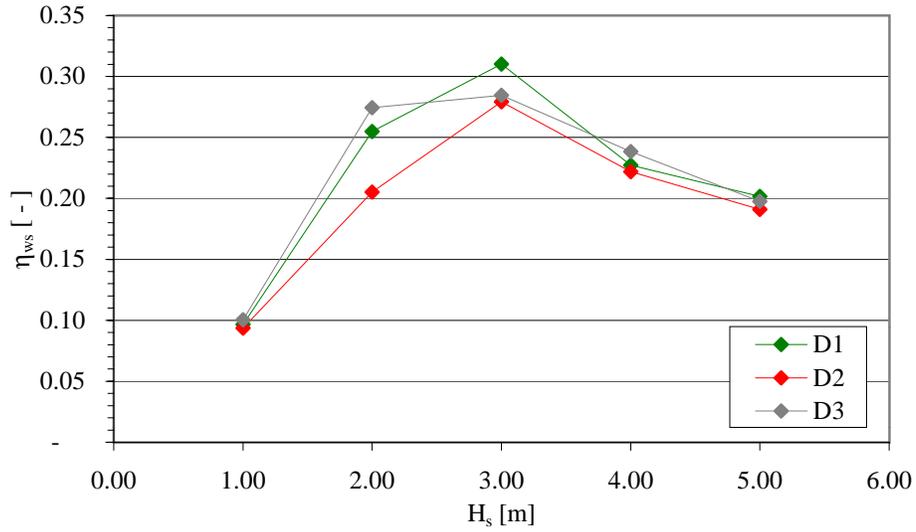
Figure 4.15: Hydraulic efficiency η_{ws} shown as a function of the sea state, characterized by the significant wave height H_s, for model tests D1 - D3.
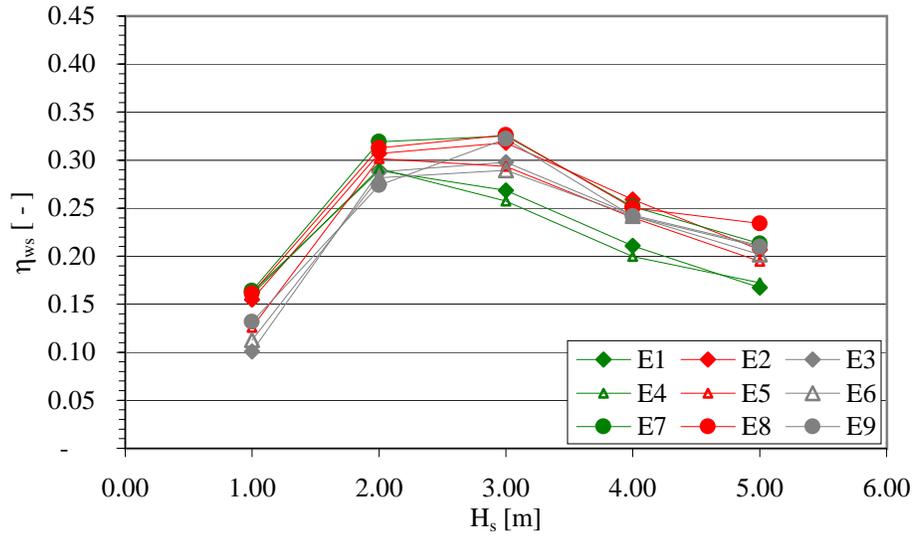
Figure 4.16: Hydraulic efficiency η_{ws} shown as a function of the sea state, characterized by the significant wave height H_s, for model tests E1 - E9.

Test series	η_{hydr} [%]	$h_{l\ n,m}$ [m]	θ_n [°]
E1	22.8	0.60	50
E2	26.4	1.20	50
E3	24.8	1.80	50
E4	22.4	0.60	35
E5	24.7	1.20	35
E6	23.4	1.80	35
E7	26.7	0.60	20
E8	27.1	1.20	20
E9	25.3	1.80	20

Table 4.7: Results of the model tests E1 - E9 in terms of overall hydraulic efficiency η_{hydr}.
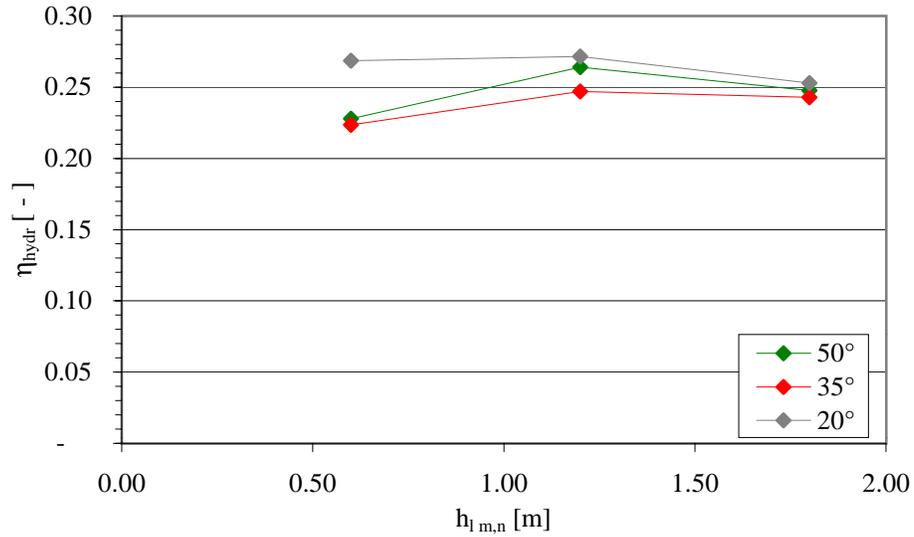
Figure 4.17: Overall hydraulic efficiency η_{hydr} shown as a function of the horizontal opening between the reservoirs $h_{l\ m,n}$.
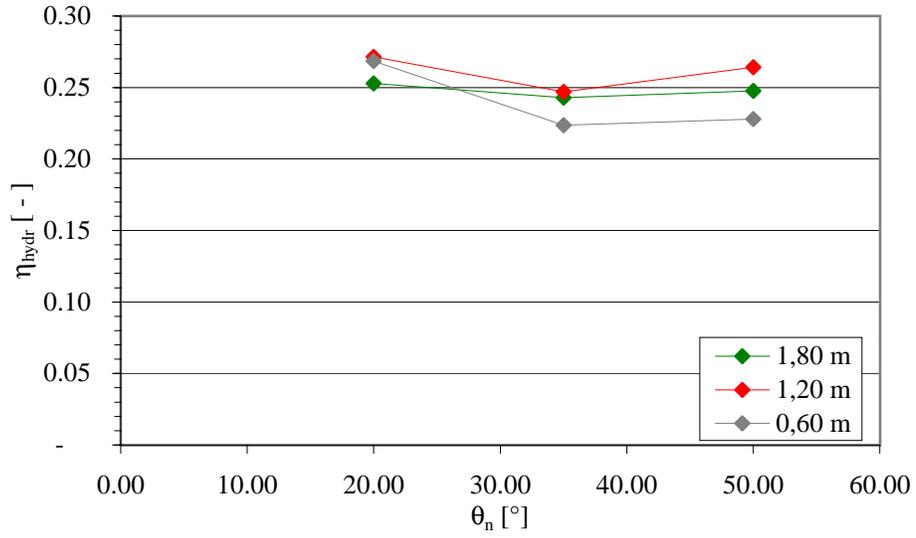
Figure 4.18: Overall hydraulic efficiency η_{hydr} shown as a function of the reservoir front angle θ_n.
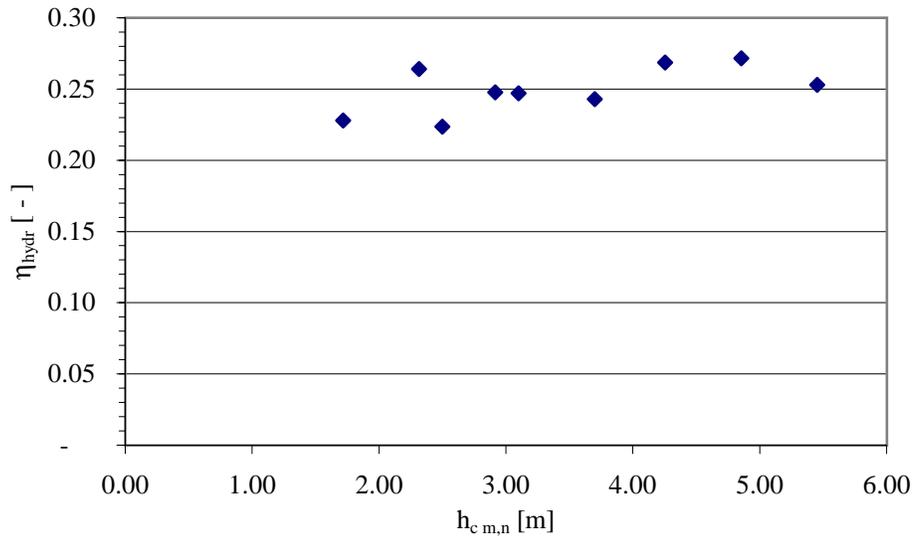
Figure 4.19: Overall hydraulic efficiency η_{hydr} shown as a function of the horizontal distance between reservoir crests $h_{c\ m,n}$.

Figure 4.17 indicates that $h_{l\ m,n} = 1.20$ m is a reasonable overall value. The figures 4.17 to 4.19 provides no other obvious conclusions as to what is an optimal configuration.

In order to try to find an optimal configuration, 4 different configurations have been tested. These configurations were selected based on more detailed studies of the results of all the tests performed so far (all these results can be found in appendix C.3). In particular, figure C.13 in appendix C.3 proved valuable in the evaluation of the test results for E1 - E9.

The geometries of these 4 configurations, F1 - F4, are shown in appendix C.3, figures C.9 to C.12.

The results for F1 - F4 are shown in figure 4.20.
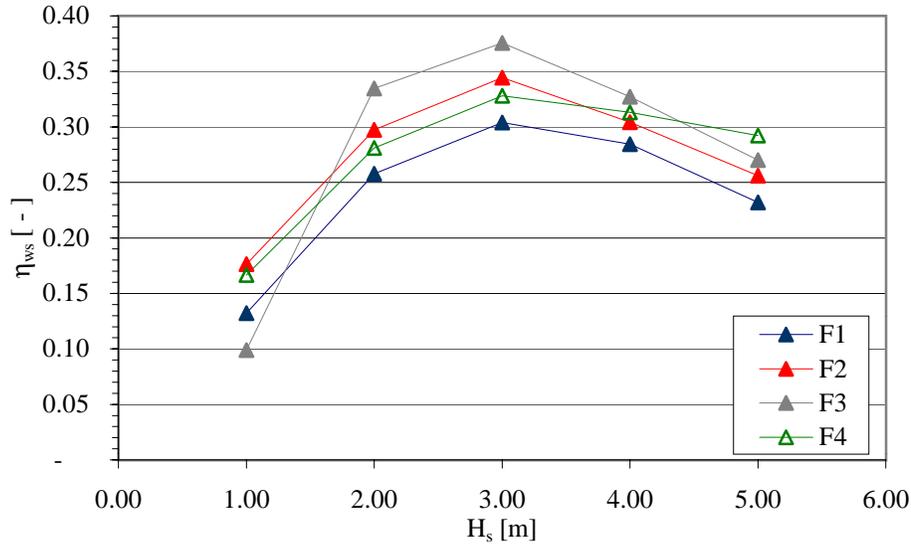
Figure 4.20: Hydraulic efficiency η_{ws} shown as a function of the wave situation characterized by the significant wave height H_s for model tests F1 - F4.

The overall hydraulic efficiencies η_{hydr} for F1, F2, F3 and F4 are 26.0, 29.3, 31.0 and 29.4 %, respectively.

In general terms, the last tests showed that by using 4 reservoirs equipped with fronts, an overall hydraulic efficiency η_{hydr} of roughly 30 % can be achieved for a crest freeboard for the lowest reservoir $R_{c,1}$ around 1.0 m.

Kofoed (2002) decided to conduct further testing of a floating model using a reservoir front configuration similar to F2, except for θ_4, which was changed from 50° to 35°. This configuration is referred to in the following as F2^{mod}.

Calculations based on eq. 4.9 resulted in $\eta_{hydr} = 16.1$ % for a vertical placement of the reservoirs as used in the tests with 4 reservoirs without fronts, $R_{c,1} = 0.5$ m (C1 - C9). The measurements showed that this was achievable for a certain horizontal reservoir placement (C4). A similar calculation for a vertical placement of the reservoirs as used in the tests E1 - E9, but without the fronts mounted on the reservoirs, results in $\eta_{hydr} = 24.2$ %. As η_{hydr} was found to be 27.1 % for E8, it appears that mounting fronts on the reservoirs can increase η_{hydr} by approx. 12 %.

A numerical optimization of $R_{c,1}$ with $\Delta z = 1.33$ m, as used in the tests E1 - E9, but without the fronts mounted on the reservoirs ($R_{c,1}$ constant in the 5 sea states but varied in the optimization) shows that using $R_{c,1} = 2.5$ m results in $\eta_{hydr} = 40.8$ %. Adding 12 % for mounting fronts on the reservoirs means that an η_{hydr} around 45 % should be expected.

Another similar numerical optimization showed that if $R_{c,1}$ is not kept constant and the same for all wave conditions, but adjusted to the optimal value for each wave condition, an $\eta_{hydr} = 43.5$ can be obtained. The detailed results of the optimizations are shown in table 4.8. Adding 12 % for mounting fronts on the reservoirs means that an η_{hydr} around 49 % should be expected.

H_s [m]	$R_{c,1}$ [m]	P [kW/m]	η_{ws} [-]
1	1.50	0.8436	0.3553
2	1.89	5.2761	0.4430
3	2.73	14.4791	0.4502
4	3.58	29.5665	0.4433
5	4.20	51.0489	0.4286

Table 4.8: Results of the optimization for a vertical placement of the reservoirs as used in the tests E1 - E9, but without the fronts, where $R_{c,1}$ is adjusted to the optimal value for each sea state.

4.9 Floating WEC with multi level reservoirs

Based on the model tests carried out using fixed structures, as described in the previous section, and drawing on experience from earlier work on the PP project (Kofoed and Frigaard [2000a]), Kofoed (2002) redesigned the PP. The results of the model tests with fixed structures were incorporated into the new version of the PP, as the front configuration F2^{mod} is used. The new version of the PP is presented in figure 4.21.

Figure 4.21: Drawings showing the redesigned Power Pyramid.

Tests using the floating model of the redesigned PP have been carried out in the deep water 3-D wave tank at the Hydraulics & Coastal Engineering Laboratory, AAU using a length scale of 1:45. Photos of the floating model are shown in figure 4.22.

4.9.1 Measuring systems

Four systems for measuring waves, overtopping, movement and mooring forces have been deployed in the test setup used with the floating model. Wave and overtopping measuring systems similar to the systems used with the fixed structure have been deployed. The tanks in the overtopping measuring system have been placed outside the basin, and long flexible hoses have been used to connect between model and tanks in order to minimize their influence on the movement of the structure.

Heave, pitch and surge movements of the model have been measured using three non-contact ultrasonic displacement sensors. Two vertical sensors measured heave and pitch, and a horizontal sensor measured surge. The results of the measurements of heave, pitch and surge will not be discussed in this work (details of this subject can be found in Kofoed [2002]). However, as the model was floating, and the water in the reservoirs was not kept at a constant level, the waves and the overtopping caused the vertical position of the crest of the reservoirs to vary over time. From the measured heave, pitch and surge, the variation in the vertical position of the crest of the reservoirs has been calculated and recorded. In the analysis of the test results, the mean value of the recorded time series of the vertical position has been used as the crest freeboard of the lowest reservoir $R_{c,1}$.

Also, the mooring force of the floating model has been measured, but the results of these measurements will not be discussed further (again, details of this subject can be found in Kofoed [2002]).

4.9.2 Test results

The test results reported in this section focus on the energy obtained from the overtopping water. The tests have been carried out in three groups. First, tests corresponding to F2 with the fixed structure were conducted, i.e., producing $R_{c,1} = 1.00$ m. Second, tests were conducted to produce $R_{c,1} = 1.25$ m in order to observe the effect of altering the $R_{c,1}$, while still keeping it constant for all sea states. Finally, tests were conducted to find the optimal $R_{c,1}$ for each sea state separately.

Figure 4.22: Photos of the floating model of the Power Pyramid in calm water (top) and in action in irregular waves (bottom).

When conducting the tests it was not possible to set the $R_{c,1}$ to an exact value prior to each individual test. Thus, when aiming for a certain $R_{c,1}$ it typically took some trial and error to reach the target value. Therefore, a larger number of tests have been performed than at first seemed necessary (a total of 43 tests were performed). The results of all the tests are given in appendix C.4, table C.6. The results are also shown in figure 4.24.

To check that the results are sound, they are at first compared with results for a single level reservoir.

Comparison with results for single level reservoir

As for the tests with the fixed structure, the overtopping discharge measured for the tests conducted with the floating model is compared with the overtopping expression given by eq. 3.10. The procedure for comparison is the same as for the fixed structure, see section 4.5. The results of the comparison are shown in figure 4.23.
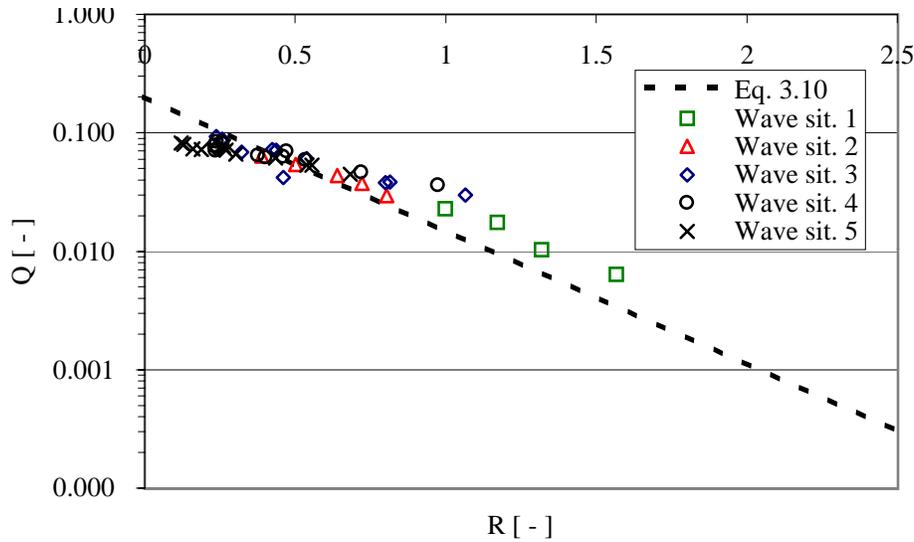
Figure 4.23: Non-dimensionalized total overtopping discharge (sum of all reservoirs) as a function of dimensionless freeboard, compared with eq. 3.10.

A fair agreement between the total overtopping discharge measured for the floating model and the prediction by eq. 3.10 can be observed from figure 4.23, although some discrepancies exists.

97

There are at least two circumstances which can explain these discrepancies. As already touched upon, $R_{c,1}$ is not very well defined throughout the tests conducted for the floating model, but is taken as the mean of the vertical position of the crest. As overtopping is a highly non-linear process, this might result in errors. Another possible reason for the discrepancy is that the capacity of the hoses leading from the reservoirs to the tanks outside the basin, where the overtopping discharges are measured, had an upper limit. Overflow of the reservoirs was for this reason occasionally observed during tests with the largest waves, combined with low crest freeboards. This mean that the overtopping discharges measured under such conditions probably are lower than the actual. This is the most likely reason why results for sea state 5 with $R < 0.4$ fall under the prediction line.

Energy obtained

To compare the performance of the fixed and floating model for the configuration $F2^{mod}$, five tests (one for each sea state) with a $R_{c,1}$ as close to 1.00 m as possible have been selected from the data in table C.6 in appendix C.4 (also shown in figure 4.24). These are summarized in table 4.9.

H_s [m]	Test	$R_{c,1}$ [m]	η_{ws} [-]	P_{occur} [%]	P_{wave} [kW/m]	P [kW/m]	Obt./year [MWh]
1	D2BS1	1.00	0.20	46.8	2.4	23.2	84.8
2	D5BS2	0.99	0.36	22.6	11.9	216.6	382.1
3	D1BS3	0.97	0.35	10.8	32.2	556.8	469.4
4	E13BS4	0.98	0.31	5.1	66.7	1018.2	405.3
5	D6BS5	0.94	0.17	2.4	119.1	1002.4	187.8
Total							1529.5

Table 4.9: Results of tests with the floating model, $R_{c,1} \sim 1.00$ m.

In table 4.9 the total amount of energy obtained from the overtopping water over a year (obt./year) is found to be 1529.5 MWh. If this is compared with the amount of energy available to the WEC (5284 MWh), the overall hydraulic efficiency is found to be $\eta_{hydr} = 28.9$ %. This compares very well with the results of tests F2 from the fixed model setup, for which $\eta_{hydr} = 29.3$ %.

Then five tests (one for each sea state) with a $R_{c,1}$ as close to 1.25 m as possible are selected from appendix C.4, table C.6. These are summarized in table 4.10.

In table 4.10 the total amount of energy obtained from the overtopping water over a year (obt./year) is found to be 2003.6 MWh. This results in an overall hydraulic efficiency of $\eta_{hydr} = 37.9$ %. This is considerably higher than the
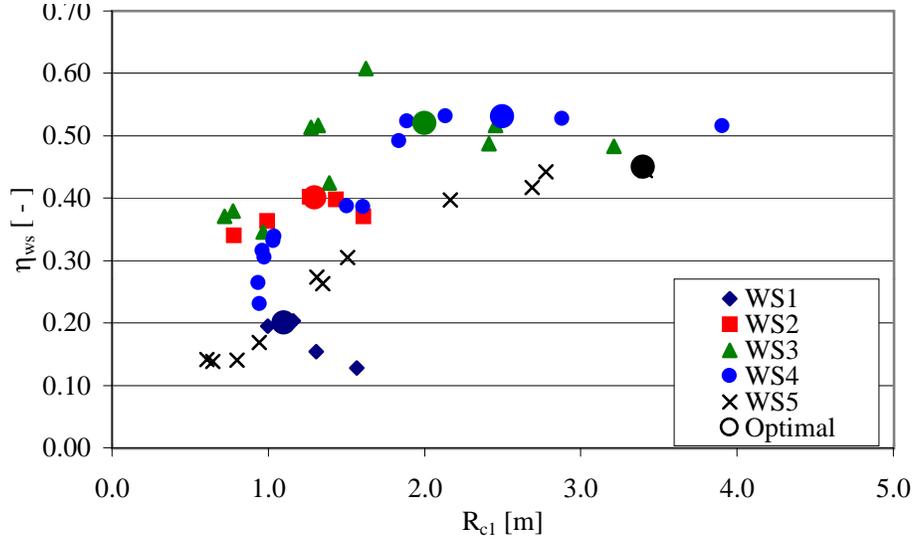
Figure 4.24: Hydraulic efficiency η_{ws} shown as a function of the crest freeboard of the lowest reservoir $R_{c,1}$ for tests with the floating model. The values of $R_{c,1}$ considered the optimal for each of the five sea states are marked with large circular dots in corresponding colors.

H_s [m]	Test	$R_{c,1}$ [m]	η_{ws} [-]	P_{occur} [%]	P_{wave} [kW/m]	P [kW/m]	Obt./year [MWh]
1	E2BS1	1.30	0.15	46.8	2.4	18.3	66.9
2	D4BS2	1.26	0.40	22.6	11.9	239.6	422.8
3	D2BS3	1.27	0.51	10.8	32.2	825.3	695.8
4	E3BS4	1.50	0.39	5.1	66.7	1287.9	512.7
5	D3BS5	1.31	0.27	2.4	119.1	1629.9	305.3
Total							2003.6

Table 4.10: Results of tests with the floating model, $R_{c,1} \sim 1.25$ m.

result obtained from F3 in the fixed model setup, where $\eta_{hydr} = 31.0$ % for a $R_{c,1} = 1.25$ m.

Finally five values of $R_{c,1}$ and η_{ws} (one for each wave situation) are selected from table C.6 in appendix C.4. Optimal here means the values of $R_{c,1}$ and η_{ws}, which seem to represent the $R_{c,1}$ that results in the highest η_{ws}, based on all the tests conducted with the floating model, for each wave situation, taking into account the scatter present in the data material. These estimated values, also presented in figure 4.24, and the resulting performance are summarized in table 4.11.

H_s [m]	$R_{c,1}$ [m]	η_{ws} [-]	P_{occur} [%]	P_{wave} [kW/m]	P [kW/m]	Obt./year [MWh]
1	1.10	0.20	46.8	2.4	23.8	86.9
2	1.30	0.40	22.6	11.9	238.2	420.2
3	2.00	0.52	10.8	32.2	836.2	704.9
4	2.50	0.53	5.1	66.7	1767.6	703.7
5	3.40	0.45	2.4	119.1	2680.0	502.1
Total						2417.8

Table 4.11: Estimated optimal conditions and the resulting performance, based on tests with the floating model.

In table 4.11 the total amount of energy obtained from the overtopping water over a year (obt./year) is found to be 2417.8 MWh. This results in an overall hydraulic efficiency of $\eta_{hydr} = 45.8$ %, which can be compared with the results of the calculations in section 4.8.2. Those results show that a geometry with $\Delta z = 1.00$ m, fronts mounted (resulting in an increase of η_{hydr} of 12 %) and $R_{c,1}$ selected to the optimal value for the individual wave situation, results in $\eta_{hydr} \sim 49$ %. However, the 49 % relies on extrapolations of measured data and calculations, and also the results from table 4.11 are estimates, so the results may be inaccurate to some degree. Nevertheless, it is reasonable to conclude that an η_{hydr} of 45 - 50 % is achievable for a floating WEC with reservoirs at 4 levels, if the floating level (crest freeboard) is adjusted to the individual wave situations.

When considering the actual output of energy from a WEC of the type tested it should be realized that the water level in each of the reservoirs cannot continuously be kept at the same level as the crests (as it is assumed in the calculation of η_{hydr}). There will be significant periods of time when the crest level and the water level in the reservoir differ. This is due to the fact that if, on one hand, the turbines are controlled so that the water level is always kept very close to the crest, and the reservoir has a limited area, large overtopping events will result in overflow of the reservoir, leading to loss of energy. On the other hand, if the turbines are controlled so that the water level in the reservoir is well below

the crest, there will be room for the next large overtopping event; however, as the water is not kept at the level it reaches when it passes the crest, but at a considerably lower level, a loss of energy also occurs under these conditions. Thus, it is of paramount importance to control the turbines very accurately, and thereby the water level in the reservoirs in order to prevent a too large a loss of energy. This problem can be helped by predicting the overtopping events to come by measuring the waves in front of the WEC and adjusting the control of the turbines accordingly.

In order to quantify the loss of energy described, a calculation has been done in which it has been assumed that the head available for the turbines is not the difference between the MWL and the crest level of the reservoir; rather it is the difference between the MWL and the water level of the reservoir. In the calculation the distance from the water level in the reservoir and the crest level has been set to 0.3 m, based on experience from the work done on the WD project, see, for example, Madsen and Frigaard (2000).

The results of this calculation are given in figure 4.25 and table 4.12.
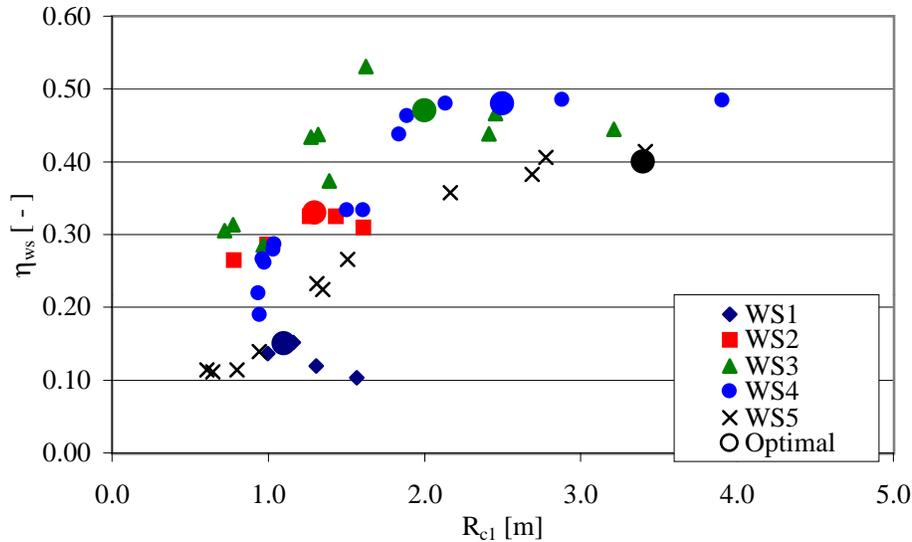
Figure 4.25: Hydraulic efficiency η_{ws} given as a function of the crest freeboard of the lowest reservoir $R_{c,1}$ for tests with the floating model. In the calculation of η_{ws}, 0.3 m is subtracted from the R_c of each reservoir. The values of $R_{c,1}$ considered the optimal for each of the 5 sea states, are marked with large circular dots in corresponding colors.

H_s [m]	$R_{c,1}$ [m]	η_{ws} [-]	P_{occur} [%]	P_{wave} [kW/m]	P [kW/m]	Obt./year [MWh]
1	1.10	0.15	46.8	2.4	17.9	65.2
2	1.30	0.33	22.6	11.9	196.5	346.7
3	2.00	0.47	10.8	32.2	755.8	637.1
4	2.50	0.48	5.1	66.7	1600.8	637.3
5	3.40	0.40	2.4	119.1	2382.2	446.3
Total						2132.6

Table 4.12: Estimated optimal conditions and the resulting performance, based on tests with the floating model. In the calculation of η_{ws}, 0.3 m is subtracted from the R_c of each reservoir.

In table 4.11 the total amount of energy obtained from the overtopping water over a year (obt./year) is now found to be 2132.6 MWh. This results in an overall hydraulic efficiency of $\eta_{hydr} = 40.4$ %. Thus, the loss of energy due to the difference between the water level in the reservoir and the reservoir crest is roughly 15 %.

CHAPTER 5

Conclusion

In this chapter conclusions are drawn from the studies conducted.

The concept of utilizing wave overtopping in WEC's has been described. Examples of such devices have been presented. It was evident from the existing knowledge that additional investigations into overtopping of these devices were needed.

Hydraulic model tests have been conducted using varying slope geometries with single and multi level reservoirs. Non-floating, as well as floating structures, have been used during the tests. All tested setups have been subjected to a wide range of sea states. An overtopping discharge measuring device was developed during the design of the model test. This device allows for the measurements of both small and large overtopping discharges with good resolution.

The results of the model tests have been compared with results from the literature. A new overtopping expression for non-breaking waves on smooth impermeable slopes with a single overtopping reservoir is presented. This new expression is based on an expression given by Van der Meer and Janssen (1995). The original formula has been modified by application of correction factors to include the effect of:

- Slope angle.
- Low relative crest freeboards.
- Limited draft.
- Various slope shapes and side wall geometries.

103

With the new expression it is possible to predict overtopping discharges of structures suited for use as part of WEC's. Therefore, it also allows for predicting the amount of energy captured from the overtopping waves. Thus, the new expression facilitates the design and optimization of WEC's of the overtopping type.

The existing empirical model for the time dependency of overtopping discharges, presented by Martinelli and Frigaard (1999a), has been validated using some of the test results.

Model tests with multiple level reservoirs have been used for establishing an expression describing the vertical distribution of overtopping discharge above the slope crest. The effect of using reservoirs at multiple levels has been quantified. Furthermore, the effect of varying the horizontal distance between the reservoirs and of mounting fronts on the reservoirs has been quantified by model tests.

The effect of adjusting the crest freeboard to suit the individual sea states has been quantified both by means of combining the results of the model tests and the established expressions, and by model tests with a floating model of a structure with multiple level reservoirs.

5.1 Single level reservoirs

The correction factor describing effects of the slope angle has been included in the new overtopping expression. This is an extension of the existing overtopping expression for non-breaking waves presented by Van der Meer and Janssen (1995).

The model tests have also "closed the gap" between existing investigations for low crest freeboards. The proposed expression allows for the prediction of overtopping discharges for relative crest freeboards down to 0.

Furthermore, the new expression also includes the effect of limited draft, allowing for the prediction of overtopping discharge for structures with limited draft, such as floating structures.

A number of slope shapes and side wall layouts have also been tested. In terms of maximizing overtopping, it is favorable to apply the following layouts:

- A horizontal plate at the slope bottom with a length of 25 % of the slope draft (BA02, $\lambda_m = 1.07$).

- A convex top of the slope with an elliptic shape (CC01, $\lambda_m = 1.18$).

- Linear guiding walls with an opening ratio of 0.848 (EA01, $\lambda_m = 1.15$).

The tests with the convex top of the slope indicate that the slope angle needs to be increased as the convexity of the slope top is increased (geometry CC01 resulting in the largest increase of the overall overtopping discharge has a slope angle of 45°, and a large part of the slope is convex with an elliptical shape).

The estimations given in section 3.5.5 for the tests with linear slopes, combined with the results of the tests with modified slopes, indicate that overall hydraulic efficiency η_{hydr} can be 20 - 35 % (depending on the geometry of the slope and the side walls) if the structure is placed in the Danish part of the North Sea.

5.2 Multi level reservoirs

Numerical calculations based on the expression for the vertical distribution of overtopping discharge have shown that using 3 or more reservoirs results in an η_{hydr} near 40 %. To obtain this efficiency in the Danish part of the North Sea, the reservoirs could be positioned at 2.5, 2.9 and 3.7 m above the MWL. However, a validation of the established expression revealed a discrepancy of ∼25 % between the measured and the calculated η_{hydr}.

Comparisons of tests with and without fronts mounted on the reservoirs indicate that an increase of η_{hydr} of ∼12 % (from $\eta_{hydr} = 24.2$ % without fronts to 27.1 % with fronts, tests E8) is achieved by mounting the fronts.

By combining numerical calculations using the expression for the vertical distribution of overtopping, and measurements from tests with fronts on the reservoirs, an optimal η_{hydr} of ∼45 % can be achieved. If the floating level is adjusted according to the individual sea state, an η_{hydr} of as high as ∼49 % can be achieved.

Tests with the floating model generally agree reasonably well with the results from the fixed model tests. An overall efficiency of 47 % was found when the floating level was optimized for the individual sea states. This is slightly lower than the figure estimated from the tests with the fixed model. It is reasonable to conclude that an η_{hydr} of 45 - 50 % is achievable for a floating WEC with reservoirs at 4 levels, if the floating level (and thereby the crest freeboards) is adjusted to the individual sea states.

5.3 Further research

The tests of modified slope shapes have disclosed areas where additional testing is needed in order to investigate in more detail the positive effects on the overtopping already found (in terms of maximizing the energy content in the

overtopping discharge). It seems that additional tests with horizontal plates at the slope bottom, with a convex top of the slope with an elliptic shape, and with linear guiding walls with an opening ratio in the range of 0.7 to 1.0 could lead to even larger increases in the overall overtopping discharges.

An investigation of how a combination of some of the geometries interact, resulting in increases of the overtopping discharge, would also be interesting. It would be interesting to find out if more than one λ_m can be applied simultaneously, as this would mean that an increase in the overtopping discharge (and thereby also in the energy obtained from the overtopping water) of up to 45 % could be obtained.

In order to improve the expression for the vertical overtopping distribution, tests should be conducted for a wider range of in particular crest freeboard, as numerical optimization resulted in values considerably larger than the ones used in the tests on which the expression is based.

5.4 Final remarks

Despite some still existing gaps in the general knowledge describing overtopping of wave energy converters, it can be concluded that a new, powerful tool has been developed for the design of the overtopping slopes on these structures.

Using the equations described in the thesis, it is possible to develop preliminary designs, and to improve existing WEC's utilizing overtopping. The future will show whether or not this can lead to large-scale utilization of wave energy for power production.

A considerable step forward in that direction is being taken in the ongoing project on the construction and testing of the "near-prototype size" model of the floating WEC, the Wave Dragon. The model is a 130 ton floating steel structure with measuring equipment enabling extensive monitoring of the performance of the device in real seas.

It is expected that the results of this project should be useful for the verification and further development of tools for the prediction of overtopping. The project will also provide valuable practical experience with the operation of a floating WEC of the overtopping type. Thus, the author is grateful to have the opportunity to participate in this project.

References

Aaen (1977). *Oversprøjt (Overtopping - in Danish)*. Bachelor Thesis, Danish Academy, Dept. of Civil Eng., Copenhagen.

Ahrens, J. (1983). Wave runup on idealized structures. *Coastal Structures '83 Specialty Conference, Arlington, Va.*, 925 − 938.

Ahrens, J. P. (1981). *Irregular Wave Run-Up on Smooth Slopes*. Tech.-Aid No. 81-17, Coastal Engineering Research Center, Waterways experiment station, Vicksburg.

Ahrens, J. P. and M. S. Heimbaugh (1988a). *Approximate Upper Limit of Irregular Wave Runup on Riprap*. Tech. Report CERC-88-5, Coastal Engineering Research Center, Waterways Experience Station, Vicksburg, Miss.

Ahrens, J. P. and M. S. Heimbaugh (1988b). Seawall overtopping model. pp. 795–806.

Ahrens, J. P. and M. F. Titus (1985). Wave Run-Up formulas for smooth slopes. *Journal of waterway, port, coastal and ocean engineering Vol. 111*(No. 1), pp. 128 − 133.

Allsop, N. (1994). Wave overtopping of seawalls, breakwaters and shoreline structures. *Proceedings of the Institution of Civil Engineers, Water Maritime and Energy 106*(4), 355–357.

Allsop, N. W. H., L. Franco, and P. Hawkes (1985b). *Wave Run-Up on Steep Slopes: A Literature Review*. HR Wallingford, Report No. SR1.

Aminti, P. and L. Franco (1988). Wave overtopping on rubble mound breakwaters. *Proc. 21st. International Conference on Coastal Engineering, Malaga, Spain*.

B. Van de Walle, J. De Rouck, L. V. and P. Frigaard (2002). Full scale measurements of wave Run-Up on a rubble mound breakwater. *Proc. 28th Int. Conf. On Coastal Eng. Cardiff, Wales*.

Battjes, J. A. (1971, Feb.). Run-Up distributions of waves breaking on slopes. *Journal of the waterways, harbors and coastal engineering division Vol. 97*(No. WW1), pp. 91 − 114.

Battjes, J. A. (1974a). *Computation of Set-Up, Long-Shore Currents, Run-Up and Overtopping Due to Wind Generated Waves.* Ph. D. thesis, Dept. Civil Engineering, Delft University of Technology.

Battjes, J. A. (1974b). Surf similarity. *Proc. 14th. ICCE, Copenhagen*, pp. 466 − 480.

Battjes, J. A. and A. Roos (1975). *Characteristics of Flow in Run-Up of Periodic Waves.* Communications on Hydraulics, Delft Unoversity of Technology, Rep. 75-3.

Besley, P. (1999). Overtopping of seawalls - design and assessment manual. Technical Report R & D W178, H. R. Wallingford & Environment Agency.

Bølgekraftudvalgets Sekretariat (1999, December). *Bølgekraftprogram, Status 2000 - Forslag Til Systematik I Forbindelse Med Sammenligning Af Bølgekraftanlæg.*

Bradbury, A. P. and N. W. H. Allsop (1988). Hydraulic effects of breakwater crown walls. *In Proc. Conf. on Design of Breakwaters, Institution of Civil Engineers, London*, pp. 385 − 396.

Bruun, P. (1985). *Design and Construction of Mounds for Breakwaters and Coastal Protection.* Elsevier, Amsterdam.

Burcharth, H. F. and S. Hughes (2000). *Coastal Engineering Manual, Fundamentals of Design. Chapter 5, Part VI.* To be published by Coastal Engineering Research Center, Waterways Experiment Station, US Army Corps of Engineers,Vicksburg, USA.

Burcharth, H. F. and Z. Liu (1999, April). Scaling of core material in rubble mound breakwater model tests. *Proc. of the 5th COPEDEC conf., Cape Town, South Africa.*

CIRIA/CUR (1991). *Manual on the Use of Rock in Coastal and Shoreline Engineering.* Special pub. 83, Constriction Industry Research and Information ass., London.

Cross, R. H. and C. K. Sollitt (1970). Wave transmission by overtopping. Technical Report 15, Ralph M. Parson Laboratory, Department of Civil Engineering, Massechussetts Institute of Technology, Cambridge, Mass.

De Gerloni, M., L. Franco, and G. Passoni (1991). The safety of breakwaters against wave overtopping. *Proc. of Coastal Structures and Breakwaters*, pp. 335 − 342.

De Rouck, J., R. Verdonck, P. Troch, L. Van Damme, F. Schlutter, and J. De Ronde (1998). Wave run-up and overtopping: prototype versus scale models. *Proceedings of the Coastal Engineering Conference 1*, 1039–1052.

de Waal, J. and J. Van der Meer (1993). Wave runup and overtopping on coastal structures. *Proceedings of the Coastal Engineering Conference 2*, 1758–1771.

de Waal, J. P., P. Tonjes, and J. W. Van der Meer (1997). Wave overtopping of vertical structures including wind effect. *Proceedings of the Coastal Engineering Conference 2*, 2216–2229.

de Waal, J. P. F. M. and J. W. Van der Meer (1992). Wave Run-Up and overtopping on coastal structures. *Proc. 23rd ICCE, Venice*, pp. 1758 – 1771.

Dodd, N. (1998). Numerical model of wave run-up, overtopping, and regeneration. *Journal of Waterway Port Coastal and Ocean Engineering 124* (2), 73–81.

Douglass, S. L. (1985). Discussion of irregular wave overtopping on gravel islands. *Paper WW 18386 by Kobayashi and Reece, Journal of Waterways, Port, Coastal and Ocean Engineering 111* (1), 146 – 147.

Douglass, S. L. (1986). *Review and Comparison of Methods for Estimating Irregular Wave Overtopping Rates*. Rep. CERC-86-12, U. S. Army Corps of Engineers.

Endoh, K. and S. Takahashi (1995). Numerically modeling personnel danger on a promenade breakwater due to overtopping waves. *Proceedings of the Coastal Engineering Conference 1*, 1016–1029.

Falnes, J. (1993). *Theory for Extraction of Ocean Wave Energy*. Division of Physics, Norwegian Institute of Technology, University of Trondheim, Norway.

Franco, C. and L. Franco (1997). Wave overtopping over caisson brakwaters: New prediction formulae based on 2d and 3d model tests. *Manus submitted to the ASCE Journal of Waterway, Port, Coastal and Ocean Engineering*.

Franco, C. and L. Franco (1999). Overtopping formulas for caisson breakwaters with nonbreaking 3d waves. *Journal of Waterway, Port, Coastal and Ocean Engineering 125* (2), 98–108.

Franco, C., L. Franco, C. Restano, and J. W. Van der Meer (1995a). The effect of obliquity and Short-Crestedness on the overtopping rate and volume distribution on caisson breakwaters. *Final proceedings MCS-project, Monolithic (vertical) breakwaters*.

Franco, L., M. de Gerloni, and J. van der Meer (1995). Wave overtopping on vertical and composite breakwaters. *Proc. 24th Int. Conf. Coastal Eng., Kobe, Japan 1*, 1030–1044.

Franco, L., M. de Gerloni, and J. W. Van der Meer (1995). Wave overtopping on vertical and composite breakwaters. *Final proceedings MCS-project, Monolithic (vertical) coastal structures, Alderney Island, UK*.

Frigaard, P. and M. Brorsen (1995). A Time-Domain method for separating incident and reflected irregular waves. *Int. Journal of Coastal Engineering Vol. 24*.

Frigaard, P., J. P. Kofoed, F. Schlütter, P. Troch, T. Versluys, B. Van der Walle, and M. Willems (1999, October). *OPTICREST - Bremen Workshop, Run-Up, Comparison Between Prototype Measurements and Laboratory Measurements.* MAS3-CT97-0116.

Frigaard, P. and F. Schlütter (1999, March). *OPTICREST Task 3.1 - Laboratory Investigations, 5th Version.* MAST III, MAS3-CT97-0116, Hydraulics and coastal engineering laboratory, Aalborg University.

Funke, E. R. and E. P. Mansard (1979). *On the Synthesis of Realistic Sea States in a Laboratory Flume.* Hydraulics Laboratory Technical Report LTR-HY-66, National Research Council Canada, Ottawa, Canada.

Goda, Y. (1971). Expected rate of irregular wave overtopping of seawalls. *Coastal Engineering in Japan 14.*

Goda, Y. (1985). *Random Seas and Design of Maritime Structures* (3rd. ed.). Univerty of Tokyo Press, Tokyo, Japan.

Gonzalez Madrigal, B. and J. Olivares Prud'Homme (1991). Reduction of wave forces and overtopping by submerged structures in front of a vertical breakwater. *Proceedings of the Coastal Engineering Conference 2*, 1348–1361.

Grantham, K. N. (1953). Wave Run-Up on sloping structures. *Transactions, American Geophysical Union Vol. 34* (No. 5), pp. 720 − 724.

Grüne, J. (1982). Wave Run-Up caused by natural storm surge. *Proc. 18th Coastal Engineering Conf., ASCE, New York Vol. I*, pp. 785 − 803.

Günbak, A. R. (1979). *Rubble Mound Breakwaters.* Div. Port and Ocean Engineering, The Norwegian Institute of Technology, Trondheim, Norway, Rep. 1.

Hasselmann, K., T. P. Barnett, E. Bouws, H. Carlson, D. E. Cartwright, K. Enke, J. A. Ewing, H. Gienapp, D. E. Hasselmann, P. Kruseman, A. Meerburg, P. Müller, D. J. Olbers, K. Richter, W. Sell, and H. Walden (1973). Measurements of Wind-Wave growth and swell decay during the joint north sea wave project (JONSWAP). *Deutsches Hydr. Zeit. A12*, pp. 1 − 95.

Hawkes, P. J. (1999). Mean overtopping rate in swell and bimodal seas. *Proceedings of the Institution of Civil Engineers - Water Maritime and Energy 136* (4), 235–238.

Hebsgaard, M., P. Sloth, and J. Juhl (1998). Wave overtopping of rubble mound breakwaters. *Proceedings of the Coastal Engineering Conference 2*, 2235–2248.

Hedges, T. S. and M. T. Reis (1997, January). *Random Wave Overtopping of Simple Seawalls: A New Regression Model.* Report no. CE/1/97, Dep. of Civil Engineering, University of Liverpool.

Hedges, T. S. and M. T. Reis (1998a). Random wave overtopping of simple sea walls: A new regression model. *Proceedings of the Institution of Civil Engineers - Water Maritime and Energy 130* (1), 1–10.

Hedges, T. S. and M. T. Reis (1998b). Random wave overtopping of simple sea walls: a new regression modeld. *Oceanographic Literature Review 45* (9), 1711.

Herbert, D., N. Allsop, and M. Owen (1995). Overtopping of sea walls under random waves. *Proceedings of the Coastal Engineering Conference 1*, 1130–1142.

Hiraishi, T. and H. Maruyama (1998). Directional wave overtopping estimation model and experimental verification. *Proceedings of the Coastal Engineering Conference 2*, 2249–2261.

Hu, K., C. G. Mingham, and D. M. Causon (2000). Numerical simulation of wave overtopping of coastal structures using the Non-Linear shllow water equations. *Coastal Engineering* (41), 433 − 465.

Hu, S.-L. J. and J. L. McCauley (1997). Estimation of wave overtopping rates for irregular waves. *Journal of Waterway Port Coastal and Ocean Engineering - American Soc of Civil Engineers 123* (5), 266–273.

Hughes, S. A. (1993). *Physical Models and Laboratory Techniques in Coastal Engineering*. Volume 7, Advanced Series on Ocean Engineering. World Scientific Publishing Co. Pte. Ltd. ISBN 981-02-1541-X (pbk).

Hunt, I. A. (1959, Sept.). Design of seawalls and breakwaters. *ASCE Vol. 85* (No. WW3, proc. paper 2172), pp. 123 − 152.

IAHR (1989). List of sea state parameters. *Journal of Waterway, Port, Coastal and Ocean Engineering, American Society of Civil Engineers Vol. 115* (No. 6), pp. 792 − 808.

Ishimoto, K., T. Chiba, and Y. Kajiya (1995). Wave overtopping detection by image processing. *'Steps Forward'. Proceedings of the Second World Congress on Intelligent Transport Systems '95 Yokohama*, 515–18 vol.1.

J. A. Gonzales-Escriva, J. R. Medina, J. G. and J. De Rouck (2002). Wind effects on runup and overtopping influencing breakwater crest design. *Proc. of 28th Int. Conf. on Coastal Eng., Cardiff, Wales*.

Jakobsen, K. P. and P. Frigaard (1999). User's manual for the program wave dragon - power simulation. Technical report, CRAFT program Low-Pressure Turbine and Control Equipment for Wave Energy Converters (Wave Dragon), Hydraulics & Coastal Engineering Laboratory, Aalborg University.

Jensen, O. J. (1984). *A Monograph on Rubble Mound Breakwaters*. Danish Hydraulic Institute.

111

Jensen, O. J. and J. Juhl (1987). Wave overtopping on breakwaters and sea dikes. *Proc., Int. Conf. Coast. and Port Engrg. in Developing Countries*.

Jensen, O. J. and T. Sørensen (1979). Overspilling/Overtopping of rubble mound breakwaters, results of studies, useful in design procedures. *Coastal Engineering, 3*, pp. 51 – 65.

Jervis, M. and D. Peregrine (1997). Overtopping of waves at a wall: A theoretical approach. *Proceedings of the Coastal Engineering Conference 2*, 2192–2205.

Johnsgard, H. (1998). A numerical model for Run-Up of breaking waves.

Johnsgard, H. and G. Pedersen (1997). A numerical model for Three-Dimensional Run-Up. *Int. journal for numerical methods in fluids Vol. 24*, pp. 913 – 931.

Josefson, U. (1978). Utvärdering av en idé till vågkraftverk. Master's thesis, Chalmers University of Technology, Gøteborg, Sweden.

Juhl, J. and P. Sloth (1995). Wave overtopping of breakwaters under oblique waves. *Proceedings of the Coastal Engineering Conference 1*, 1182–1196.

Kamphuis, J. W. and N. Mohamed (1978, May). Run-Up of irregular waves on plane smooth slope. *Journal of the waterway, port, coastal and ocean division Vol. 104*(WW2).

Kataoka, Y., O. Otani, T. Nakaoka, Y. Hamazaki, N. Takehana, and Y. Ichikawa (1999). Wave overtopping and dissipation for a new type of shore protection. *R and D: Research and Development Kobe Steel Engineering Reports 49*(2), 53–56.

Kikkawa, H., H. Shi-Igai, and T. Kono (1968). Fundamental study of wave overtopping on levees. *Coastal Engineering in Japan Vol. 11*, pp. 107 – 115.

Knott, G. and J. Flower (1979). Simulation studies of the basic nonlinear effects of wave energy conversion by an overtopping water column. *Energy Conversion 19*(1), 59–69.

Kobayashi, N. (1998). *Wave Run-Up and Overtopping on Beaches and Coastal Structures*, Volume 5 of *Advances in Coastal and Ocean Engineering*, pp. 95 – 154.

Kobayashi, N. and A. W. Raichle (1994, Jan - Feb). Irregular wave overtopping of revetments in surf zones. *Journal of Waterway, Port, Coastal and Ocean Engineering 120*(1), 56 – 73.

Kobayashi, N. and A. M. Reece (1983). Irregular wave overtopping on gravel islands. *Journal of Waterway, Port and Ocean Engineering 109*(WW4), 429 – 444.

Kobayashi, N. and A. Wurjanto (1989). Wave overtopping on coastal structures. *Journal of Waterway, Port, Coastal and Ocean Engineering 115* (2), 235–251.

Kofoed, J. P. (2000a, July). Model study of overtopping of marine structures for a wide range of geometric parameters. *Poster presented at 27th In. Conf. on Coastal Eng. (ICCE-2000), Sidney, Australia.*

Kofoed, J. P. (2000b). Optimization of overtopping ramps for utilization of wave energy. Technical report, Hydraulic & Coastal Engineering Laboratory, Department of Civil Engineering, Aalborg University.

Kofoed, J. P. (2000c). Time variation of overtopping rates applied to WD. Technical report, Non-nuclear Energy RTD Programme (CRAFT), "Low-pressure Turbine and Control Equipment for Wave Energy Converters (Wave Dragon), Hydraulic & Coastal Engineering Laboratory, Aalborg University.

Kofoed, J. P. (October 2002). Hydraulic investigations of the wave energy converter power pyramid - Phase 2 (in danish). Technical report, Hydraulics & Coastal Engineering Laboratory, Aalborg University.

Kofoed, J. P. and H. F. Burcharth (2000, Dec.). Experimental verification of an empirical model for time variation of overtopping discharge. *4th European Wave Energy Conference (EWEC 2000), Aalborg, Denmark.*

Kofoed, J. P. and P. Frigaard (2000a). Indledende hydrauliske undersøgelser af bølgeenergianlægget power pyramid (report in danish. english title: Preliminary hydraulic investigation of the wave energy device power pyramid). Technical report, Hydraulics & Coastal Engineering Laboratory, Aalborg University.

Kofoed, J. P. and P. Frigaard (2000b, Nov.). Marine structures with heavy overtopping. *4th Int. Conf. on Coasts, Ports and Marine Structures (ICOPMAS"2000"), Bandar Abbass, Iran.*

Kofoed, J. P., P. Frigaard, H. C. Sørensen, and E. Friis-Madsen (1998). Wave dragon - a slack moored wave energy converter. *Proc. of the Third European Wave Energy Conference in Patras, Greece.*

Kofoed, J. P., T. Hald, and P. Frigaard (May 2002). Experimental study of a multi level overtopping wave power device. *The Tenth Congress of International Maritime Association of the Mediterranean (IMAM 2002).*

Kofoed, J. P. and A. Nielsen (1997, September). The wave dragon - evaluation of a wave energy converter. Master's thesis, Aalborg University. Graduate report in Civil Engineering.

Kudale, M. D. and N. Kobayashi (1997). Hydraulic stability analysis of leeside slopes of overtopped breakwaters. *Proceedings of the 25th (1996) International Conference on Coastal Engineering 2*, 1721 − 1734.

Lab., H. (Nov. 2000). Breakwater for the new port of la coruna at punta langosteira - final report of the model test. Technical report, Hydraulics & Coastal Engineering Laboratory, Aalborg University.

Le Méhauté, B. (1963). On nonsaturated breakers and the wave Run-Up. *Proceedings, 8th Conference on Coastal Engineering, Mexico City, Mexico*, pp. 77 − 92.

Le Méhauté, B., R. C. Y. Koh, and L. Hwang (1968, Feb.). A synthesis of wave Run-Up. *Journal of the waterways and coastal engineering division, ASCE Vol. 94* (No. WW1, proc. paper 5807), pp. 77 − 92.

Lee, J., F. Zhuang, and C. Chang (1994). Kinematics of wave overtopping on marine structure. pp. 821–834.

Longuet-Higgins, M. S. (1975). On the joint distribution of the periods and amplitudes of sea waves. *Journal of Geophysical Research 80* (18), 2688 −.

Losada, M. A. and L. A. Gimenez-Curto (1981). Flow characteristics on rough, permeable slopes under wave action. *Coastal Engineering, 4*, pp. 187 − 206.

Madsen, J. B. and P. Frigaard (2000). The wave dragon: Operation strategy of the turbines. joule craft project: JOR3-CT98-7027, Low-Pressure turbine and control equipment for wave energy converters (wave dragon). Technical report, CRAFT program Low-Pressure Turbine and Control Equipment for Wave Energy Converters (Wave Dragon), Hydraulics & Coastal Engineering Laboratory, Aalborg University.

Martinelli, L. and P. Frigaard (1999a). Example of overtopping time series. Technical report, CRAFT program Low-Pressure Turbine and Control Equipment for Wave Energy Converters (Wave Dragon), Hydraulics & Coastal Engineering Laboratory, Aalborg University.

Martinelli, L. and P. Frigaard (1999b). The wave dragon: Tests on a modified model. Technical report, CRAFT-project, Department of Civil Engineering, Aalborg University.

Massel, S. R. (1996). *Ocean Surface Waves: Their Physics and Prediction.* Volume 11, Advanced Series on Ocean Engineering. World Scientific Publishing Co. Pte. Ltd. ISBN 981-02-2109-6(pbk).

Monso, J. L., A. Vidaor, C. Cadevall, and C. Garcia (1997). Overtopping reduction in crownwall design. *Proceedings of the Coastal Engineering Conference 2*, 1816–1825.

Murakami, K., I. Irie, and Y. Kamikubo (1997). Experiments on a non-wave overtopping type seawall. *Proceedings of the Coastal Engineering Conference 2*, 1840–1851.

Murphy, J. (1999, March). *OPTICREST Task 3.2 - Wave Run-Up Measurement Techniques.* MAST III, MAS3-CT97-0116, HMRC, University College Cork, Ireland.

Nelis, P. M., D. Branford, and M. H. Unsworth (1994). Model of the transfer of radioactivity from sea to land in sea spray. *Atmospheric environment Vol. 28*(No. 20), 3213 – 3223.

Oezhan, E. and A. C. Yalciner (1991). Overtopping of solitary waves at model sea dikes. *Proceedings of the Coastal Engineering Conference 2*, 1487–1498.

Oumeraci, H. (1999). Physical modelling, field measurements and numerical modelling in coastal energy: Synergy or competition? *Second German-Chinese Joint Seminar on Recent Developments in Coastal Engineering - The Sustainable Development in the Coastal Zone, Tainan, Taiwan.*

Oumeraci, H. and H. Schüttrumpf (1999, March). *OPTICREST Task 3.5 - Litterature Review on Wave Run-Up and Run-Down Velocities.* MAST III, MAS3-CT97-0116, Dep. of Hydromechanics and Coastal Engineering, Braunschweig.

Oumeraci, H., H. Schüttrumpf, and M. Bleck (1999, October). *OPTICREST Task 3.5 and 5 - Wave Overtopping at Seadikes, Comparison of Physical Model Tests and Numerical Computations.* MAS3-CT97-0116, Dept. of Hydromechanics and Coastal Engineering, Technical University of Braunschweig, Germany.

Owen, M. W. (1980). *Design of Sea Walls Allowing for Wave Overtopping.* Rep. EX 924, HR Wallingford.

Owen, M. W. (1982a). The hydraulic design of seawall profiles. *Proc. Conf. on Shoreline Protection, ICE, London*, 185 – 192.

Owen, M. W. (1982b). Overtopping of sea defences. *International Conference on the Hydraulic Modeling of Civil Engineering Structures*, 469 – 480.

Paape, A. (1960). *Experimental Data in the Overtopping of Seawalls by Waves.* Delft Hydraulics, Publ. No. 23.

Pedersen, J. (1996). *Wave Forces and Overtopping on Crown Walls of Rubble Mound Breakwaters.* Ph. D. thesis, Hydraulics & Coastal Engineering Laboratory, Department of Civil Engineering, Aalborg University, Denmark.

Pedersen, J. and H. F. Burcharth (1992). Wave forces on crown walls. *Proc. 23rd International Conference on Coastal Engineering, Venice, Italy.*

Pilarczyk, K. and R. Zeidler (1996). *Offshore Breakwaters and Shore Evolution Control.* A. A. Balkema, Rotterdam.

Pohl, R. (1999). DISCUSSION - estimation of wave overtopping rates for irregular waves by Sau-Lon james hu, and james l McCauley. *Journal of Waterway Port Coastal and Ocean Engineering 125*(5), 272.

Roos, A. and J. A. Battjes (1976). Characteristics of flow in Run-Up of periodic waves. *Proc. 15th ICCE, Honolulu*, pp. 781–795.

Sakakiyama, T. (1995). Wave overtopping and pressure dependent on crest elevation. *Coastal Dynamics - Proceedings of the International Conference*, 209–220.

Sakakiyama, T. and R. Kajima (1997). Wave overtopping and stability of armor units under multidirectional waves. *Proceedings of the Coastal Engineering Conference 2*, 1862–1875.

Sakakiyama, T., R. Kajima, S. Imai, H. Katayama, and T. Shimizu (1997). Field measurements of wave overtopping on seawall covered with armor units. *Proc. 3rd Int. Symp. Waves97, Virginia, USA Vol. II*, 1336 – 1350.

Saville, T. (1955). Laboratory data on the wave runup and overtopping on shore structures. Technical Report TM-64, US Army Corps of Engineers, Beach Erosion Board.

Saville, T. (1956, April). Wave Run-Up on shore structures. *ASCE Vol. 82* (No. WW2, proc. paper 925).

Saville, T. and J. M. Caldwell (1953). Experimental study of wave overtopping on shore structures. *Proc. Minnesota Int. Hydraulics Conv., IAHR, ASCE, Minneapolis, Minnesota, USA*.

Schüttrumpf, H., A. Kortenhaus, and H. Oumeraci (1998). Application of overtopping models to vertical walls against storm surges. *Proceedings of the Coastal Engineering Conference 2*, 1553 – 1556.

Schüttrumpf, H., J. Moller, H. Oumeraci, J. Grune, and R. Weissmann (2001). Effects of natural sea states on wave overtopping of seadikes. *Proceedings of The Fourth International Symposium on Ocean Wave Measurement and Analysis (Waves 2001), San Francisco*.

Schüttrumpf, H. and H. Oumeraci (2000). EAK-Empfehlungen a2 - wellenauflauf und wellenüberlauf (kurzfassung) hansa - schiffahrt - schiffbau - hafen. (in german).

Sekimoto, T., H. Kunisu, and T. Yamazaki (1995). Short term wave overtopping rate of block armored seawall. *Proceedings of the Coastal Engineering Conference 2*, 1568–1579.

Sibul, O. V. and E. G. Tickner (1956). Model study of overtopping of Wind-Generated wave on levees with slopes 1:3 and 1:6. Technical Report TM-80, US Army Corps of Engineers, Beach Erosion Board.

Sørensen, H. C. and E. Friis-Madsen (1999). Wave dragon. forsøg til belysning af hydraulisk respons. rapport fase a.

SPM (1984). *Shore Protection Manual* (4th edition ed.). Department of The Army, Waterways Experiment Station, Corps of Engineers, Coastal Engineering Research Center.

Svendsen, I. A. and I. G. Jonsson (1976). *Hydrodynamics of Coastal Regions.* Den Private Ingeniørfond, Technical University of Denmark, Lyngby. ISBN 87-87245-57-4.

TACPAI (1974). *Wave Run-Up and Overtopping.* Technical Advisory Committee on Protection Against Inundation, Government Publishing Office, The Hague.

Tautenhain, E., S. Kohlase, and H. W. Partenscky (1982). Wave Run-Up at sea dikes under oblique wave attack. *Proc. 18th ICCE, Cape Town*, pp. 804 − 810.

Tjugen, K. J. (1993). Tapchan ocean wave energy project. *Proc. European Wave Energy Symposium, Edinburgh, Scotland* (ISBN 0-903640-84-8).

Tsuruta, S. and Y. Goda (1968). Expected discharge of irregular wave overtopping. *11th Conference on Costal Engineering, London*, 833 − 852.

Umeyama, M. (1993). Wave overtopping on vertical boundary and water-surface displacement. *Journal of Waterway, Port, Coastal and Ocean Engineering 119*(3), 243–260.

Van der Meer, J. W. (1993). *Conceptual Design of Rubble Mound Breakwaters.* Delft Hydraulics, Publ. No. 483.

Van der Meer, J. W. (1998a). Applications and stability criteria for rock and artificial units. *Chapter 11 in "Seawalls, dikes and revetments". Edited by K. W. Pilarczyk, Balkema, Rotterdam.*

Van der Meer, J. W. (1998b). Geometrical design of coastal structures. *Chapter 9 in "Seawalls, dikes and revetments". Edited by K. W. Pilarczyk, Balkema, Rotterdam.*

Van der Meer, J. W. (1998c). Wave Run-Up and overtopping. *Chapter 8 in "Seawalls , dikes and revetments". Edited by K. W. Pilarczyk, Balkema, Rotterdam.*

Van der Meer, J. W. and L. Franco (1995). Vertical breakwaters. *Delft Hydraulics, Publ. No. 487..*

Van der Meer, J. W. and J. P. F. M. Janssen (1994). Wave Run-Up and wave overtopping of dikes. *Wave forces on inclined and vertical wall structures, ed. N. Kobayashi and Z. Demirbilek, pp. 1 - 27, ASCE. Also Delft Hydraulics, Publ. No. 485..*

Van der Meer, J. W. and J. P. F. M. Janssen (1995). Wave run-up and wave overtopping at dikes. Technical report, Task Committee Reports, ASCE.

Van der Meer, J. W. and K. W. Pilarczyk (1995). Lowcrested rubble mound structures. *In " River, coastal and shoreline protections; Erosion control using riptap and armourstone". John Wiley & Sons, England. Edited by C. R. Thorne et al., proc. Riprap workshop, Fort Collins, Colorado, USA, pp. 233 - 250..*

Van der Meer, J. W. and C. J. Stam (1992). Wave Run-Up on smooth and rock slopes of coastal structures. *Journal of Waterway, Port, Coastal and Ocean Engineering Vol. 118*(No. 5), pp. 534 − 550.

Van Oorschot, J. H. and K. D'Angremond (1968). The effect of wave energy spectra on wave Run-Up. *Proc. 11th. conf. on coastal engineering, London Vol. II*, pp. 888 − 900.

Verdonck, R., J. D. Rouck, P. Troch, and L. V. Damme (1999). Prototype measurements of wave Run-Up on a rubblemound breakwater. *Proc. of the 5th. COPEDEC conf., Cape Town, South Africa*.

Verdonck, R., P. Troch, J. D. Rouck, and H. F. Burcharth (1998, June). *OPTICREST Task 1 - Review of Available Information*. MAST III, MAS3-CT97-0116, Ghent University, Aalborg University.

Ward, D. L., C. G. Wibner, J. Zhang, and B. Edge (1995). Wind effects on runup and overtopping. *Proceedings of the Coastal Engineering Conference 2*, 1687–1699.

Ward, D. L., J. Zhang, C. G. Wibner, and C. M. Cinotto (1997). Wind effects on runup and overtopping of coastal structures. *Proceedings of the Coastal Engineering Conference 2*, 2206–2215.

Wassing, F. (1958). Model investigations on wave run-up carried out in the Netherlands during the past twenty years. *Proc. 6th ICCE, Florida*, pp. 700 − 714.

Weggel, J. R. (1976). Wave overtopping equation. *Proceedings of the 15th Coastal Engineering Conference, ASCE, Honolulu, Hawaii*, pp. 2737 − 2755.

Wens, F. and M. Willems (1999, April). *OPTICREST Task 3.3 - Laboratory Investigations: Two Dimensional Testing, The Zeebrugge Breakwater, 1st Year Report*. MAST III, MAS3-CT97-0116, Flemish Community Flanders Hydraulics, Belgium.

Wolf, F. C. J., P. Troch, J. D. Rouck, and L. V. Damme (1998, November). *Mast III - OPTICREST Task 2.1 - Methodology and Analysis of Available Data, Description of Fields Sites for Measurement of Wave Run-Up*. National Institute for Coastal and Marine Management/RIKZ, the Netherlands.

Yamamoto, Y. and K. Horikawa (1993). New methods of evaluate wave run-up height and wave overtopping rate. *Proceedings of the Coastal Engineering Conference 2*, 1734–1747.

Zhuang, F., C. Chang, and J. Lee (1994). Kinematic measurements of wave overtopping using lasser doppler velocimeter. *ASME, Fluids Engineering Division (publicatino) FED 191*, 83 − 88.

118

Zhuang, F., C. Chang, and J. Lee (1995). Modelling of wave overtopping over breakwater. *Proceedings of the Coastal Engineering Conference 2*, 1700–1712.

Zhuang, F. and J.-J. Lee (1997). Viscous rotational model for wave overtopping over marine structure. *Proceedings of the Coastal Engineering Conference 2*, 2178–2191.

APPENDIX A

Harmonic Wave Overtopping a String

The purpose of this appendix is to determine the maximum overtopping volume of water passing over a string placed in a harmonic regular wave at a point between the still water level and the amplitude of the wave. Furthermore, the power present in this overtopping volume of water is calculated and compared with the total amount of power in the wave.
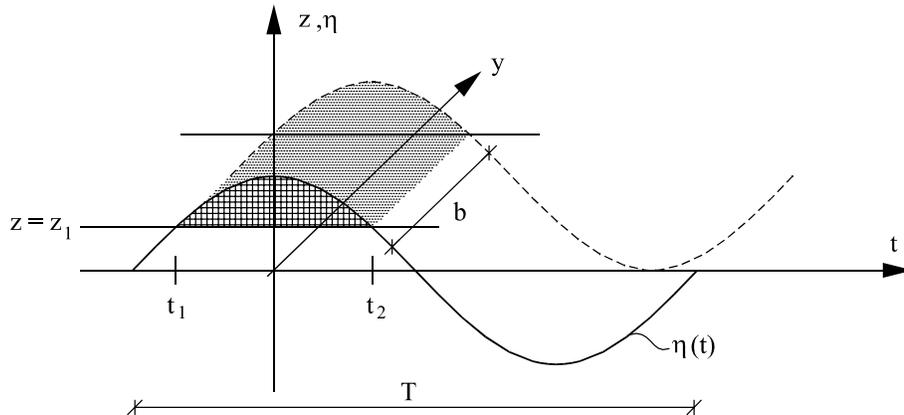
Figure A.1: Definition sketch.

A harmonic regular wave can be expressed as

$$\eta(x, t) = a \cos(kx - \omega t) \tag{A.1}$$

where $\eta(x, t)$ is the water elevation, a the wave amplitude, $\omega = \frac{2\pi}{T}$ the cyclic frequency, T the wave period, t the time, $k = \frac{2\pi}{L}$, L the wave length and x the horizontal coordinate in the direction of the wave.

A string is imagined placed at $z = z_1$ as shown in figure A.1. Now the flow of water that is passing over this string at a fixed point, $x = 0$ (on average over one wave period T), $q(z_1)$ [m^3/s], is calculated for a section with the width b in the direction perpendicular to the wave direction.

$$
\begin{aligned}
q(z_1) &= \frac{1}{T} \int_{t_1}^{t_2} bc(\eta(t) - z_1) dt \\
&= \frac{bL}{T^2} \int_{x_1}^{x_2} (a \cos(-\frac{2\pi}{T}t) - z_1) dt \\
&= \frac{bL}{T^2} \left(\int_{-\frac{T}{2\pi}\cos^{-1}(\frac{z_1}{a})}^{\frac{T}{2\pi}\cos^{-1}(\frac{z_1}{a})} \cos(\frac{2\pi}{T}t) dt - z_1 \frac{T}{\pi} \cos^{-1}(\frac{z_1}{a}) \right) \\
&= \frac{bL}{\pi T} \left(a \sin(\cos^{-1}(\frac{z_1}{a})) - z_1 \cos^{-1}(\frac{z_1}{a}) \right) \\
&= \frac{bL}{\pi T} \left(a\sqrt{1 - (\frac{z_1}{a})^2} - z_1 \cos^{-1}(\frac{z_1}{a}) \right) \tag{A.2}
\end{aligned}
$$

where $c = \frac{L}{T}$ is the wave velocity.

From this overtopping discharge, the power obtained if the water is captured at the height of the string (as potential energy), $P(z_1)$ [W], can be calculated as:

$$
\begin{aligned}
P(z_1) &= \gamma_w q_{mean}(z_1) z_1 \\
&= \frac{bL\gamma_w}{\pi T} \left(az_1 \sqrt{1 - (\frac{z_1}{a})^2} - z_1^2 \cos^{-1}(\frac{z_1}{a}) \right) \\
&= \frac{bL\gamma_w}{\pi T} az_1 \left(\sqrt{1 - (\frac{z_1}{a})^2} - \frac{z_1}{a} \cos^{-1}(\frac{z_1}{a}) \right) \tag{A.3}
\end{aligned}
$$

where $\gamma_w = \rho_w g$ is the specific weight of water, ρ_w is the density of water and g is the gravity acceleration.

A plot of equation (A.2) and (A.3) (for the following values of parameters: $a = 1$ m, $T = 7.7$ s, $L = 83.9$ m, $d = 20$ m, $b = 1$ m and $\gamma_w = 10,016$ kg/(m^{2}s^2)) is shown in figure A.2.
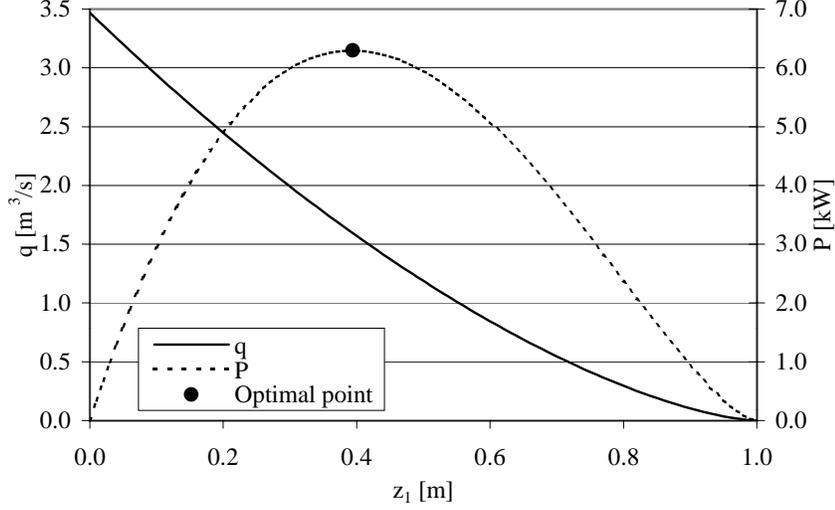
Figure A.2: Plot of overtopping discharge q, and obtained power, $P(z_1)$, as a function of the z-level of the string, z_1.

Now the optimal choice of z_1, z_1^{max}, in terms of maximum power that can be obtained is determined:

$$
\begin{aligned}
\frac{d}{dz_1}P(z_1) &= \frac{bL\gamma_w}{\pi T}(a\sqrt{1 - (\frac{z_1}{a})^2} - \frac{z_1^2}{a\sqrt{1 - (\frac{z_1}{a})^2}} \\
&\qquad - (2z_1\cos^{-1}(\frac{z_1}{a}) - \frac{z_1^2}{a\sqrt{1 - (\frac{z_1}{a})^2}}) \\
&= \frac{bL\gamma_w}{\pi T}(a\sqrt{1 - (\frac{z_1}{a})^2} - 2z_1\cos^{-1}(\frac{z_1}{a})) \\
&= 0 \qquad\qquad\qquad\qquad\qquad\qquad\qquad\qquad\text{(A.4)}
\end{aligned}
$$

An attempt to solve equation (A.4) for z_1, in order to obtain z_1^{max}, leads to a recursive equation:

$$
\sqrt{1 - (\frac{z_1^{max}}{a})^2} = 2\frac{z_1^{max}}{a}\cos^{-1}(\frac{z_1^{max}}{a}) \qquad\qquad\qquad\text{(A.5)}
$$

A numerical evaluation of equation (A.5) shows two possible solutions, namely $z_1^{max} = a$ and $z_1^{max} = 0.3942a$. Obviously, the first solution is trivial and of no interest, while the second is relevant to the solution of the problem.

Using this value of z_1^{max} the maximum power that can be obtained, P^{max}, is determined by insertion into equation (A.3).

$$
\begin{aligned}
P^{max} &= P(z_1^{max}) \\
&= \frac{bL\gamma_w}{\pi T}(0.3942a^2\sqrt{1-(\frac{0.3942a}{a})^2} - (0.3942a)^2\cos^{-1}(\frac{0.3942a}{a})) \\
&= 0.1812\frac{a^2bL\gamma_w}{\pi T}
\end{aligned}
\tag{A.6}
$$

Finally, the ratio between P^{max} and the power that is moving through a vertical cross section of the water column, perpendicular to the wave direction with the width b, P_{wave}, can be calculated. This ratio is referred to below as the efficiency.

$$
\begin{aligned}
\text{Efficiency} &= \frac{P^{max}}{P_{wave}} \\
&= \frac{0.1812\frac{a^2bL\gamma_w}{\pi T}}{\frac{1}{16}\gamma_w(2a)^2\frac{L}{T}(1+\frac{2\frac{2\pi}{L}d}{\sinh(2\frac{2\pi}{L}d)})b} \\
&= \frac{0.2307}{(1+\frac{2\frac{2\pi}{L}d}{\sinh(2\frac{2\pi}{L}d)})}
\end{aligned}
\tag{A.7}
$$

where d is the water depth.

Using (A.7) for shallow water shows that the efficiency in this case is ≈ 11.5 %, while for deep water it is ≈ 23.1 %.

The variation in the non-dimensionalized mean power, P', defined as

$$
\begin{aligned}
P' &= \frac{P}{P_{wave}} \\
&= \frac{P}{\frac{1}{16}\gamma_w(2a)^2\frac{L}{T}(1+\frac{2\frac{2\pi}{L}d}{\sinh(2\frac{2\pi}{L}d)})b}
\end{aligned}
\tag{A.8}
$$

is shown in figure A.3.

If, instead of capturing the water at the level of the string, each infinitesimal volume of water over $z = z_1$ is captured at the level it reaches, the mean power obtained is:

124
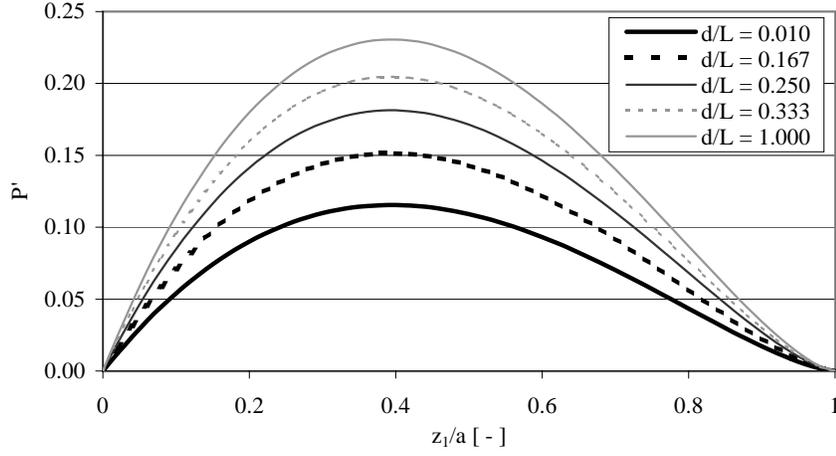
Figure A.3: Plot of non-dimensionalized obtained power, $P'(\frac{z_1}{a})$, as a function of the non-dimensionalized z-level of the string, $\frac{z_1}{a}$.

$$
\begin{aligned}
P &= \frac{1}{T} \int_0^a \gamma_w b z c(t_2 - t_1) dz \\
&= \frac{\gamma_w b L}{T^2} \int_0^a z \left(\frac{T}{\pi} \cos^{-1} \frac{z}{a} - \left(-\frac{T}{\pi} \cos^{-1} \frac{z}{a} \right) \right) dz \\
&= \frac{\gamma_w b L}{\pi T} \int_0^a z \cos^{-1} \frac{z}{a} dz \\
&= \frac{a^2 \gamma_w b L}{8T} \left(1 - \frac{4 z_1^2}{\pi a^4} \cos^{-1} \left(\frac{z_1}{a} \right) + \frac{2 z_1}{\pi a^3} \sqrt{1 - \left(\frac{z_1}{a} \right)^2} - \frac{2}{\pi} \sin^{-1} \left(\frac{z_1}{a} \right) \right)
\end{aligned}
\tag{A.9}
$$

P obtain its maximum value for $z_1 = 0$ and, thus, the maximum obtainable power P^{max} for this case becomes:

$$
P^{max} = \frac{a^2 \gamma_w b L}{8T}
\tag{A.10}
$$

The efficiency for this case then becomes:

$$
\text{Efficiency} = \frac{P^{max}}{P_{wave}}
$$

125

$$= \frac{1}{2} \frac{1}{1 + \frac{2\frac{2\pi}{L}d}{\sinh(2\frac{2\pi}{L}d)}} \tag{A.11}$$

Thus, the efficiency in deep water becomes 50 % and in shallow water 25 %.

APPENDIX B

Results – Overtopping Discharges with Single Level Reservoir

In the following pages the results of the model tests conducted are presented in terms of non-dimensional average overtopping discharges Q (defined as $Q = \frac{q}{\sqrt{gH_{m0}^3}}$) as a function of dimensionless crest freeboard R (defined as R_c/H_{m0}, where H_{m0} is the incident significant wave height).

The dimensions given in this appendix are all in model scale.

The data provided are also accessible on CD-ROM.

B.1   Linear overtopping slope

In this section results of tests conducted with a linear slope are presented. Three series of tests have been performed with a linear slope geometry:

- Varying slope angle α.
- Varying crest freeboard R_c.
- Varying draft d_r.

For the principal layout of the slope and the parameters describing it, please refer to figure 3.2 in section 3.3.

B.1.1 Varying slope angle

Test AA01

Slope angle: 20°   Draft: 0.162 m   Crest freeboard: 0.077 m
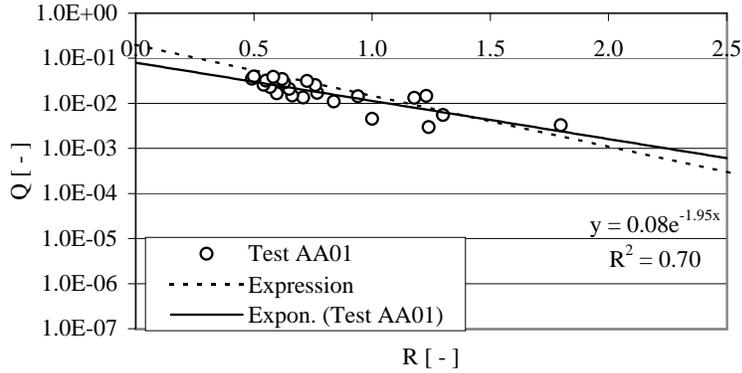
Figure B.1: Results of tests with test geometry AA01.

Test AA02

Slope angle: 30°   Draft: 0.166 m   Crest freeboard: 0.083 m
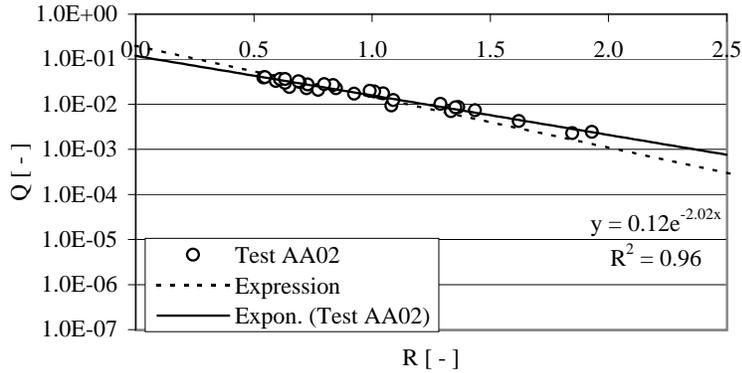
Figure B.2: Results of tests with test geometry AA02.

Test AA03

Slope angle: 40°   Draft: 0.162 m   Crest freeboard: 0.086 m
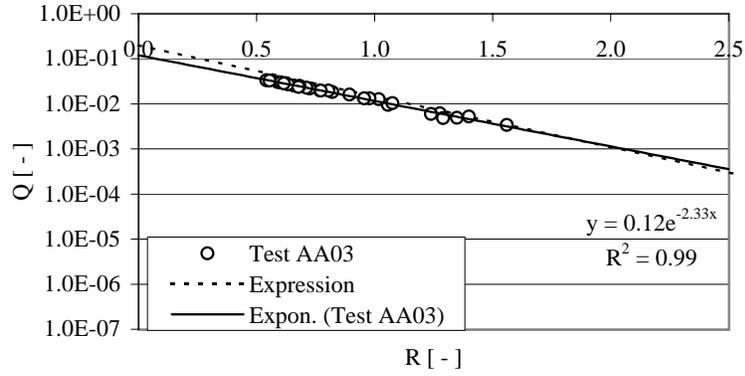
Figure B.3: Results of tests with test geometry AA03.

Test AA04

Slope angle: 50°   Draft: 0.162 m   Crest freeboard: 0.082 m
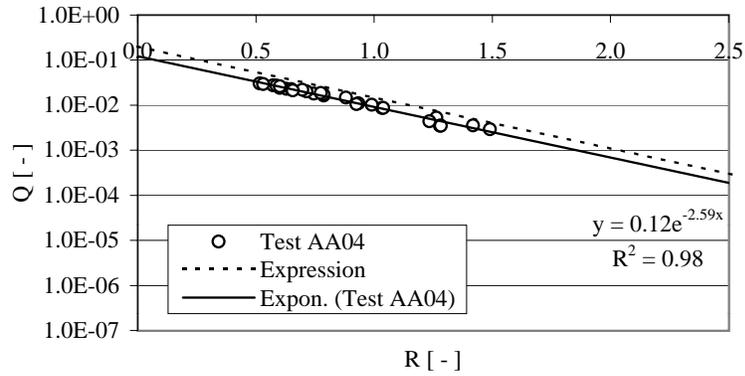
Figure B.4: Results of tests with test geometry AA04.

129

Test AA05
Slope angle: 60°   Draft: 0.123 m   Crest freeboard: 0.081 m
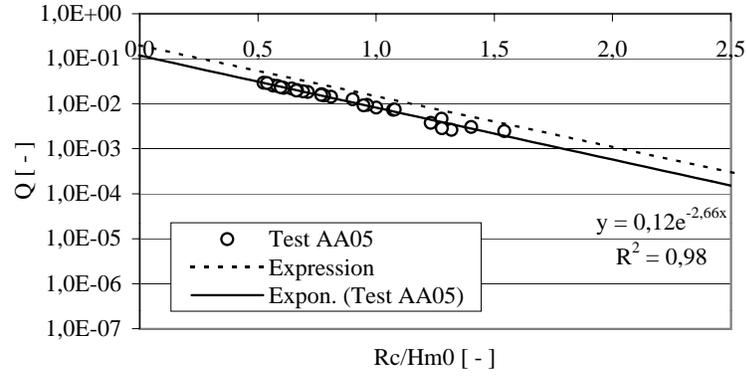
Figure B.5: Results of tests with test geometry AA05.

B.1.2 Varying crest freeboard

AB01

Slope angle: 40°   Draft: 0.166 m   Crest freeboard: 0.021 m
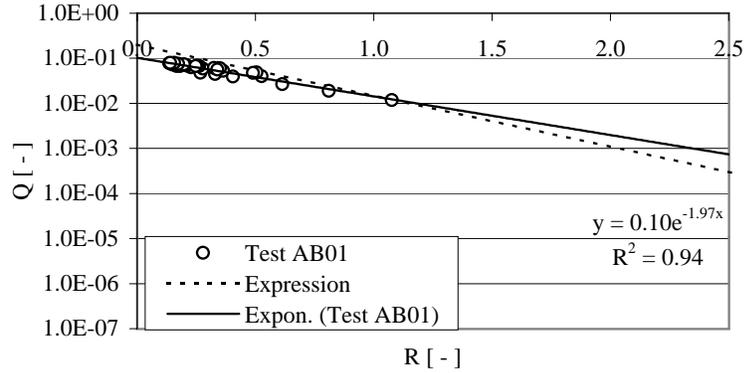
Figure B.6: Results of tests with test geometry AB01.

AB02

Slope angle: 40°   Draft: 0.166 m   Crest freeboard: 0.052 m
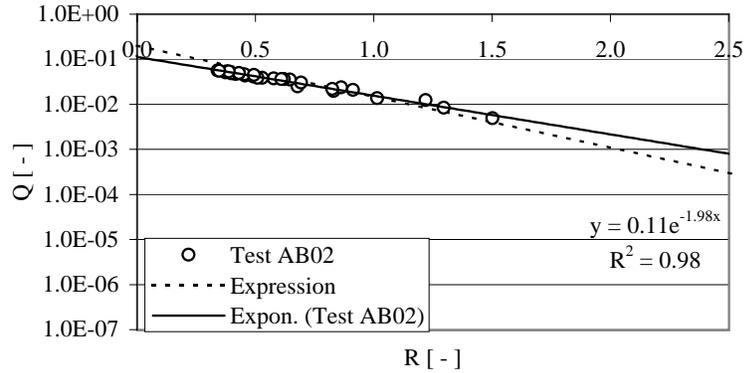
Figure B.7: Results of tests with test geometry AB02.

131

AB03

Slope angle: 40°   Draft: 0.163 m   Crest freeboard: 0.098 m
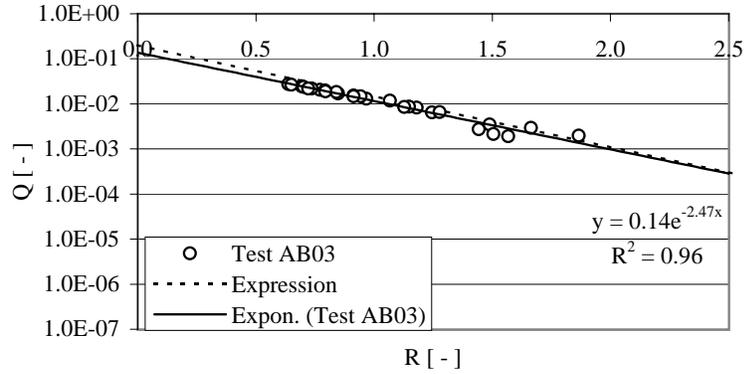
Figure B.8: Results of tests with test geometry AB03.

AB04

Slope angle: 40°   Draft: 0.167 m   Crest freeboard: 0.142 m
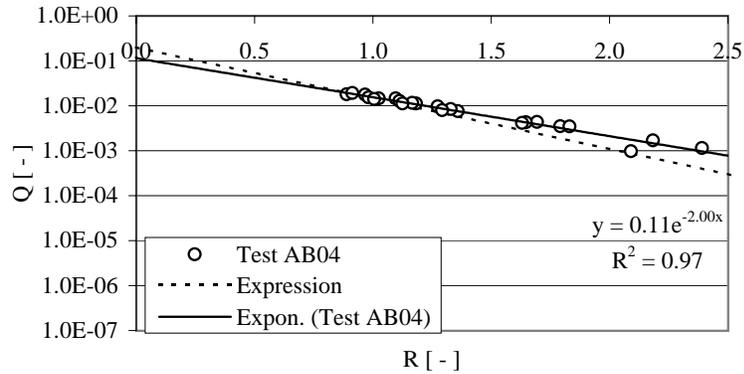
Figure B.9: Results of tests with test geometry AB04.

B.1.3   Varying draft

AC01

Slope angle: 40°   Draft: 0.100 m   Crest freeboard: 0.087 m
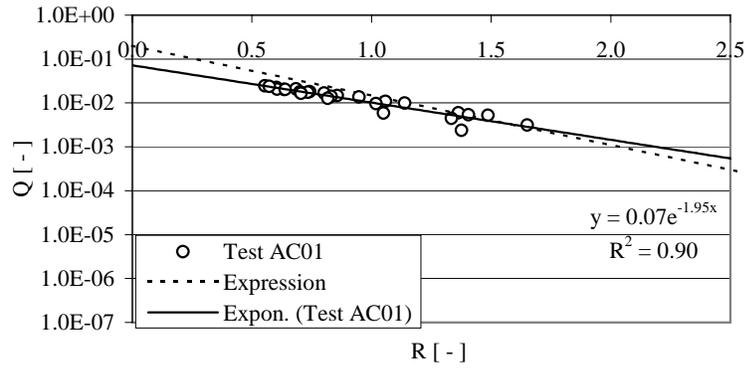
Figure B.10: Results of tests with test geometry AC01.

AC02

Slope angle: 40°   Draft: 0.243 m   Crest freeboard: 0.087 m
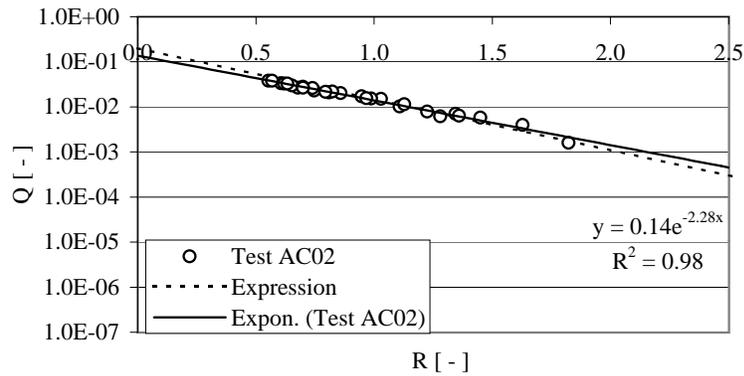
Figure B.11: Results of tests with test geometry AC02.

133

AC03

Slope angle: 40°   Draft: 0.358 m   Crest freeboard: 0.087 m
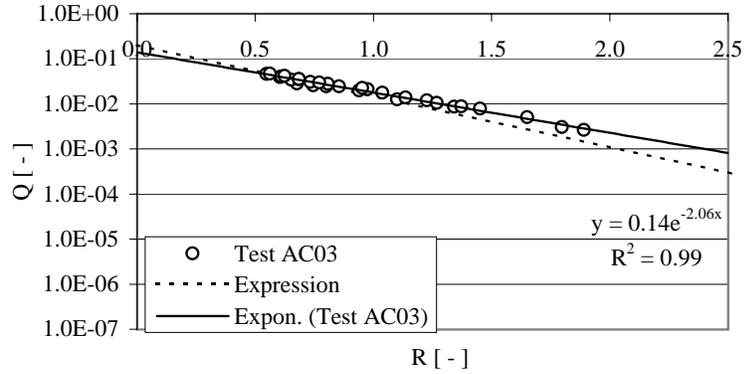
Figure B.12: Results of tests with test geometry AC03.

AC04

Slope angle: 40°   Draft: 0.500 m   Crest freeboard: 0.087 m
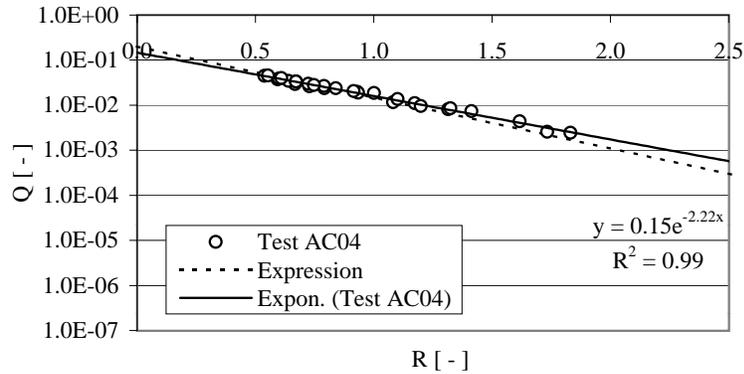
Figure B.13: Results of tests with test geometry AC04.

B.2   Modifications of the slope profile

In this section results of tests conducted with modifications of the slope profile geometry are presented. First, results of a test series with a reference geometry (linear slope, principal layout as shown in figure 3.2, section 3.3) are presented. These are used to evaluate the tested modifications. The tested modifications are:

- Horizontal plate at slope bottom.

- Convex top of slope.

- Concave top of slope.

B.2.1   Reference geometry

Test BA04
Basic setup, linear ramp, no modifications
Slope angle: 30°   Draft: 0.200 m   Crest freeboard: 0.050 m
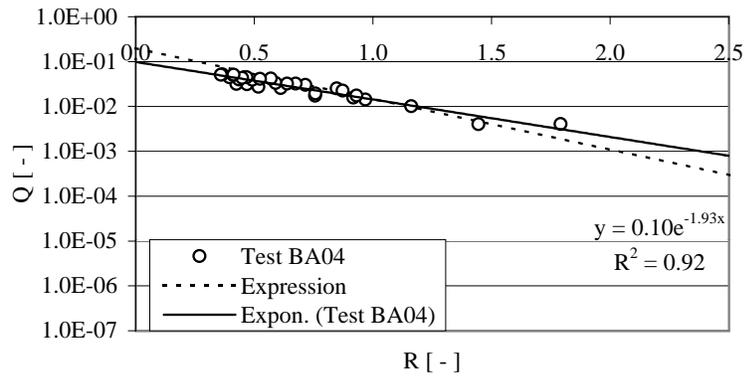
Figure B.14: Results of tests with test geometry BA04.

B.2.2 Horizontal plate at slope bottom
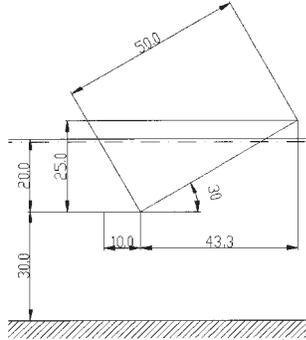
Figure B.15: The geometry of the slope in the BA01 tests. Measures are in cm.

Test BA01

Horizontal plate at ramp bottom: 0.100 m

Slope angle: 30°　　　　Draft: 0.200 m　　　　　Crest freeboard: 0.050 m
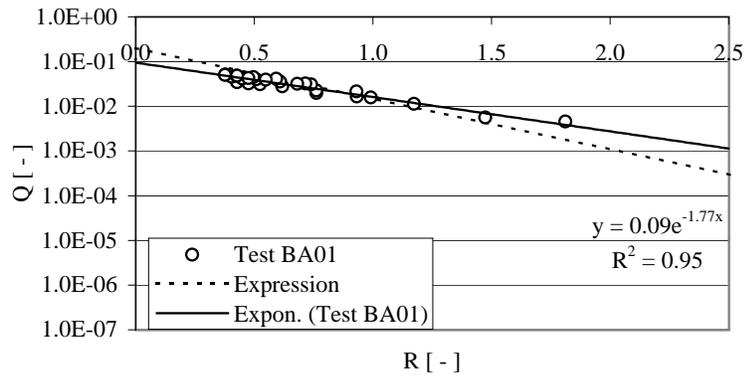
Figure B.16: Results of tests with test geometry BA01.
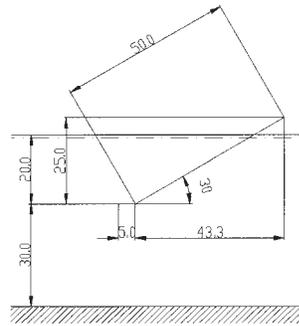
Figure B.17: The geometry of the slope in the BA02 tests. Measures are in cm.

Test BA02
Horizontal plate at ramp bottom: 0.050 m
Slope angle: 30°   Draft: 0.200 m   Crest freeboard: 0.050 m
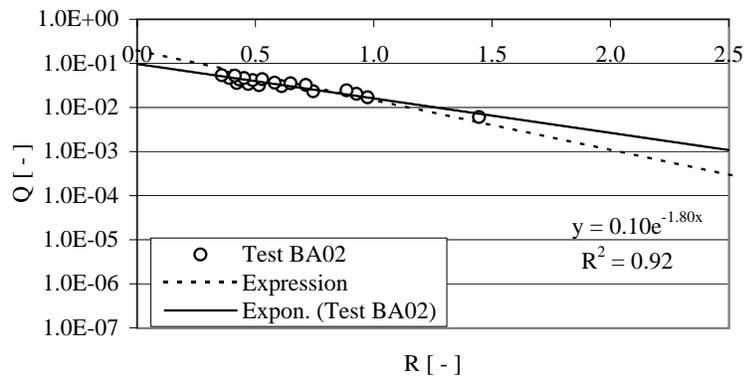
Figure B.18: Results of tests with test geometry BA02.
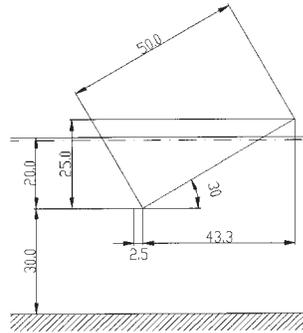
Figure B.19: The geometry of the slope in the BA03 tests. Measures are in cm.

Test BA03

Horizontal plate at ramp bottom: 0.025 m

Slope angle: 30°　　　　Draft: 0.200 m　　　　Crest freeboard: 0.050 m
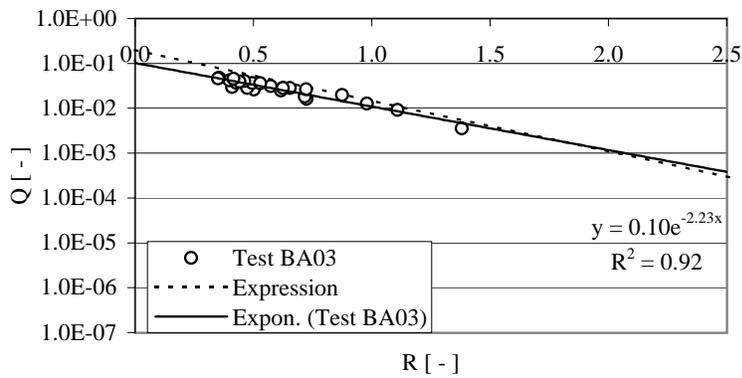
Figure B.20: Results of tests with test geometry BA03.

B.2.3   Convex top of slope
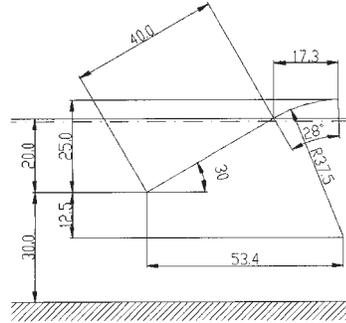
Figure B.21: The geometry of the slope in the CA01 tests. Measures are in cm.

Test CA01

Convex ramp	Curve radius: 0.375 m	Sector of circle: 28°
Slope angle: 30°	Draft: 0.200 m	Crest freeboard: 0.050 m
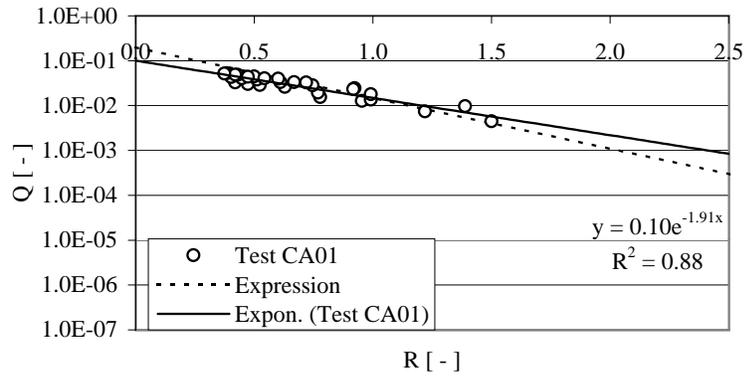
Figure B.22: Results of tests with test geometry CA01.
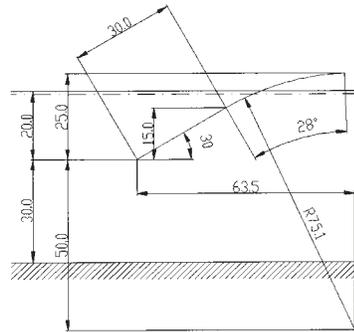
Figure B.23: The geometry of the slope in the CA02 tests. Measures are in cm.

Test CA02

Convex ramp	Curve radius: 0.751 m	Sector of circle: 28°
Slope angle: 30°	Draft: 0.200 m	Crest freeboard: 0.050 m

$$y = 0.08e^{-1.59x}$$
$$R^2 = 0.83$$
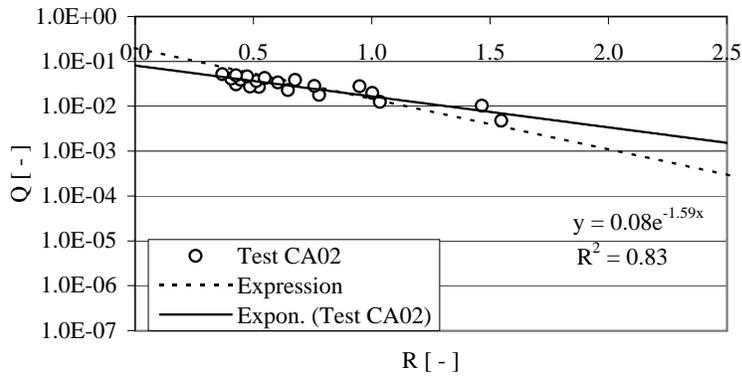
Figure B.24: Results of tests with test geometry CA02.
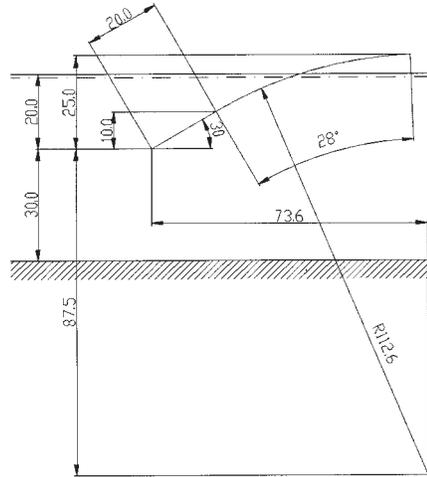
Figure B.25: The geometry of the slope in the CA03 tests. Measures are in cm.

Test CA03

Convex ramp	Curve radius: 1.126 m	Sector of circle: 28°
Slope angle: 30°	Draft: 0.200 m	Crest freeboard: 0.050 m
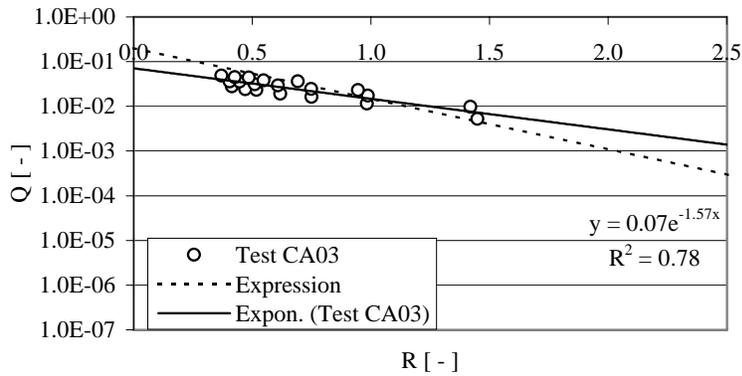
Figure B.26: Results of tests with test geometry CA03.

141
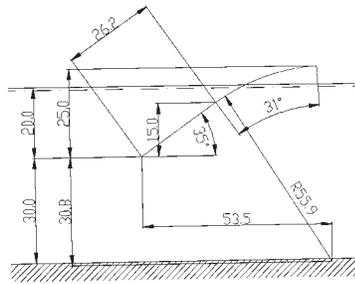
Figure B.27: The geometry of the slope in the CB01 tests. Measures are in cm.

Test CB01

Convex ramp	Curve radius: 0.559 m	Sector of circle: 31°
Slope angle: 35°	Draft: 0.200 m	Crest freeboard: 0.050 m
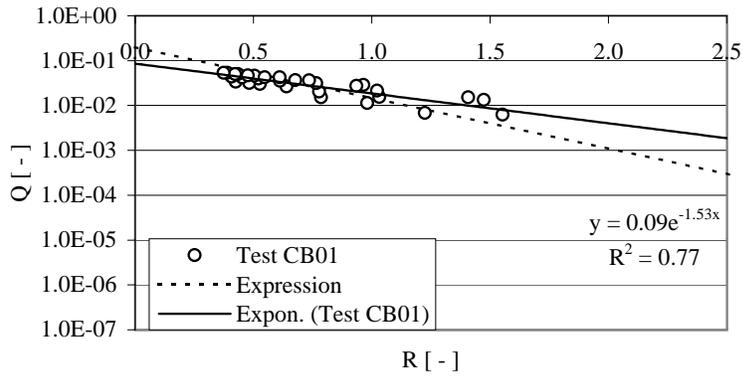
Figure B.28: Results of tests with test geometry CB01.
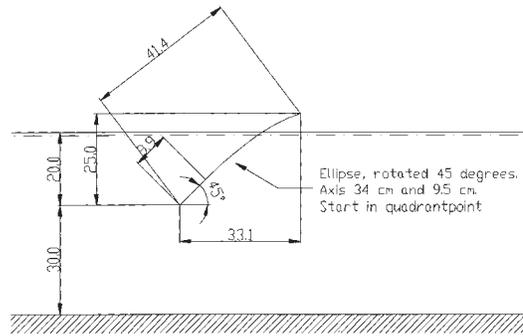
Figure B.29: The geometry of the slope in the CC01 tests. Measures are in cm.

Test CC01

Convex ramp, elliptic

Slope angle: 45°   Draft: 0.200 m   Crest freeboard: 0.050 m
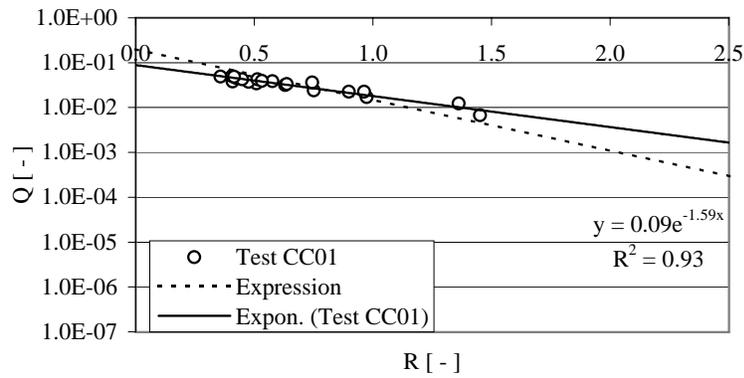
Figure B.30: Results of tests with test geometry CC01.

B.2.4   Concave top of slope
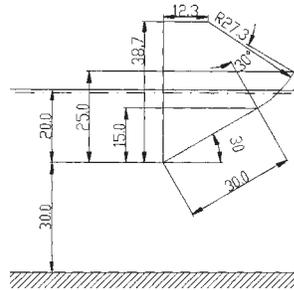
Figure B.31: The geometry of the slope in the DA01 tests. Measures are in cm.

Test DA01

Concave ramp   Curve radius: 0.273 m   Sector of circle: 30°
Slope angle: 30°   Draft: 0.200 m   Crest freeboard: 0.050 m
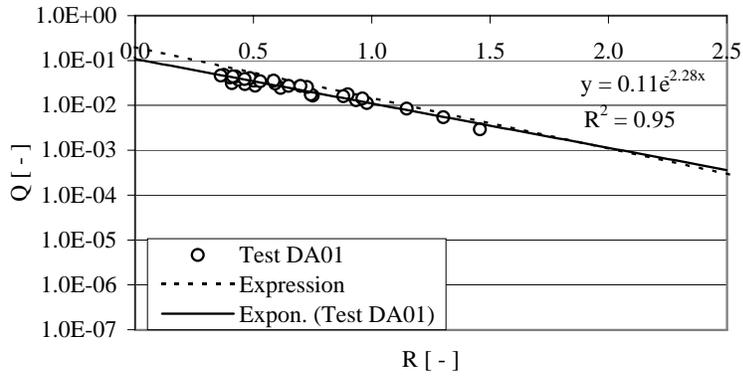
Figure B.32: Results of tests with test geometry DA01.

B.3 Modifications of the side walls of the slope

In this section results of tests performed with modifications of the side walls of the slope are presented. The tested modifications are:

- Linear converging guiding walls.
- Curved converging guiding walls.

B.3.1 Linear converging guiding walls
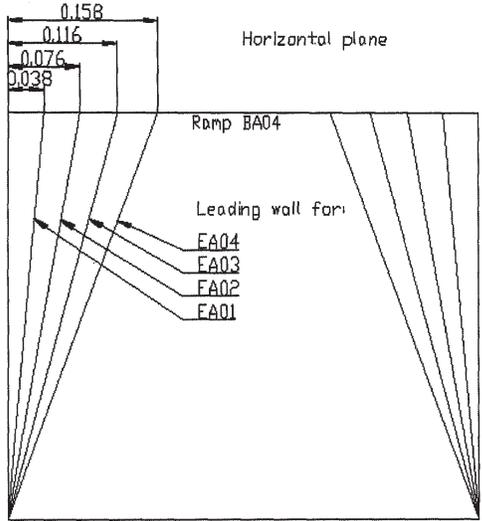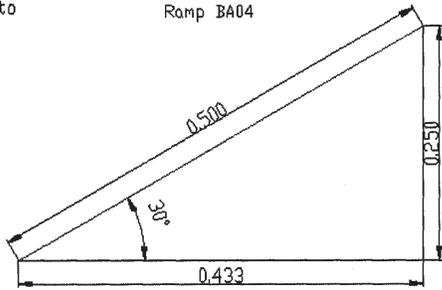
Figure B.33: The geometry of the slope in the EA01 to EA04 tests.
Measures are in m.

Test EA01
Linear converging guiding walls, opening ratio: 0.848
Slope angle: 30°   Draft: 0.200 m   Crest freeboard: 0.050 m
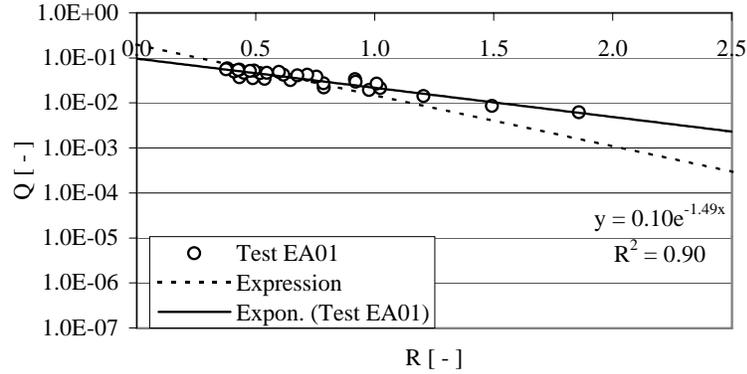
Figure B.34: Results of tests with test geometry EA01.

Test EA02
Linear converging guiding walls, opening ratio: 0.696
Slope angle: 30°   Draft: 0.200 m   Crest freeboard: 0.050 m
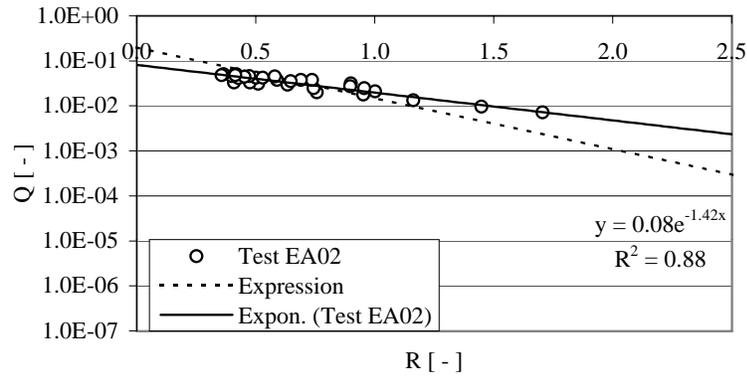
Figure B.35: Results of tests with test geometry EA02.

147

Test EA03

Linear converging guiding walls, opening ratio: 0.536

Slope angle: 30°   Draft: 0.200 m   Crest freeboard: 0.050 m

$$y = 0.07e^{-1.18x}$$
$$R^2 = 0.89$$
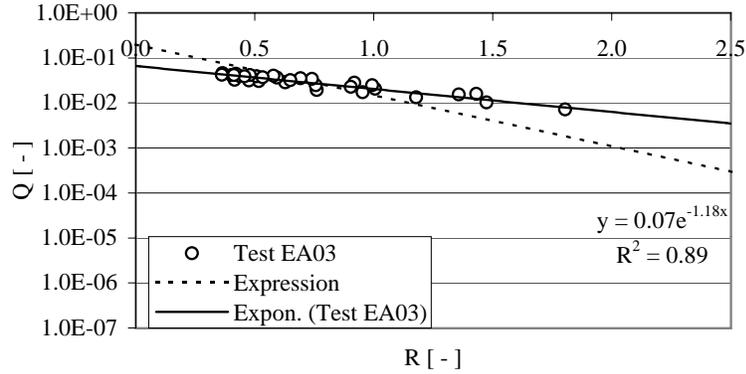
Figure B.36: Results of tests with test geometry EA03.

Test EA04

Linear converging guiding walls, opening ratio: 0.368

Slope angle: 30°   Draft: 0.200 m   Crest freeboard: 0.050 m

$$y = 0.05e^{-1.10x}$$
$$R^2 = 0.92$$
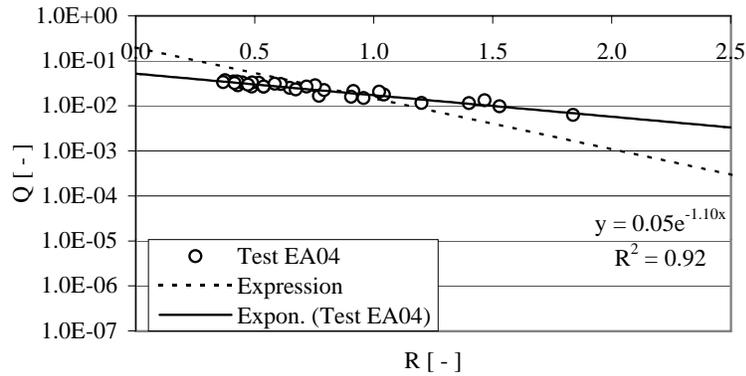
Figure B.37: Results of tests with test geometry EA04.

B.3.2 Curved converging guiding walls
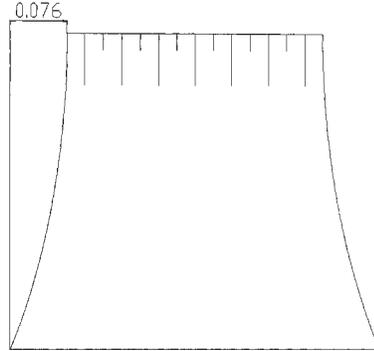
Figure B.38: The shape the of curved converging guiding walls (horizontal projection) for geometry FA02. Measure is in m

Test FA02

Curved converging guiding walls

Opening ratio: 0.696   Large radius in ellipse: 0.095 m

Slope angle: 30°   Draft: 0.200 m   Crest freeboard: 0.050 m
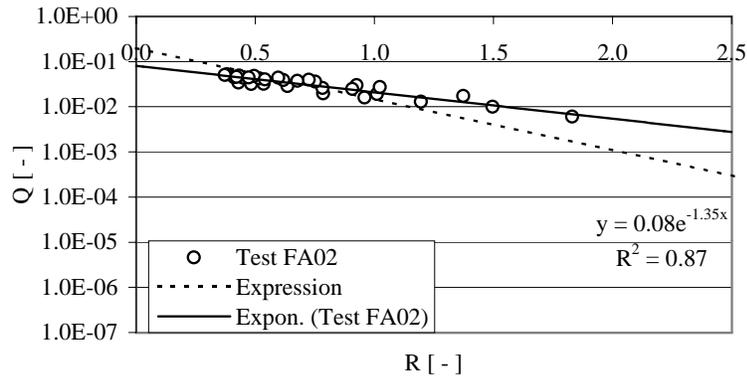
Figure B.39: Results of tests with test geometry FA02.

150

APPENDIX C

Results – Overtopping Discharges with Multi Level Reservoirs

In the following pages the geometries for multi level reservoirs are shown through figures and pictures. Additionally, the results of the model tests conducted are presented in tables in terms of overtopping discharges q_n and amount of captured energy P_n for the individual reservoirs, as well as the total amount of captured energy P and hydraulic efficiency η_{hydr}. All results have been scaled up to prototype values.

The data provided are also accessible on CD-ROM.

C.1 Vertical distribution of overtopping discharge

The geometries of the tested models, on which the expression for the vertical distribution of overtopping is based, are equipped with 8 reservoirs without fronts. The configurations are shown in table 4.1, section 4.2. A photo from the 8 reservoir setup is shown in figure C.1.

The results from the model tests A1 - B are given in table C.1.

C.2 Varied horizontal distance between reservoirs, no fronts

The geometries of the tested models with varying horizontal distance between reservoirs without fronts are shown in table 4.2, section 4.2. Examples of the geometries are shown in figures C.2 and C.3.

The results of the model tests are presented in section 4.8.1 in terms of graphs, figures 4.13 and 4.14. In table C.2 the data from the model tests are shown.

C.3 Various front geometries

The geometries of the tested models with varying horizontal distance between reservoirs and front angles are shown in table 4.3, section 4.2. Photos of selected geometries are shown in figures C.5 and C.6.

The results of the model tests are presented in section 4.8.2 in terms of graphs. In table C.3 the data from model tests D1 to D3 are shown. Corresponding graphs can be found in figure 4.15, section 4.8.2.

In table C.4 the data from model tests E1 to E9 are shown. Corresponding graphs can be found in figures 4.16 to 4.19, section 4.8.2.

Model test have also been conducted using 4 selected geometries with 4 levels of reservoirs, all of them with fronts. The geometries of these models are shown in section 4.2. Furthermore, the geometries are shown in figures C.9 to C.12.

In table C.5 the data from model tests F1 to F4 are shown. Corresponding graphs can be found in figure 4.20, section 4.8.2.

Figure C.1: Photo of model test setup A1.

Test series	H_s [m]	q_1 [m³/s/m]	q_2 [m³/s/m]	q_3 [m³/s/m]	q_4 [m³/s/m]	q_5 [m³/s/m]	q_6 [m³/s/m]	q_7 [m³/s/m]	q_8 [m³/s/m]
A1	1	0.09680	0.00010	0.00004	0.00006	0.00004	0.00000	0.00001	0.00001
	2	0.49292	0.02877	0.00577	0.00082	0.00020	0.00001	0.00000	0.00000
	3	0.91092	0.22935	0.03707	0.00611	0.00194	0.00051	0.00066	0.00047
	4	0.98160	0.40888	0.09613	0.02970	0.01266	0.00234	0.00282	0.00148
	5	0.95155	0.50853	0.15617	0.05961	0.00735	0.00525	0.00655	0.00598
A2	1	0.03672	0.00002	0.00003	0.00002	0.00002	0.00000	0.00003	0.00000
	2	0.34449	0.00992	0.00152	0.00024	0.00000	0.00001	0.00000	0.00000
	3	0.62186	0.11201	0.01800	0.00513	0.00129	0.00030	0.00028	0.00004
	4	0.76431	0.26821	0.06666	0.01876	0.00283	0.00146	0.00171	0.00095
	5	0.82248	0.38792	0.11227	0.03620	0.00420	0.00270	0.00357	0.00336
A3	1	0.01540	0.00000	0.00002	0.00005	0.00002	0.00001	0.00000	0.00000
	2	0.24188	0.00842	0.00208	0.00022	0.00001	0.00000	0.00000	0.00000
	3	0.53346	0.07813	0.01310	0.00399	0.00101	0.00021	0.00024	0.00031
	4	0.70312	0.23502	0.05503	0.01472	0.00258	0.00120	0.00120	0.00083
	5	0.82134	0.36688	0.09849	0.03285	0.00714	0.00268	0.00345	0.00246
B	1	0.00111	0.00041	0.00010	0.00007	0.00000	0.00001	0.00001	0.00000
	2	0.12299	0.00010	0.00006	0.00000	0.00004	0.00000	0.00000	0.00001
	3	0.41301	0.01554	0.00379	0.00070	0.00012	0.00001	0.00001	0.00001
	4	0.77585	0.09763	0.00958	0.00222	0.00043	0.00004	0.00001	0.00000
	5	1.06347	0.26514	0.03236	0.00905	0.00131	0.00024	0.00030	0.00003

Table C.1: Results of model tests A1 - B with 8 reservoirs without fronts.
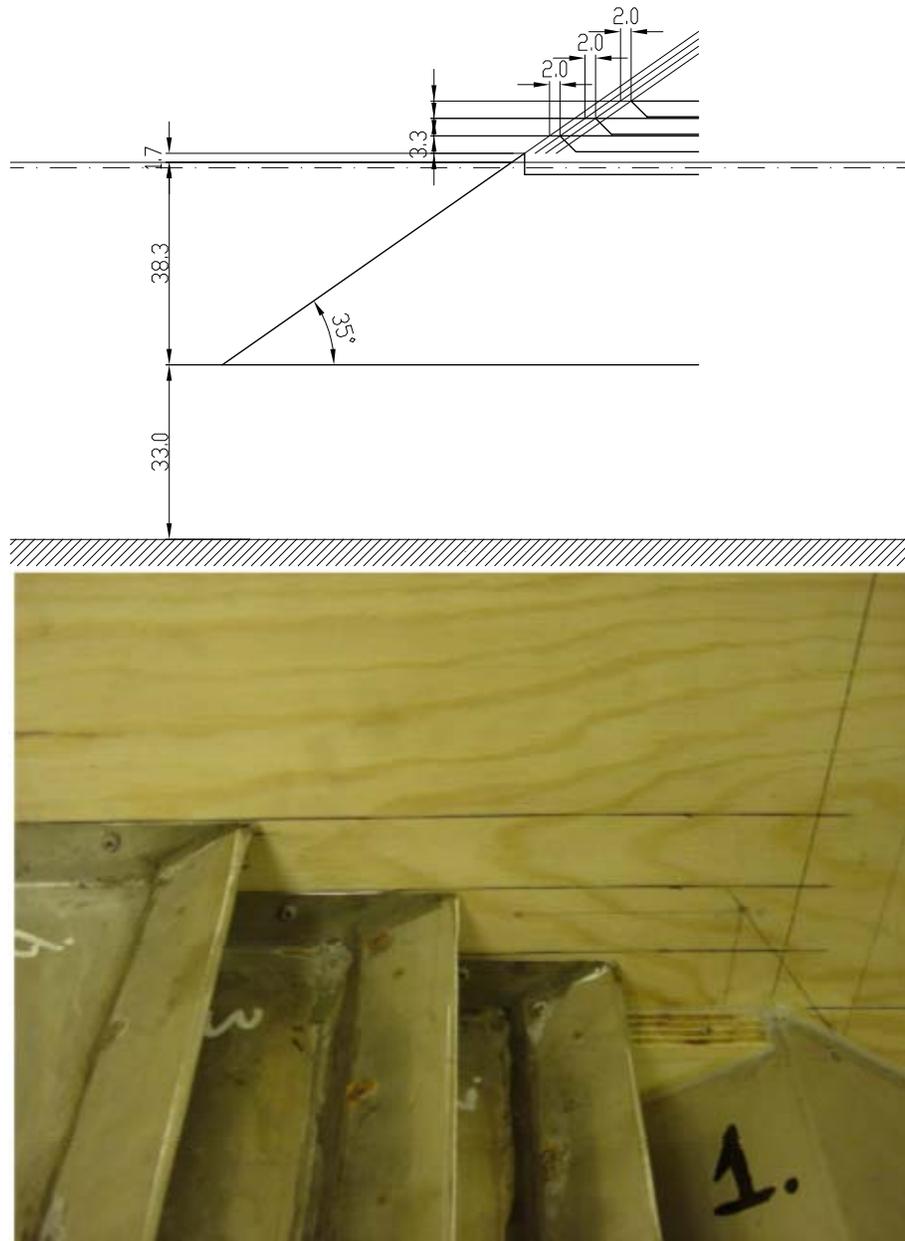
Figure C.2: Drawing (top) and photo (bottom) of model test setup C1, model scale. Measures are in cm.
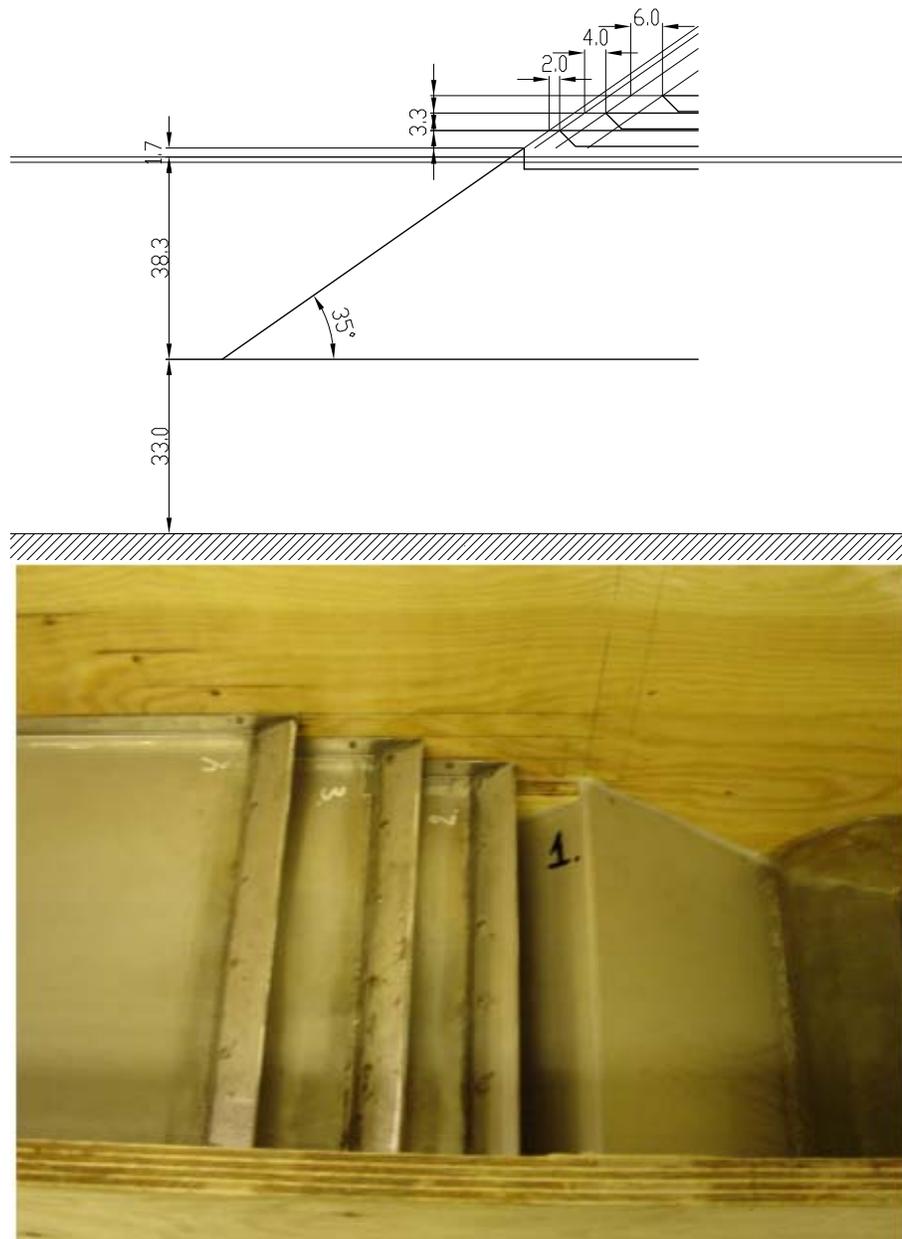
*Figure C.3: Drawing (top) and photo (bottom) of model test setup C2, model scale. Measures are in cm.*

Test series	H_s [m]	q_1 [m³/s/m]	q_2 [m³/s/m]	q_3 [m³/s/m]	q_4 [m³/s/m]	P_1 [kW/m]	P_2 [kW/m]	P_3 [kW/m]	P_4 [kW/m]	P [kW/m]	η_{hydr} [-]
C1	1	0.1034	0.0002	0.0003	0.0001	0.1726	0.0034	0.0088	0.0048	0.1896	0.0796
	2	0.6446	0.0191	0.0005	0.0001	1.0761	0.2877	0.0120	0.0022	1.3780	0.1157
	3	1.0564	0.1213	0.0098	0.0024	1.7635	1.8226	0.2459	0.0831	3.9151	0.1217
	4	1.3452	0.4021	0.0663	0.0138	2.2456	6.0413	1.6601	0.4827	10.4298	0.1564
	5	1.5817	0.5886	0.1293	0.0392	2.6404	8.8442	3.2390	1.3746	16.0982	0.1352
η_{hydr} 12.9 %											
C2	1	0.1347	0.0003	0.0002	0.0001	0.2249	0.0049	0.0057	0.0035	0.2390	0.1003
	2	0.6118	0.0326	0.0011	0.0001	1.0213	0.4901	0.0277	0.0037	1.5428	0.1295
	3	1.0411	0.1415	0.0104	0.0003	1.7381	2.1266	0.2595	0.0093	4.1335	0.1285
	4	1.3717	0.3916	0.0421	0.0066	2.2899	5.8842	1.0536	0.2324	9.4600	0.1418
	5	1.7412	0.6684	0.1232	0.0340	2.9068	10.0428	3.0845	1.1937	17.2278	0.1446
η_{hydr} 13.3 %											
C3	1	0.1188	0.0003	0.0001	0.0002	0.1983	0.0050	0.0016	0.0069	0.2118	0.0889
	2	0.6188	0.0098	0.0008	0.0002	1.0331	0.1468	0.0212	0.0078	1.2089	0.1015
	3	1.0000	0.1089	0.0178	0.0078	1.6694	1.6366	0.4454	0.2735	4.0248	0.1252
	4	1.4010	0.3477	0.0611	0.0156	2.3389	5.2234	1.5297	0.5483	9.6403	0.1445
	5	1.6743	0.5846	0.1430	0.0511	2.7950	8.7827	3.5820	1.7923	16.9519	0.1423
η_{hydr} 12.6 %											
C4	1	0.1205	0.0001	0.0000	0.0002	0.2012	0.0013	0.0010	0.0065	0.2100	0.0882
	2	0.6409	0.0214	0.0026	0.0002	1.0700	0.3218	0.0655	0.0057	1.4630	0.1228
	3	0.9390	0.2264	0.0421	0.0195	1.5676	3.4016	1.0537	0.6833	6.7063	0.2085
	4	1.4157	0.3999	0.0774	0.0309	2.3633	6.0085	1.9372	1.0842	11.3933	0.1708
	5	1.6654	0.5945	0.1280	0.0486	2.7802	8.9316	3.2046	1.7021	6.6185	0.1395
η_{hydr} 15.8 %											
C5	1	0.1300	0.0007	0.0002	0.0002	0.2171	0.0109	0.0050	0.0084	0.2414	0.1013
	2	0.5869	0.0271	0.0021	0.0005	0.9798	0.3216	0.0532	0.0164	1.3711	0.1151
	3	1.0432	0.1931	0.0213	0.0051	1.7415	2.9010	0.5321	0.1795	5.3542	0.1665
	4	1.4007	0.3186	0.0390	0.0045	2.3383	4.7862	0.9763	0.1571	8.2578	0.1238
	5	1.7855	0.5593	0.0996	0.0209	2.9807	8.4029	2.4939	0.7327	14.6102	0.1227
η_{hydr} 13.1 %											
C6	1	0.0990	0.0002	0.0001	0.0001	0.1653	0.0030	0.0020	0.0042	0.1744	0.0732
	2	0.6212	0.0145	0.0004	0.0001	1.0370	0.2179	0.0108	0.0050	1.2707	0.1067
	3	0.9535	0.2019	0.0183	0.0024	1.5918	3.0335	0.4577	0.0845	5.1674	0.1607
	4	1.4633	0.3279	0.0302	0.0067	2.4428	4.9267	0.7556	0.2337	8.3588	0.1253
	5	1.9092	0.5603	0.0676	0.0162	3.1872	8.4185	1.6938	0.5673	3.8668	0.1164
η_{hydr} 12.5 %											
C7	1	0.1612	0.0011	0.0001	0.0003	0.2691	0.0158	0.0020	0.0103	0.2972	0.1248
	2	0.6663	0.0171	0.0008	0.0001	1.1124	0.2571	0.0200	0.0030	1.3924	0.1169
	3	1.0318	0.1891	0.0219	0.0006	1.7225	2.8416	0.5484	0.0219	5.1344	0.1597
	4	1.4881	0.3401	0.0402	0.0052	2.4843	5.1105	1.0054	0.1839	8.7841	0.1317
	5	1.9062	0.5316	0.0899	0.0148	3.1823	7.9867	2.2512	0.5197	13.9399	0.1170
η_{hydr} 13.2 %											
C8	1	0.1080	0.0002	0.0000	0.0000	0.1803	0.0029	0.0000	0.0010	0.1842	0.0773
	2	0.6017	0.0271	0.0011	0.0005	1.0045	0.4075	0.0284	0.0171	1.4575	0.1224
	3	0.9332	0.2321	0.0300	0.0156	1.5579	3.4866	0.7507	0.5455	6.3407	0.1972
	4	1.3819	0.3607	0.0534	0.0256	2.3070	5.4194	1.3370	0.8963	9.9597	0.1493
	5	1.7292	0.6041	0.1220	0.0620	2.8867	9.0759	3.0544	2.1732	17.1902	0.1443
η_{hydr} 14.9 %											
C9	1	0.1034	0.0002	0.0000	0.0001	0.1726	0.0034	0.0010	0.0024	0.1793	0.0753
	2	0.5842	0.0258	0.0014	0.0000	0.9752	0.3880	0.0342	0.0000	1.3975	0.1173
	3	0.9637	0.2023	0.0201	0.0120	1.6087	3.0400	0.5022	0.4208	5.5717	0.1732
	4	1.3695	0.3681	0.0545	0.0167	2.2863	5.5302	1.3642	0.5856	9.7663	0.1464
	5	1.7518	0.5829	0.1107	0.0432	2.9245	8.7580	2.7709	1.5151	15.9686	0.1341
η_{hydr} 13.9 %											

Table C.2: Results of model tests C1 - C9 with varying horizontal distance between the reservoirs without fronts.
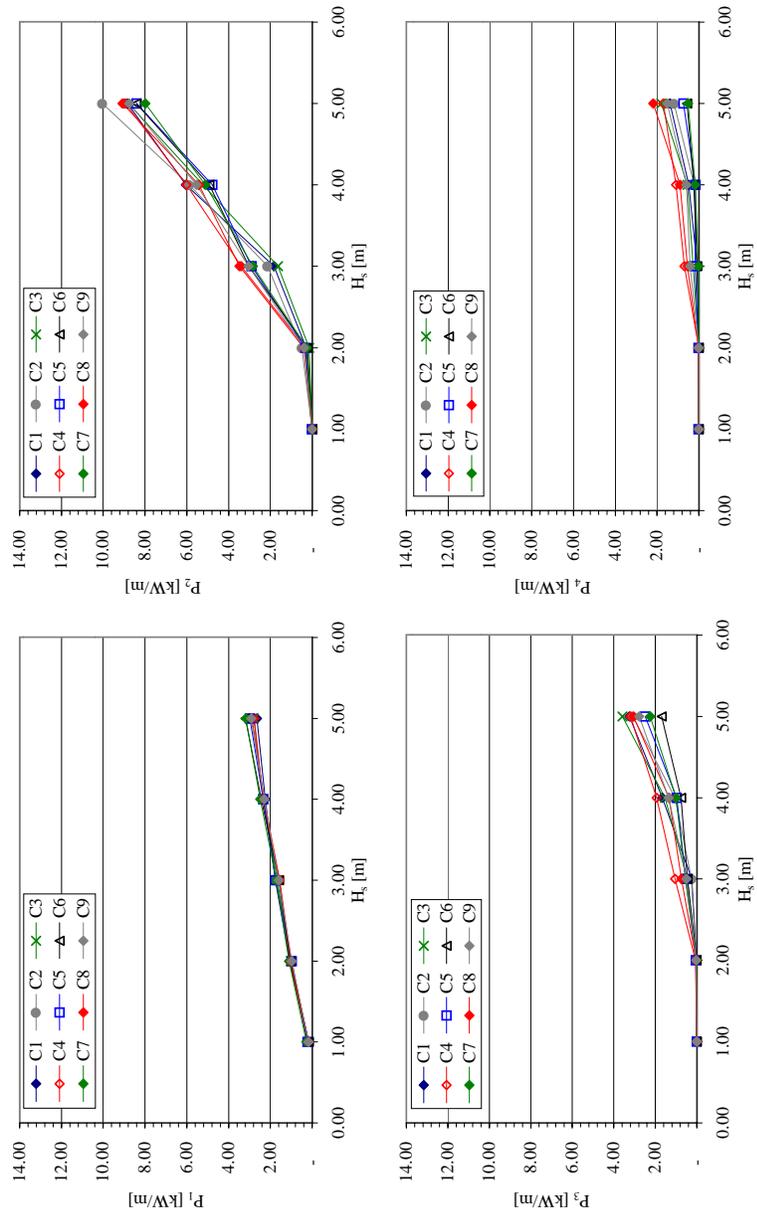
*Figure C.4: Power obtained as potential energy in individual reservoirs
P_n given as a function of the wave situation characterized
by the significant wave height H_s for model tests C1 - C9.*

Figure C.5: Photos of model test setups D1, D2 and D3 (left to right).

Figure C.6: Photos of model test setups E4, E5, E7 and E8 (top left to bottom right)

Test series	H_s [m]	q_1 [m³/s/m]	q_2 [m³/s/m]	q_3 [m³/s/m]	q_4 [m³/s/m]	P_1 [kW/m]	P_2 [kW/m]	P_3 [kW/m]	P_4 [kW/m]	P [kW/m]	η_{hydr} [-]
D1	1	0.1184	0.0009	0.0006	0.0001	0.1976	0.0132	0.0162	0.0033	0.2303	0.0967
	2	0.5107	0.0984	0.0161	0.0086	0.8525	1.4785	0.4031	0.3031	3.0372	0.2550
	3	0.6138	0.2833	0.0754	0.0801	1.0246	4.2567	1.8886	2.8088	9.9788	0.3103
η_{hydr}	4	0.7837	0.4039	0.1205	0.1358	1.3083	6.0680	3.0170	4.7605	15.1539	0.2272
23.8 %	5	0.9370	0.6013	0.2051	0.2359	1.5643	9.0349	5.1360	8.2718	24.0069	0.2016
D2	1	0.1308	0.0003	0.0000	0.0000	0.2184	0.0045	0.0000	0.0000	0.2229	0.0936
	2	0.5989	0.0567	0.0167	0.0049	0.9998	0.8513	0.4193	0.1733	2.4437	0.2052
	3	0.8631	0.2274	0.0778	0.0621	1.4408	3.4163	1.9470	2.1756	8.9798	0.2792
η_{hydr}	4	1.2060	0.3699	0.1279	0.1150	2.0133	5.5577	3.2037	4.0305	14.8052	0.2220
21.6 %	5	1.4982	0.5603	0.2100	0.1878	2.5011	8.4188	5.2588	6.5830	22.7617	0.1911
D3	1	0.1205	0.0002	0.0011	0.0002	0.2011	0.0033	0.0271	0.0078	0.2393	0.1005
	2	0.4940	0.1141	0.0204	0.0063	0.8247	1.7145	0.5105	0.2201	3.2699	0.2745
	3	0.6340	0.3108	0.0740	0.0447	1.0584	4.6693	1.8533	1.5688	9.1498	0.2845
η_{hydr}	4	0.8865	0.4828	0.1477	0.0989	1.4800	7.2536	3.6993	3.4680	15.9009	0.2384
23.7 %	5	1.0893	0.6654	0.2245	0.1741	1.8185	9.9971	5.6228	6.1021	23.5405	0.1976

*Table C.3: Results of model tests D1 - D3 with fronts.*

Figure C.7: Power obtained as potential energy in individual reservoirs P_n given as a function of the wave situation characterized by the significant wave height H_s for model tests D1 - D3.

Test series	H_s [m]	q_1 [m³/s/m]	q_2 [m³/s/m]	q_3 [m³/s/m]	q_4 [m³/s/m]	P_1 [kW/m]	P_2 [kW/m]	P_3 [kW/m]	P_4 [kW/m]	P [kW/m]	η_{hydr} [-]
E1	1	0.0517	0.0010	0.0004	0.0001	0.3451	0.0234	0.0145	0.0044	0.3875	0.1626
	2	0.2613	0.0376	0.0109	0.0084	1.7446	0.8766	0.3993	0.4229	3.4434	0.2891
	3	0.3344	0.0928	0.0417	0.0540	2.2328	2.1653	1.5312	2.7036	8.6329	0.2684
	4	0.4823	0.1529	0.0694	0.0942	3.2205	3.5691	2.5520	4.7158	14.0574	0.2107
η_{hydr} 22.8 %	5	0.6066	0.2128	0.1062	0.1400	4.0503	4.9673	3.9052	7.0123	19.9351	0.1674
E2	1	0.0527	0.0001	0.0003	0.0001	0.3517	0.0012	0.0109	0.0050	0.3688	0.1548
	2	0.3426	0.0339	0.0097	0.0044	2.2880	0.7912	0.3555	0.2216	3.6564	0.3070
	3	0.5277	0.1243	0.0530	0.0372	3.5238	2.9004	1.9466	1.8620	10.2328	0.3182
	4	0.7792	0.2301	0.0945	0.0647	5.2031	5.3702	3.4745	3.2404	17.2882	0.2592
η_{hydr} 26.4 %	5	0.9449	0.3317	0.1413	0.1077	6.3098	7.7410	5.1942	5.3922	24.6373	0.2068
E3	1	0.0342	0.0000	0.0002	0.0001	0.2284	0.0004	0.0082	0.0032	0.2402	0.1008
	2	0.3732	0.0263	0.0062	0.0019	2.4921	0.6129	0.2285	0.0932	3.4267	0.2877
	3	0.6512	0.1137	0.0416	0.0210	4.3482	2.6538	1.5287	1.0524	9.5832	0.2980
	4	0.9178	0.2093	0.0791	0.0456	6.1285	4.8848	2.9064	2.2851	16.2048	0.2429
η_{hydr} 24.8 %	5	1.2160	0.3558	0.1325	0.0774	8.1203	8.3035	4.8721	3.8769	25.1727	0.2113
E4	1	0.0494	0.0016	0.0002	0.0001	0.3301	0.0374	0.0089	0.0056	0.3820	0.1604
	2	0.2226	0.0446	0.0151	0.0077	1.4861	1.0402	0.5560	0.3854	3.4678	0.2911
	3	0.2891	0.0951	0.0361	0.0558	1.9305	2.2184	1.3277	2.7961	8.2727	0.2572
	4	0.3958	0.1471	0.0619	0.0990	2.6428	3.4330	2.2760	4.9594	13.3112	0.1996
η_{hydr} 22.4 %	5	0.5649	0.2204	0.1041	0.1552	3.7721	5.1433	3.8275	7.7726	20.5155	0.1722
E5	1	0.0430	0.0001	0.0001	0.0001	0.2870	0.0025	0.0042	0.0064	0.3000	0.1259
	2	0.3225	0.0407	0.0090	0.0031	2.1538	0.9496	0.3320	0.1567	3.5920	0.3016
	3	0.5035	0.1354	0.0400	0.0288	3.3623	3.1607	1.4713	1.4420	9.4363	0.2934
	4	0.7242	0.2433	0.0729	0.0563	4.8358	5.6787	2.6810	2.8183	16.0138	0.2401
η_{hydr} 24.7 %	5	0.9856	0.3158	0.1166	0.0987	6.5817	7.3702	4.2865	4.9447	23.1831	0.1946
E6	1	0.0377	0.0002	0.0002	0.0001	0.2521	0.0044	0.0080	0.0040	0.2684	0.1127
	2	0.3538	0.0228	0.0088	0.0027	2.3628	0.5318	0.3239	0.1367	3.3552	0.2817
	3	0.6541	0.1180	0.0307	0.0211	4.3676	2.7551	1.1288	1.0556	9.3071	0.2894
	4	0.9442	0.2157	0.0719	0.0430	6.3050	5.0336	2.6435	2.1549	16.1370	0.2419
η_{hydr} 23.4 %	5	1.2014	0.3368	0.1129	0.0798	8.0224	7.8613	4.1497	3.9971	24.0305	0.2017
E7	1	0.0477	0.0014	0.0003	0.0006	0.3184	0.0316	0.0100	0.0302	0.3902	0.1638
	2	0.2157	0.0811	0.0108	0.0015	1.4404	1.8925	0.3965	0.0730	3.8024	0.3192
	3	0.2888	0.2334	0.0519	0.0234	1.9287	5.4472	1.9087	1.1740	10.4586	0.3252
	4	0.4137	0.3577	0.0873	0.0492	2.7627	8.3480	3.2103	2.4625	16.7835	0.2516
η_{hydr} 26.7 %	5	0.5470	0.5039	0.1445	0.0930	3.6526	11.7600	5.3102	4.6568	25.3796	0.2131
E8	1	0.0461	0.0014	0.0003	0.0006	0.3081	0.0322	0.0117	0.0321	0.3841	0.1612
	2	0.3215	0.0511	0.0081	0.0018	2.1467	1.1919	0.2968	0.0902	3.7257	0.3128
	3	0.4793	0.2222	0.0401	0.0126	3.2009	5.1850	1.4752	0.6312	10.4923	0.3263
	4	0.7478	0.3523	0.0702	0.0181	4.9938	8.2212	2.5815	0.9052	16.7018	0.2504
η_{hydr} 27.1 %	5	0.9339	0.5689	0.1474	0.0590	6.2361	13.2769	5.4183	2.9546	27.8860	0.2341
E9	1	0.0396	0.0000	0.0005	0.0006	0.2647	0.0009	0.0177	0.0302	0.3135	0.1316
	2	0.3488	0.1983	0.0045	0.0005	2.3291	0.7426	0.1669	0.0235	3.2621	0.2739
	3	0.6141	0.3319	0.0282	0.0118	4.1006	4.6269	1.0377	0.5902	10.3554	0.3220
	4	0.9520	0.4407	0.0428	0.0088	6.3570	7.7469	1.5718	0.4407	16.1164	0.2416
η_{hydr} 25.3 %	5	1.2366	0.4992	0.0828	0.0409	8.2575	11.6514	3.0427	2.0488	25.0005	0.2099

Table C.4: Results of model tests E1 - E9 with varying horizontal distance between the reservoirs and varying font angles.
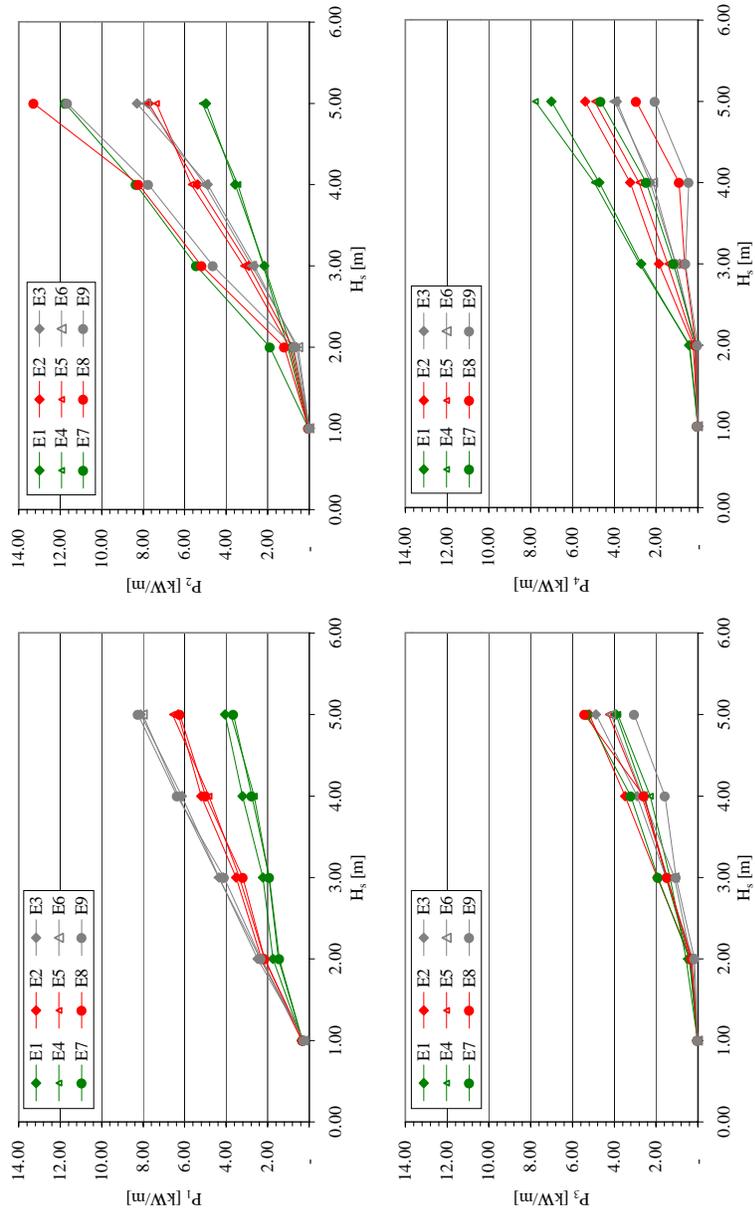
Figure C.8: Power obtained as potential energy in individual reservoirs P_n given as a function of the wave situation characterized by the significant wave height H_s for model tests E1 - E9.
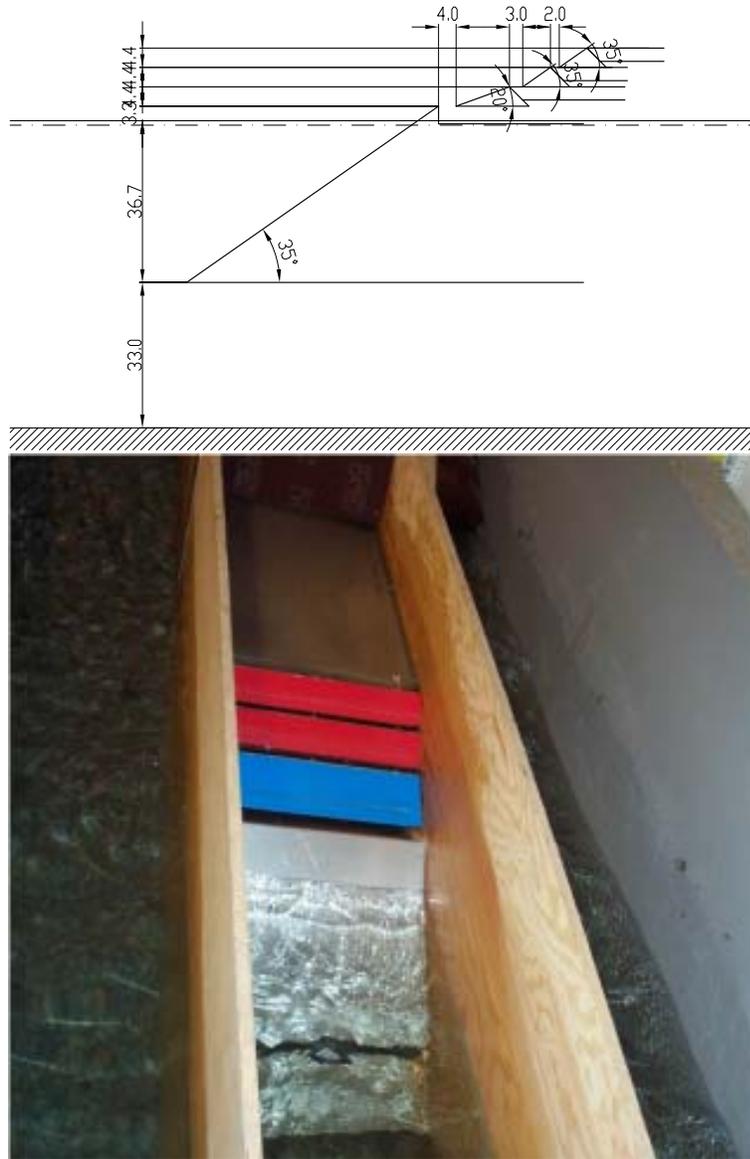
*Figure C.9: Drawing (top) and photo (bottom) of model test setup F1,
model scale. Measures are in cm.*

Figure C.10: Drawing (top) and photo (bottom) of model test setup F2,
model scale. Measures are in cm.
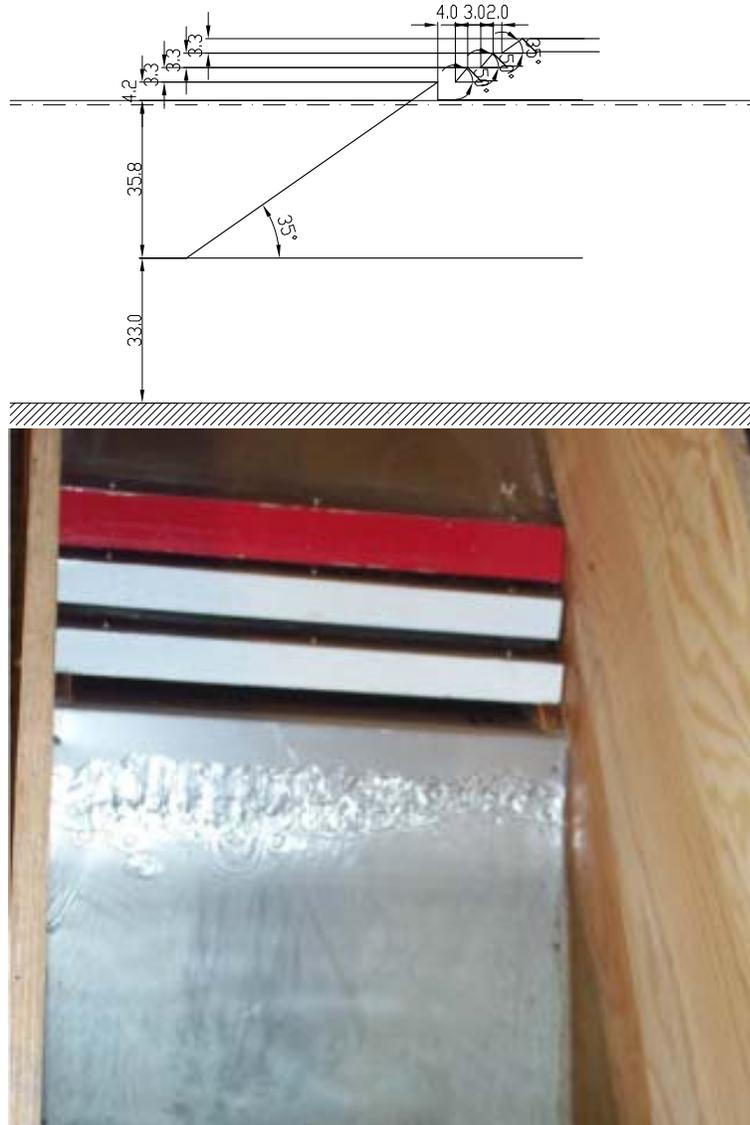
Figure C.11: Drawing (top) and photo (bottom) of model test setup F3, model scale. Measures are in cm.

Figure C.12: Drawing (top) and photo (bottom) of model test setup C1, model scale. Measures are in cm.

Test series	H_s [m]	q_1 [m³/s/m]	q_2 [m³/s/m]	q_3 [m³/s/m]	q_4 [m³/s/m]	P_1 [kW/m]	P_2 [kW/m]	P_3 [kW/m]	P_4 [kW/m]	P [kW/m]	η_{hydr} [-]
F1	1	0.0471	0.0000	0.0000	0.0000	0.3148	0.0000	0.0000	0.0000	0.3148	0.1322
	2	0.3013	0.0454	0.0000	0.0000	2.0119	1.0593	0.0000	0.0000	3.0712	0.2578
	3	0.5430	0.1749	0.0185	0.0276	3.6262	4.0813	0.6804	1.3839	9.7718	0.3038
η_{hydr} 26.0 %	4	0.8343	0.3409	0.0445	0.0759	5.5713	7.9561	1.6353	3.8037	8.9665	0.2843
	5	1.1155	0.4768	0.0778	0.1237	7.4487	1.1275	2.8612	6.1948	7.6322	0.2320
F2	1	0.0629	0.0000	0.0000	0.0000	0.4200	0.0000	0.0000	0.0000	0.4200	0.1763
	2	0.3237	0.0530	0.0061	0.0034	2.1618	1.0611	0.1822	0.1375	3.5425	0.2974
	3	0.5813	0.1960	0.0365	0.0543	3.8817	3.9255	1.0954	2.1743	11.0768	0.3444
η_{hydr} 29.3 %	4	0.8647	0.3521	0.0751	0.1302	5.7741	7.0541	2.2555	5.2181	20.3018	0.3044
	5	1.1450	0.5075	0.1339	0.2162	7.6456	10.1662	4.0247	8.6624	30.4989	0.2561
F3	1	0.0226	0.0000	0.0000	0.0000	0.2254	0.0005	0.0000	0.0000	0.2259	0.0990
	2	0.2629	0.0354	0.0052	0.0065	2.7431	0.7967	0.1698	0.2771	3.9867	0.3347
	3	0.5024	0.1575	0.0257	0.0577	5.2419	3.5499	0.8354	2.4573	12.0845	0.3758
η_{hydr} 31.0 %	4	0.7286	0.3078	0.0565	0.1278	7.6024	6.9365	1.8390	5.4410	21.8189	0.3271
	5	0.9964	0.4663	0.0853	0.1992	10.3965	10.5083	2.7774	8.4785	32.1608	0.2700
F4	1	0.1055	0.0000	0.0000	0.0000	0.3963	0.0004	0.0000	0.0000	0.3967	0.1665
	2	0.5060	0.0683	0.0081	0.0007	1.9006	1.1970	0.2236	0.0247	3.3460	0.2809
	3	0.8489	0.2911	0.0604	0.0159	3.1885	5.1032	1.6639	0.5959	10.5515	0.3281
η_{hydr} 29.4 %	4	1.2277	0.6168	0.1358	0.0460	4.6112	10.8114	3.7403	1.7274	20.8904	0.3132
	5	1.6861	1.0400	0.2368	0.0988	6.3332	18.2297	6.5235	3.7111	34.7976	0.2921

*Table C.5: Results of model tests F1 - F4 with selected geometries.*
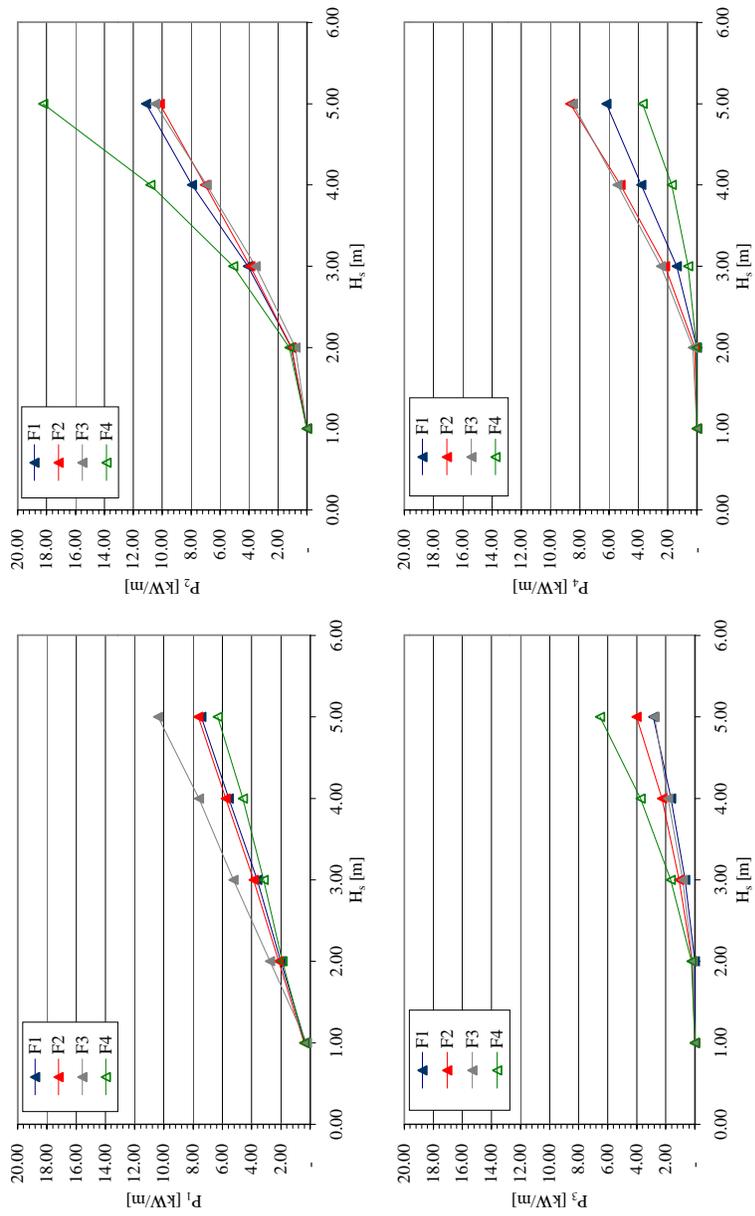
Figure C.13: *Power obtained as potential energy in individual reservoirs P_n given as a function of the wave situation characterized by the significant wave height H_s for model tests F1 - F4.*

169

C.4 Floating model

Tests have been performed with a floating model with a front geometry like F2^{mod}. The floating model is further described in section 4.9. The results of the tests with the floating model are described in table C.6.

H_s [m]	q_1 [m³/s/m]	q_2 [m³/s/m]	q_3 [m³/s/m]	q_4 [m³/s/m]	$R_{c,1}$ [m]	P_1 [kW/m]	P_2 [kW/m]	P_3 [kW/m]	P_4 [kW/m]	P [kW/m]	η_{hydr} [-]
1	0.0194	0.0000	0.0000	0.0000	1.566	0.3036	0.0000	0.0000	0.0000	0.3036	0.128
	0.0699	0.0000	0.0000	0.0000	0.998	0.4644	0.0000	0.0000	0.0000	0.4644	0.195
	0.0297	0.0013	0.0000	0.0000	1.305	0.3375	0.0290	0.0000	0.0000	0.3665	0.154
	0.0521	0.0007	0.0000	0.0000	1.160	0.4686	0.0152	0.0000	0.0000	0.4839	0.203
2	0.1995	0.0336	0.0044	0.0035	1.609	3.2148	0.8785	0.1585	0.1630	4.4149	0.371
	0.3395	0.0880	0.0237	0.0121	0.778	1.3725	1.5678	0.6598	0.4582	4.0582	0.341
	0.2755	0.0568	0.0117	0.0043	1.264	2.9407	1.2872	0.3823	0.1827	4.7929	0.402
	0.3178	0.0675	0.0196	0.0077	0.992	2.0902	1.3467	0.5861	0.3084	4.3313	0.364
	0.2549	0.0368	0.0067	0.0030	1.430	3.4832	0.8959	0.2299	0.1336	4.7426	0.398
3	0.5053	0.2046	0.0735	0.0448	0.965	3.1448	4.0279	2.1826	1.7814	11.1367	0.346
	0.5343	0.2609	0.0970	0.0376	1.273	5.7785	5.9396	3.1781	1.6098	16.5060	0.513
	0.6491	0.1384	0.1553	0.0745	0.775	2.6063	2.4604	4.3172	2.8189	12.2028	0.379
	0.6864	0.1312	0.1764	0.0670	0.720	2.3735	2.2598	4.8058	2.4961	11.9352	0.371
	0.5749	0.1721	0.1718	0.0056	1.319	6.6746	3.9960	5.7100	0.2415	16.6221	0.517
	0.5078	0.0812	0.1761	0.0597	1.623	8.2566	2.1345	6.3928	2.7664	19.5503	0.608
	0.3344	0.1245	0.0335	0.0341	2.412	8.0794	4.2557	1.4793	1.8508	15.6653	0.487
	0.2594	0.0930	0.0262	0.0302	3.213	8.3471	3.9241	1.3700	1.8808	15.5220	0.483
	0.3163	0.1387	0.0409	0.0406	2.455	7.7767	4.8002	1.8250	2.2160	16.6179	0.517
	0.1662	0.2240	0.0877	0.0718	1.390	2.1423	5.3626	2.9792	3.1555	13.6395	0.424
4	0.7070	0.3540	0.1928	0.1076	1.039	5.1003	7.2313	5.8689	4.3516	22.5521	0.338
	0.8280	0.1992	0.2344	0.1261	0.964	5.1428	3.9200	6.9593	5.0075	21.0296	0.315
	0.8372	0.2104	0.2611	0.0961	1.033	5.9686	4.2853	7.9319	3.8829	22.0687	0.331
	0.6642	0.3400	0.0492	0.0943	1.607	10.6941	8.8783	1.7793	4.3515	25.7032	0.385
	0.6716	0.3259	0.0910	0.0949	1.503	10.1120	8.1714	3.1926	4.2823	25.7584	0.386
	0.7521	0.3508	0.0634	0.1145	0.939	4.4239	6.8119	1.8659	4.5161	17.6178	0.264
	0.6891	0.3419	0.0492	0.0794	0.947	4.1304	6.6695	1.4537	3.1391	15.3928	0.231
	0.7062	0.4014	0.1173	0.1093	1.887	13.3472	11.6061	4.5660	5.3485	34.8678	0.523
	0.6544	0.2036	0.1926	0.1618	0.975	4.1546	4.0272	5.7383	6.4429	20.3630	0.305
	0.6175	0.1971	0.1778	0.1690	2.136	13.2097	6.1913	7.3657	8.6937	35.4605	0.532
	0.4804	0.2054	0.1225	0.1244	2.881	13.8611	7.9830	5.9897	7.3282	35.1620	0.527
	0.5690	0.3284	0.1642	0.1376	1.839	10.4845	9.3408	6.3152	6.6692	32.8097	0.492
	0.3555	0.1865	0.0794	0.0961	3.907	13.9103	9.1659	4.6978	6.6464	34.4204	0.516
5	0.9463	0.3912	0.2274	0.0630	0.606	2.3184	6.2915	5.9358	2.2746	16.8203	0.141
	0.9265	0.4408	0.1814	0.0502	0.645	2.5754	7.2632	4.8070	1.8344	16.4799	0.138
	1.0526	0.3478	0.2311	0.1121	1.310	12.0535	8.0464	7.6595	4.8383	32.5977	0.274
	1.0130	0.2629	0.1603	0.0825	0.799	4.3178	4.7374	4.4937	3.1402	16.6891	0.140
	0.9854	0.3148	0.2492	0.0832	1.348	11.9593	7.4036	8.3584	3.6223	31.3437	0.263
	1.0130	0.2273	0.2085	0.0885	0.941	5.9930	4.4199	6.1439	3.4921	20.0489	0.168
	0.8833	0.2170	0.2425	0.1991	1.507	13.3313	5.4492	8.5197	8.9871	36.2872	0.305
	0.8687	0.2198	0.2518	0.2111	2.166	18.8448	6.9697	10.5075	10.9210	47.2431	0.397
	0.6914	0.3372	0.2083	0.1842	2.777	19.2305	12.7576	9.9678	10.6606	52.6164	0.442
	0.5510	0.3195	0.1704	0.1665	3.414	18.8442	14.1272	9.2403	10.7003	52.9120	0.444
	0.7069	0.3516	0.1860	0.1576	2.688	19.0354	12.9897	8.7337	8.9798	49.7386	0.418

Table C.6: Results of tests with the floating model.